The role of root suberin in protecting barley plants from copper stress

Dissertation

zur

Erlangung des Doktorgrades (Dr. rer. nat.)

der

Mathematisch-Naturwissenschaftlichen Fakultät

der

Rheinischen Friedrich-Wilhelms-Universität Bonn

vorgelegt von

Qihui Zhang

aus

Zhejiang, China

Bonn, 2025

Angefertigt mit Genehmigung der Mathematisch-Naturwissenschaftlichen Fakultät der
Rheinischen Friedrich-Wilhelms-Universität Bonn

Gutachter/Betreuer: Prof. Dr. Lukas Schreiber
Gutachterin: PD Dr. Caroline Marcon

Tag der Promotion: 15.07.2025
Erscheinungsjahr: 2025

Abstract

Copper (Cu) contamination in agricultural soil significantly threatens crop growth, yield, and overall agricultural productivity. Although barley *(Hordeum vulgare* L.) exhibits a relatively high tolerance to metal stress, the mechanisms underlying its tolerance to Cu stress, particularly the specific role of suberin, remain unclear. Therefore, this study investigated the morphological, physiological, biochemical, and transcriptomic responses of barley (cv. Scarlett) seedlings exposed to 50 μM and 100 μM Cu for six days.

The results of this study indicated that Cu exposure significantly inhibited barley growth, with roots exhibiting greater sensitivity than shoots. Despite growth inhibition, photosynthetic performance in leaves remained unaffected. Cu stress induced oxidative stress, as evidenced by increased hydrogen peroxide (H_2O_2) accumulation in roots, superoxide radical ($O_2^{\bullet -}$) level in leaves, and enhanced lipid peroxidation in both tissues, reflected by increased malondialdehyde (MDA) content. In response, barley plants accumulated proline in both roots and leaves, likely mitigating oxidative stress. Histochemical staining and chemical quantification revealed enhanced suberin deposition in roots under Cu stress, particularly through increased synthesis of aliphatic suberin monomers.

Additionally, Cu stress disrupted nutrient homeostasis by affecting the uptake of essential mineral nutrients. Histochemical analysis of Cu distribution in root cross-sections and mineral nutrition analysis further indicated that suberin functioned as an effective endodermis barrier, limiting the xylem loading of Cu ions. As a result, Cu primarily accumulated in root apoplastic regions, reducing its translocation to shoots and alleviating shoot toxicity. Transcriptomic analysis identified extensive transcriptional reprogramming involving cell wall modifications, antioxidant defense, detoxification processes, Cu transporters, and plant hormone signaling transduction pathways in response to Cu stress. Furthermore, suberin-defective mutants (lacking

very long chain C22-C26 ω-hydroxy acids) exhibited increased Cu sensitivity, enhanced oxidative damage, and greater Cu translocation to shoots, underscoring the importance of suberin monomer composition in root barrier function.

In summary, this study provides a comprehensive understanding of Cu-induced phytotoxicity in barley and highlights suberin's critical function as an endodermal barrier limiting Cu uptake and translocation. The findings of this study provide novel insights for genetic improvement strategies aimed at enhancing Cu tolerance in barley and other crops and contribute to phytoremediation in Cu-contaminated soil.

Content

1. Introduction

Heavy metal contamination of agricultural soils caused by anthropogenic activities is a major environmental problem worldwide (Timothy and Tagui Williams, 2019; Zhang and Wang, 2020). Such contamination adversely impacts human and animal health, agricultural productivity, and food quality (Rashid et al., 2023). Copper (Cu), while an essential micronutrient for plant growth, represents one of the most prevalent heavy metal pollutants in soil (Luo et al., 2024). Excess Cu exposure negatively affects plant growth and development, subsequently reducing crop yields (Mir et al., 2021). Consequently, mitigating Cu pollution remains an essential goal for sustainable agriculture. Phytoremediation, the utilization of plants to absorb and immobilize heavy metals from contaminated soils, has been recognized as an environmentally friendly and cost-effective remediation strategy (Wan et al., 2016). Nevertheless, the effectiveness of phytoremediation is highly dependent on the plant species' capacity for specific heavy metal tolerance and accumulation (Memon and Schröder, 2009; Gupta et al., 2013). Therefore, understanding the mechanisms of plant tolerance to specific metals is important for developing plants suitable for the phytoremediation of contaminated sites (Jabeen et al., 2009). Barley (*Hordeum vulgare* L.), ranking fourth among cereal crops globally, is recognized as relatively tolerant to heavy metal stress (Ebbs and Kochian, 1998; Mostofa et al., 2014). An important feature of plant tolerance to environmental stress, including heavy metal stress, is the formation of an endodermal suberin barrier in roots (Doblas et al., 2017; Peralta Ogorek et al., 2023). However, the mechanisms underlying barley's tolerance to Cu stress, particularly the specific role of suberin deposition in Cu tolerance, still remain unclear. Given barley's significant potential for phytoremediation of heavy metal-contaminated soils (Ebbs and Kochian, 1998), elucidating the physiological and molecular responses to Cu stress and clarifying the functional role of suberin deposition are essential. This knowledge would promote

varietal selection and genetic improvement aimed at enhancing Cu tolerance and ultimately contribute valuable insights into effective phytoremediation strategies.

1.1 The function of copper in plants

Copper is an essential redox-active micronutrient that functions optimally within a narrow concentration range to support fundamental physiological processes in plants (Mir et al., 2021). As a transition metal existing predominantly as Cu^{2+} (cupric) and Cu^{+} (cuprous) ions in planta (Jun et al., 2023), its redox cycling capacity enables participation in critical biochemical pathways, including mitochondrial respiration, photosynthetic electron transport, cell wall lignification, and oxidative stress responses (Peers and Price, 2006; Thounaojam et al., 2012; Lacey and Binder, 2014; Ruiz et al., 2021; Zhou et al., 2025). The catalytic versatility of Cu enables its ability to serve as a cofactor in key enzymes, such as plastocyanin (a photosystem electron carrier), Cu/Zn superoxide dismutase (a ROS scavenger), laccases (involved in lignin polymerization), and cytochrome c oxidase (a component of the respiratory chain) (Hoegger et al., 2006; Abdel-Ghany, 2009; Boden et al., 2021). Moreover, Cu also modulates phytohormone signaling through its incorporation into ethylene receptors like CTR1 (constitutive triple response 1), which governs ethylene perception and downstream responses (Light et al., 2016).

1.2 Copper toxicity in plants

A Cu concentration of 5-30 mg/kg in plant tissues is generally optimal for normal growth and development (Shabbir et al., 2020; Kumar et al., 2021). However, this range may vary depending on plant species, varieties, and environmental factors. When concentrations exceed this optimal range, Cu becomes toxic to most plants (Yruela, 2009). Increased Cu concentrations exert adverse effects on plant growth and development, affecting plants at morphological, physiological, and molecular levels. In addition to reducing plant productivity and crop yields, Cu toxicity may also pose risks

to human health by entering the food chain (Adrees et al., 2015). The following summarizes the toxic effects of Cu in plants (**Figure 1. 1**).

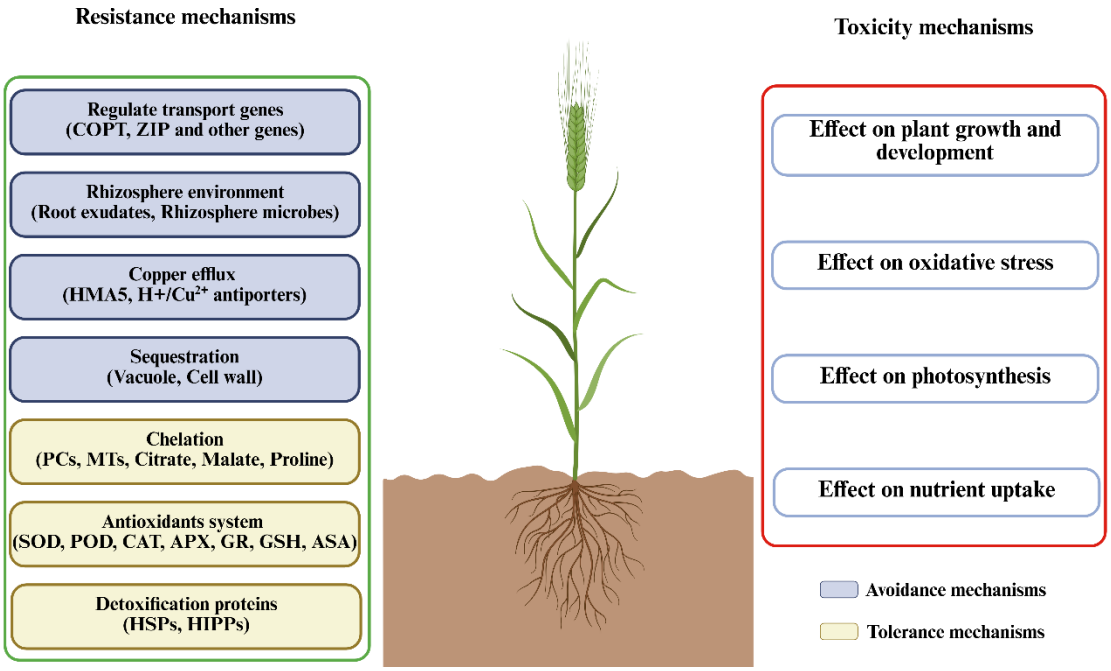

Figure 1. 1 Plant toxicity and resistance mechanisms under Cu stress. Modified from (Wang et al., 2025).

1.2.1 Effect on plant growth and development

Growth inhibition is one of the most notable symptoms observed in plants under Cu stress (Adrees et al., 2015; Mir et al., 2021). Cu tends to accumulate in roots, causing toxicity that first affects root structure and function before impacting aboveground physiological processes (Cambrollé et al., 2013). Cu toxicity induces structural changes, including root shortening, thickening and darkening, reduced root hair growth, and tearing of the root epidermis and cortex, ultimately inhibiting root growth and biomass production (Kopittke et al., 2009; Madejón et al., 2009; Juang et al., 2012). Batool et al. (2015) demonstrated that inhibited root growth under heavy metal stress is related to reduced cell division and subsequent increases in root cell wall thickness. Several studies have confirmed the inhibitory effects of excess Cu on root and shoot growth across various plant species. For instance, in rice (*Oryza sativa*), Cu toxicity markedly

reduced plant biomass and grain yield when soil Cu concentrations exceeded 100 mg/kg, with yield declines increasing as soil Cu concentration increased (Xu et al., 2006). Similarly, hydroponic studies conducted on rice (*Oryza sativa* L.) exposed to Cu concentrations of 0, 10, 50, and 100 μM for five days revealed a gradual decrease in shoot and root growth, with root growth showing the greatest sensitivity to increasing Cu levels and exposure durations (Thounaojam et al., 2012). Moreover, Htwe et al. (2020) reported that Cu stress significantly reduced rice plant height and grain yield. Kumar et al. (2008) further observed that maize seedlings treated with 100 μM Cu for 14 days exhibited significantly reduced fresh and dry weights of stems and roots, accompanied by visible leaf chlorosis. Studies showed that excess Cu concentrations inhibited root growth in both tomato (*Solanum lycopersicum* L.) and cucumber (*Cucumis sativus* L.), and cucumber roots were more sensitive to Cu toxicity than tomato roots under the same treatment conditions (İşeri et al., 2011). Moreover, barley (*Hordeum vulgare* L.) seedlings exposed to Cu concentrations increasing from 0.1 to 1 mg/L showed marked reductions in both root and shoot lengths, with roots demonstrating greater susceptibility to Cu stress than shoots (Žaltauskaitė and Šliumpaitė, 2013). These studies indicate that Cu toxicity significantly inhibits plant growth, with the severity of effects dependent upon species, genotype, metal concentration, and duration of exposure. Thus, detailed assessments of Cu toxicity responses across diverse plant species and cultivars are essential for accurately understanding plant-metal interactions.

1.2.2 Effect on photosynthetic performance

Cu, as a cofactor of plastocyanin, participates in the photosynthetic electron transport process. It is also an activator of certain enzymes involved in chlorophyll biosynthesis (Sun et al., 2022). While optimal Cu concentrations enhance photosynthetic processes, excessive Cu can negatively impact photosynthesis by altering pigment composition, damaging chloroplast ultrastructure, impairing thylakoid membrane integrity, reducing net photosynthetic rates, decreasing RuBisCo enzyme efficiency, and inhibiting

electron transfer in photosystem II (PSII) (Parveen et al., 2020; Mir et al., 2021). Studies indicate that Cu toxicity inhibits photosynthesis primarily by disrupting chlorophyll synthesis or causing its degradation (Li et al., 2019b). Sheng et al. (2024) reported that excess Cu decreases chlorophyll content by replacing Mg^{2+} ions with Cu^{2+} ions within chlorophyll molecules and inducing lipid peroxidation of chloroplast membranes. Furthermore, Pätsikkä et al. (2002) suggested that Cu-induced iron deficiency reduces leaf chlorophyll concentrations, resulting in increasing Cu toxicity to PSII. Several studies reported the toxic effects of Cu on chlorophyll biosynthesis in various crop species. For example, in wheat, 200 mg/kg Cu treatment significantly reduced chlorophyll content after 14 days (Xu et al., 2017). Similarly, in lentil plants, high Cu concentrations (3.0 mM) significantly reduced chloroplast pigments, including chlorophyll a, chlorophyll b, and carotenoids (Hossain et al., 2020). Cu toxicity affects chlorophyll content differently across plant species and even within the same species. For instance, 100 μM Cu treatment reduced total chlorophyll content by 37.02% and 55.83% in maize varieties SC 122 and SC 10, respectively, compared with control levels (Aly and Mohamed, 2012). While some studies have reported Cu's inhibitory effects on both photosystem I (PSI) and PSII (Mishra and Dubey, 2005), more studies have shown that PSII is the most sensitive site to Cu toxicity (Yruela, 2009). In green algae (*Chlorella*), Cu toxicity primarily inhibits photosynthesis by damaging PSII (Chen et al., 2016). Similarly, in water hyacinth (*Eichhornia crassipes*), Cu treatment reduced photosynthesis by decreasing chlorophyll content and damaging PSII functions (Jin et al., 2021). Studies have also shown that excess Cu (75-150 μM) disrupts thylakoid membrane composition, leading to reduced PSII activity and electron transport (Xu et al., 2013).

1.2.3 Effect on oxidative stress

In plants, reactive oxygen species (ROS) such as hydrogen peroxide (H_2O_2), superoxide anion ($O_2^{\bullet -}$), and hydroxyl radicals (•OH) are generated as byproducts of aerobic metabolism (Pourrut et al., 2011). Among these ROS, hydroxyl radicals (•OH) are

particularly reactive, causing immediate oxidative damage to essential biomolecules such as lipids, proteins, and nucleic acids (Pai et al., 2018; Møller et al., 2020; Arslan et al., 2022). Cu is a redox-active metal that can catalyze ROS generation via Haber-Weiss and Fenton reactions, thereby producing superoxide ($O_2^{\bullet -}$), hydrogen peroxide (H_2O_2), and hydroxyl radicals (•OH) (Florence, 1984; Pham et al., 2013). Thus, excess Cu disturbs redox homeostasis by overwhelming the plant's antioxidant defense systems, leading to increased ROS accumulation and subsequent oxidative damage (Lin et al., 2023; Khorashad et al., 2024). Cu-induced ROS overproduction has been widely documented in various plant species. For example, in barley (*Hordeum vulgare* L.), hydrogen peroxide levels increased proportionally with rising Cu concentrations (Tamás et al., 2017). Similarly, rice (*Oryza sativa* L.) exposed to 0-100 μM Cu for 5 days showed dose-dependent increases in H_2O_2 and malondialdehyde (MDA), a biomarker of lipid peroxidation (Thounaojam et al., 2012). Furthermore, *Medicago sativa* displayed contrasting responses: $O_2^{\bullet -}$ levels increased steadily with Cu concentration, whereas •OH levels peaked at 50 μM Cu before declining at 100 μM, possibly due to antioxidant induction (Wang et al., 2011). These findings indicate that ROS generation under Cu stress is dependent on multiple factors, including plant species, Cu concentration, and exposure duration.

1.2.4 Effect on nutrient uptake

Cu toxicity typically affects roots before shoots, with root damage being an early symptom (Chen et al., 2022b). Excessive Cu ions in the soil significantly inhibit root elongation, disrupt the integrity of the root epidermis, reduce root hair density, and cause disordered root architecture (Madejón et al., 2009; Juang et al., 2012). These morphological changes directly impair the root system's ability to absorb water and essential nutrients, leading to a global imbalance in the plant's nutrient homeostasis. Further studies have shown that high concentrations of Cu can induce dysfunction in transmembrane ion transport systems. Some studies reported that Cu ions competitively inhibit the uptake of essential cations such as Fe^{2+}, Zn^{2+}, and Mn^{2+} at absorption sites

(Yruela, 2009). Some studies also reported that Cu-induced ROS production can damage cell membrane integrity through lipid peroxidation, resulting in nutrient leakage and loss of selective absorption capacity (Adrees et al., 2015). For example, when Cu concentrations exceeding 20 mg/kg were applied to maize, the uptake of phosphorus (P), zinc (Zn), and iron (Fe) decreased progressively with increasing Cu concentrations (Azeez et al., 2015). In *Inga subnuda*, Cu concentrations above 0.16 mmol/L caused ultrastructural damage to root cells, including the cell membrane, endodermis, mitochondria, and vacuoles, which in turn impaired the root system's ability to absorb and transport mineral nutrients (De Freitas et al., 2015). In rice, excess Cu downregulated the expression of key nutrient transporters such as *OsNPF6.5*, *OsNPF2.2*, and *OsNPF2.4*, resulting in decreased nitrate (NO_3^-) uptake and translocation, leading to reduced nitrate concentration and nitrate reductase (NR) activity in shoots (Huo et al., 2020). These findings indicated that Cu toxicity affects nutrient uptake by altering root morphology, competing with metal transporters, downregulating the expression of genes involved in nutrient uptake, and disrupting plasma membrane permeability (Roy et al., 2017; Mir et al., 2021).

1.3 Copper in soil

Studies have shown that Cu concentrations in natural soils range from 3 to 100 mg/kg, with higher concentrations (>100 mg/kg) found in certain locations (Marschner, 1995; Rehman et al., 2019). In agricultural soils, typical Cu levels suitable for plant growth range from 5 to 30 mg/kg, depending on soil type. However, vineyard soils can have Cu concentrations between 200 and 500 mg/kg due to the long-term use of copper-based agrochemicals (Brun et al., 1998). While Cu levels above 30 mg/kg can induce toxicity in plants, the amount depends on multiple factors, including plant species, growth stage, cultivation practices, and environmental conditions (Lamichhane et al., 2018). Particularly in acidic soils, Cu concentrations above 20 mg/kg may be toxic to sensitive plants (Rehman et al., 2019). Furthermore, the World Health Organization

(WHO) has set permissible limits for Cu in soil and plants at 36 mg/kg and 10 mg/kg, respectively (Alengebawy et al., 2021).

Although soil Cu concentrations vary, only about 20% of the Cu, primarily in the form of hydroxides and carbonates, is bioavailable to plants. The remaining 80%, in forms such as oxides and sulfides, is difficult for plants to utilize (Fernández-Calviño et al., 2008; Mihaljevič et al., 2019). Therefore, assessing Cu toxicity in soils based solely on total Cu content is insufficient. Instead, toxicity is primarily determined by the bioavailable fraction, which is the plant-usable form of Cu (La Torre et al., 2018). The bioavailability of Cu depends on various factors, including soil properties that influence Cu mobility and its availability in the soil's solid/solution phase (Violante et al., 2010). Key factors influencing Cu bioavailability include total Cu concentration, cation exchange capacity (CEC), soil organic matter (SOM), and soil pH (Chaignon et al., 2009). Among these factors, soil pH has the most significant impact on Cu mobility and plant uptake. Cu availability to plants increases as pH decreases, and Cu^{2+} activity and soluble Cu concentrations decrease with rising pH (Tye et al., 2004; Morel et al., 2014; Qu et al., 2018). In acidic Cu-contaminated soils, rhizosphere pH, influenced by root and microbial activity, can play a larger role in Cu bioavailability than bulk soil pH (Chaignon et al., 2009; Hinsinger et al., 2009; Bravin et al., 2012).

Cu concentrations in soils have risen dramatically due to human activities, particularly industrial and agricultural practices, and Cu is now considered a significant soil contaminant in many regions (Apori et al., 2018). The extensive use of copper-containing fertilizers, fungicides, herbicides, and pesticides has contributed to Cu accumulation in agricultural soils (Adrees et al., 2015; Brunetto et al., 2016; Rehman et al., 2019). Several studies have reported increased Cu levels in soils under the long-term cultivation of crops such as grapes, citrus, and other fruits (Brunetto et al., 2016; Ballabio et al., 2018). Since Cu cannot be easily degraded biologically or chemically, and only minimal amounts are removed through leaching, runoff, or plant uptake, it can persist as a soil contaminant, causing bioaccumulation and toxicity. This long-term

persistence poses risks to the environment, food security, and human health (Mackie et al., 2012; Lamichhane et al., 2018).

1.4 Uptake and translocation mechanisms of copper in plants

The mechanisms of Cu uptake and transport in plant roots remain poorly understood, particularly regarding long-distance transport and processes at the root level. However, the identification of several different metal transporters has greatly expanded knowledge of Cu uptake and transport mechanisms (Yruela, 2009; Shabbir et al., 2020; Mir et al., 2021). Based on previous studies, the mechanisms of Cu uptake and transport in plants have been described (**Figure 1. 2**) (Robbins et al., 2014; Printz et al., 2016; Ishka et al., 2022).

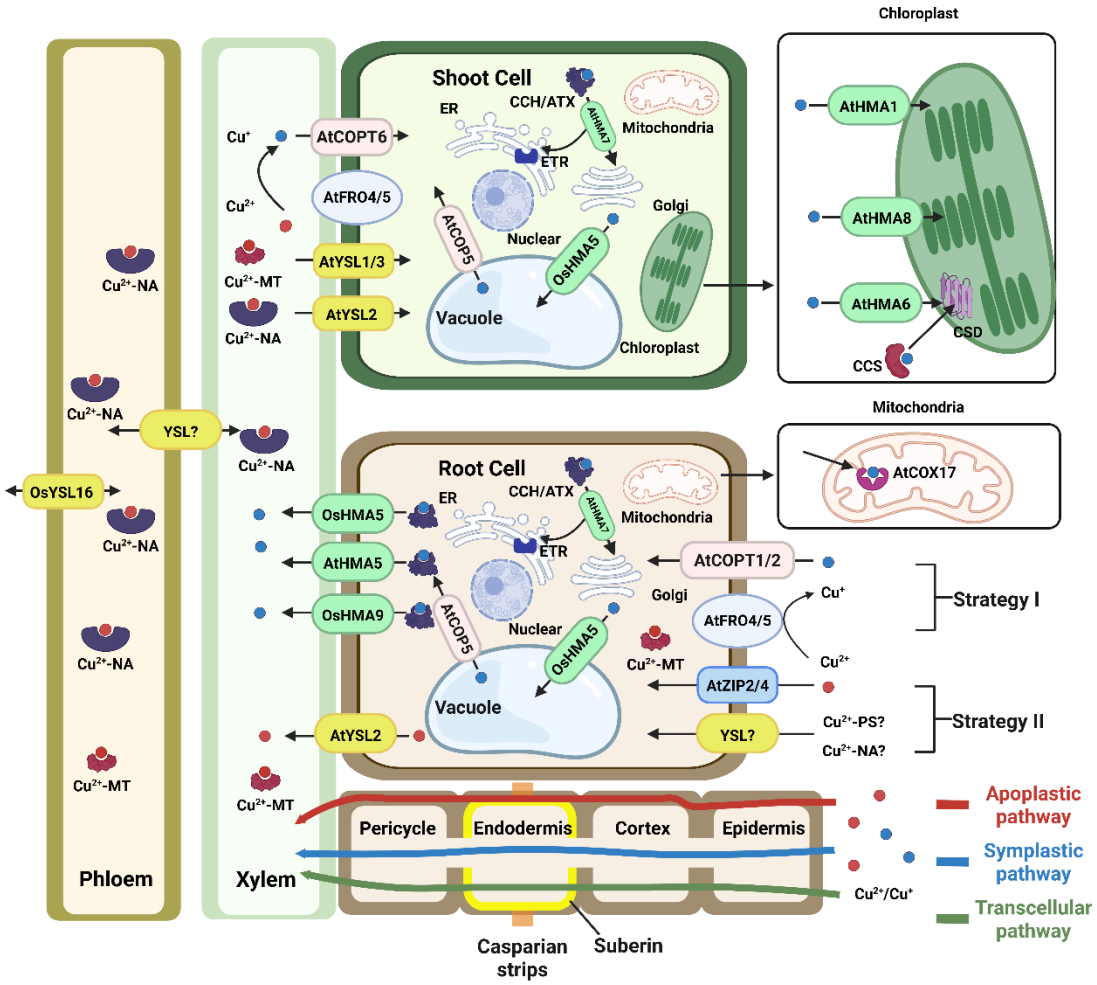

Figure 1. 2 Overview of Cu transport in plants based on studies in *Arabidopsis thaliana* and *Oryza sativa*. Note: FRO, ferric reductase oxidase; COPT, copper transporter; ZIP, Zrt-/Irt-like

protein; YSL, yellow-stripe-like protein; PS, phytosiderophore; NA, nicotianamine; MT, metallothionein; HMA, heavy metal ATPase; CCH/ATX-like, antioxidant protein-like Cu chaperone; CSD, Cu/Zn superoxide dismutase; CCS, Cu chaperone for Cu/Zn superoxide dismutase; COX, cytochrome c oxidase; ER, endoplasmic reticulum; ETR, ethylene receptor. Modified from (Ishka et al., 2022).

1.4.1 Copper uptake by root cells

Cu exists in soils mainly in two forms, Cu^{2+} and Cu^{+}, with Cu^{2+} complexes being dominant (Rehman et al., 2019). Notably, the bioavailability of Cu^{2+} is extremely limited in soils with high organic matter content (Sierra Aragón et al., 2019). As a result, it is hypothesized that grasses and non-grass plants may adopt two Cu uptake strategies: the reduction-based strategy (Strategy I) and the chelation-based strategy (Strategy II), similar to their iron uptake mechanisms (**Figure 1. 2**) (Kobayashi and Nishizawa, 2012). Non-grass monocots and dicots utilize this reduction-based strategy (Strategy I), where Cu^{2+} is reduced to Cu^{+} by membrane-bound ferric reductases of the ferric reductase oxidase (FRO) family (Burkhead et al., 2009). Subsequently, the reduced Cu^{+} is then transported into root cells by specific Cu transporters. *AtFRO4* and *AtFRO5* have been implicated in the reduction of Cu^{2+} to Cu^{+} (Bernal et al., 2012). However, no evidence has been found for FRO-like genes reducing Cu^{2+} in grasses, and oats, as a grass species, show no preference for Cu^{+} uptake (Ryan et al., 2013). Thus, grasses may instead use a chelation-based strategy (Strategy II) to absorb Cu^{2+}. This approach likely involves the secretion of phytosiderophores (PS) or other chelators that solubilize Cu^{2+} in the rhizosphere, facilitating root uptake (Ishka et al., 2022). It remains unclear whether grasses rely on reduction, chelation, or both strategies to uptake Cu. Cu uptake in plants is regulated by several Cu transporters, most notably the copper transporter (COPT) protein family, which specifically transports Cu^{+} (Sanz et al., 2019). Among these, *AtCOPT1* and *AtCOPT2* are considered key transporters for root Cu uptake (Sancenón et al., 2004; Peñarrubia et al., 2010; Puig, 2014). In addition to the COPT family, members of the Zrt-/Irt-like protein (ZIP) family, such as *AtZIP2* and *AtZIP4*, are

thought to mediate the uptake of Cu^{2+} into root cells (Wintz et al., 2003). Moreover, yellow stripe-like (YSL) transporters, part of the oligopeptide transporter (OPT) superfamily (Curie et al., 2001), are involved in transporting metal ions complexed with PS or nicotianamine (NA) (Colangelo and Guerinot, 2006; Curie et al., 2009). Recent research suggests that *ZmYSL1* can transport Cu^{2+} in heterologous systems (Sheng et al., 2021). This finding indicates that some YSL transporters may also mediate Cu entry into root cells.

1.4.2 Copper transport in cellular

The intracellular transport is mediated by Cu transporter families and Cu chaperones, which are involved in maintaining Cu intracellular homeostasis. Cu transporter genes include the COPT, ZIP, YSL, and HMA (heavy metal ATPase) family genes (Wang et al., 2021). Cu chaperones fall into three main types: CCH/ATX-like (antioxidant protein-like Cu chaperone), CCS (Cu chaperone for Cu/Zn SOD), and COX (cytochrome c oxidase) (Markossian and Kurganov, 2003). Generally, once Cu ions enter root cells, they bind to metallothioneins (MTs) or specific soluble Cu chaperones in the cytoplasm and are transported to various organelles (e.g., vacuoles, chloroplasts, mitochondria) to prevent cytoplasmic Cu overload (**Figure 1. 2**) (Migocka and Malas, 2018). For instance, Cu ions chelated by ATX1 are transported by the vacuolar membrane transporter protein HMA5 to the vacuole for storage, thereby reducing Cu toxicity (Andrés-Colás et al., 2006; Del Pozo et al., 2010). Similarly, HMA5 and COPT5 are thought to control the movement of Cu ions into and out of the vacuole to regulate Cu ion levels, thereby maintaining intracellular Cu homeostasis (Garcia-Molina et al., 2011; Wang et al., 2024). Cu chaperone CCH, highly homologous to ATX1, binds Cu^{+} and interacts directly with HMA7 (RAN1) to transport Cu to the endoplasmic reticulum (ER), where it plays a crucial role in synthesizing the ethylene receptor (ETR) (Hoppen et al., 2019). The mechanism of Cu transport into mitochondria is less well understood. However, some studies have shown that COX17 likely mediates Cu transport to mitochondria, where it assists in the assembly of

functional cytochrome c oxidase complexes (Garcia et al., 2016). Cu transport to chloroplasts is thought to be facilitated by the transporters *AtHMA1*, *AtHMA6*, and *AtHMA8*, which deliver Cu to chloroplasts for use as a cofactor in Cu/Zn SOD (Catty et al., 2011; Blaby-Haas et al., 2014; Boutigny et al., 2014). Additionally, the Cu chaperone CCS is believed to assist in delivering Cu to Cu/Zn SOD within chloroplasts (Abdel-Ghany et al., 2005).

1.4.3 Long-distance transport of copper in plants

After being absorbed by the roots, Cu is transported to the aerial parts through the xylem (Cao et al., 2020). Therefore, root-to-shoot Cu transport depends on xylem loading (Printz et al., 2016). In roots, water and solutes move to the xylem through three primary radial pathways: the apoplastic pathway—water and solutes move through cell walls and intercellular spaces in the root cortex toward the pericycle; the symplastic pathway—water and solutes move from one cell to another via plasmodesmata, providing a cytoplasmic connection; and the transcellular pathway—water and solutes move across cell membranes through diffusion gradients and transporter proteins (Robbins et al., 2014; Kreszies et al., 2018). Therefore, similar to other solutes, Cu may also be transported radially into the xylem via these three pathways in roots (**Figure 1. 2**). Although the Cu xylem loading mechanism has not yet been sufficiently investigated, several Cu transporters and Cu chaperones have been reported to be involved. For instance, *OsATX1* transfers Cu^{+} to *OsHMA5*, which loads Cu^{+} into the xylem, thereby transporting Cu from roots to shoots (Deng et al., 2013; Zhang et al., 2018b). Similarly, the *AtHMA5* mutant accumulates more Cu in roots, suggesting a role in Cu xylem loading (Andrés-Colás et al., 2006). Additionally, *OsHMA9* is primarily expressed in vascular tissues and is thought to promote Cu^{+} entry into the xylem (Lee et al., 2007). Although the exact mechanism of root-to-shoot Cu transport in plants remains to be clarified, several Cu transporters and metal chelates, such as MT and NA, are believed to be involved (Xu et al., 2024). Studies have shown that Cu^{2+} can be chelated by NA and transferred from the root to the shoots via *AtYSL2*, or Cu^{2+} can be

reduced to Cu^{+} via *AtFRO4/5* and imported into shoot cells via *AtCOPT6* (DiDonato et al., 2004; Chen et al., 2022a). Whereas *AtYSL1/3* are likely involved in the transport of Cu^{2+}-MT complexes into shoot cells (Wintz et al., 2003; Chu et al., 2010; Printz et al., 2016). In addition, the study found that *OsYSL16* in rice is not only involved in the transport of iron from roots to aerial parts but is also responsible for transporting Cu^{2+}-NA complexes in nutritional organs to new tissues and seeds through the phloem (Zhang et al., 2018a).

1.5 Copper resistance mechanism of plants

Over time, plants have evolved two primary resistance mechanisms to cope with Cu ion toxicity (**Figure 1. 1**). The first is the avoidance mechanism, which aims to prevent the accumulation of toxic Cu concentrations in sensitive plant parts or cells. Strategies for this include reducing Cu absorption, sequestering Cu ions into vacuoles and cell walls, and expelling excess Cu through efflux systems (Adrees et al., 2015). The second is the tolerance mechanism, where plants mitigate Cu toxicity within the body by utilizing chelation, antioxidant systems, and detoxification proteins to detoxify and manage Cu ions (Wang et al., 2025).

1.5.1 Avoidance mechanism

1.5.1.1 Reduce copper uptake

The main mechanism for reducing the toxicity of excess Cu is to reduce or prevent uptake from the soil (Mir et al., 2021). This mechanism is mainly achieved through the regulation of Cu transporters, rhizosphere microbes, or root exudates. Cu transporters and chaperones are essential for ensuring sufficient Cu is available for cellular functions while also preventing toxic accumulation (Gaetke et al., 2014). For example, excessive Cu levels down-regulated the expression of transporters *AtCOPT1* and *AtCOPT2* (Perea-García et al., 2020). Similarly, ZIP transporter genes *AtZIP2* and *AtZIP4* are downregulated in the presence of excess Cu (Milner et al., 2013). Except for the downregulation of Cu transporter expression, certain rhizobacteria are also thought to

be able to protect plants from the toxic effects of Cu by reducing Cu uptake (He et al., 2010). Studies have shown that rhizobacterial *Enterobacter* sp. P36 was able to reduce the Cu accumulation in plant parts, thereby alleviating Cu toxicity to the mung bean plants (Sharaff et al., 2017). Additionally, root exudates were able to inhibit Cu uptake by changing the bioavailability of Cu in the soil (Vives-Peris et al., 2020). Citrate released by roots inhibits Cu absorption by forming extracellular complexes with Cu ions (Adeleke et al., 2017). Similar observations have also been reported in various plants under Cu stress, including the release of organic acids such as citrate and malate outside the root surface (Osmolovskaya et al., 2018).

1.5.1.2 Chelation and sequestration into the vacuole and cell wall

Plants alleviate Cu toxicity by sequestering absorbed Cu into metabolically inactive tissues or organelles, such as vacuoles and cell walls (Printz et al., 2016; Xu et al., 2024). This sequestration is crucial for managing Cu toxicity. For instance, in cucumbers, melatonin enhances the sequestration of Cu ions in vacuoles and cell walls to mitigate Cu toxicity (Cao et al., 2019). Similarly, vacuole sequestration is thought to contribute to soybean acclimation to excess Cu (Bernal et al., 2006). Furthermore, the plant cell wall mitigates Cu toxicity by adsorbing and immobilizing Cu^{2+} through carboxyl and hydroxyl groups, forming a physicochemical barrier that restricts their entry into the cytoplasm (Xu et al., 2024). Changes in cell wall composition are also involved in Cu tolerance, as seen in wheat sprouts, where Cu stress induces the production of cell wall proteins (Al-Hakimi and Hamada, 2011).

1.5.1.3 Cu efflux

Cu efflux may be one of the effective mechanisms to reduce intracellular Cu toxicity. Studies on Cu-sensitive, moderately Cu-tolerant, and highly Cu-tolerant populations of *Silene vulgaris* suggest that Cu efflux across the root plasma membrane mediated by $H+/Cu^{2+}$ antiporters plays a role in the Cu tolerance mechanism of *Silene vulgaris* (Van Hoof et al., 2001). Similarly, HMA5 is a copper ATPase that is thought to play a role

in Cu compartmentalization and detoxification in roots by transferring Cu from the symplast to the apoplast (Andrés-Colás et al., 2006; Del Pozo et al., 2010).

1.5.2 Tolerance mechanism

1.5.2.1 Intracellular detoxification

Plants detoxify Cu by chelating Cu ions once they enter cells. Chelators help buffer cytosolic metal concentrations and are central to Cu detoxification. In plants, metal chelators include phytochelatins (PCs), MTs, organic acids, and amino acids (Emamverdian et al., 2015). PCs are peptides synthesized from glutathione that can chelate Cu ions to form non-toxic complexes (Sharma et al., 2016). Excess Cu induces the synthesis of PCs, suggesting a role in detoxification (Navarrete et al., 2019). However, in some species, excess Cu does not always induce PC synthesis (Roncarati et al., 2015), indicating that PCs may not be the sole Cu detoxification mechanism. MTs are cysteine-rich proteins that also play a role in detoxifying Cu due to their high copper-binding capacity (Calvo et al., 2017). Excess Cu induces MT gene expression, aiding plants in managing rapid changes in Cu levels (Duan et al., 2019; Navarrete et al., 2019). However, this induction may be species-specific (Buapet et al., 2019). Other Cu chelators, such as citrate, malate, proline, and histidine, are also synthesized in response to high Cu levels (Sharma and Dietz, 2006; Dresler et al., 2014). Proline is particularly important, as it chelates Cu and acts as a hydroxyl radical scavenger, protecting plants from heavy metal damage (Anwar Hossain et al., 2014). Furthermore, some studies indicated that heat shock proteins (HSPs) and heavy-metal-associated isoprenylated plant proteins (HIPPs) that served as detoxification proteins also play an important role in Cu tolerance (Cui et al., 2019; Khan et al., 2019).

1.5.2.2 Antioxidants

Plants respond to Cu-induced oxidative stress by activating both enzymatic and non-enzymatic antioxidant systems (Khatun et al., 2008). Enzymatic defenses include superoxide dismutase (SOD), peroxidase (POD), catalase (CAT), ascorbate peroxidase

(APX), and glutathione reductase (GR), while non-enzymatic defenses involve substances like glutathione (GSH) and ascorbic acid (ASA) (Buapet et al., 2019). Under Cu stress, antioxidant enzyme activity increases, helping to mitigate the damaging effects of reactive oxygen species (ROS) (Gong et al., 2019). Numerous studies have shown that high Cu concentrations stimulate the production of enzymes like SOD, POD, CAT, APX, and GR, which scavenge ROS and prevent oxidative damage (Lai and Luo, 2019). GSH and ASA are critical non-enzymatic antioxidants that work through the GSH-ASA cycle to neutralize ROS. Cu stress enhances GSH and ASA accumulation, increasing plant tolerance to Cu toxicity (Mostofa et al., 2014). GSH is thought likely to play a dual role in Cu tolerance, functioning both as an antioxidant and as a precursor for phytochelatins, which chelate Cu ions (Shabbir et al., 2020).

1.6 Suberin, a multifunctional and plastic endodermis barrier

Plants have evolved specialized lipid- and phenolic-based barriers to protect against diverse environmental stresses (Peralta Ogorek et al., 2023). Among these protective structures, the apoplastic barrier in the root endodermis, composed primarily of Casparian strips and suberin, plays an essential role in stress tolerance by regulating water and solute transport (Shukla and Barberon, 2021). Suberin, along with lignin, has been recognized mainly as an apoplastic barrier that restricts uncontrolled apoplastic transport (Wang et al., 2019). However, recent advances using suberin-defective mutants have revealed a more specific role. Specifically, suberin deposition in the endodermis also acts as a bidirectional barrier in the transcellular pathway, selectively controlling nutrient uptake into vascular tissues and preventing nutrient leakage from the stele (Doblas et al., 2017). For example, in the Arabidopsis mutant *cyp86a1*/*horst*, reduced aliphatic suberin content weakens the apoplastic barrier, thereby increasing the radial transport of water and sodium chloride (Ranathunge and Schreiber, 2011). Conversely, increased suberin accumulation in the esb1 mutant leads to decreased shoot uptake of essential minerals such as calcium (Ca), manganese (Mn), and zinc (Zn) (Baxter et al., 2009). Other studies suggest suberin regulates calcium uptake and

prevents potassium leakage from the vascular system (Moore et al., 2002; Persson et al., 2016). Together, these findings highlight suberin as a multifunctional barrier important for regulating water and solute transport by the apoplastic pathway and the transcellular pathway.

During root development, suberin deposition follows a specific pattern with three distinct root zones: a non-suberized zone (no suberin deposition), a patchy suberized zone (some and random suberized endodermis cells), and a continuously suberized zone (full suberized in all endodermal cells except passage cells) (Barberon, 2017). This deposition pattern is thought to be regulated by developmental cues and environmental stresses (Shukla et al., 2021). Studies show that various abiotic stresses, such as salt stress and osmotic stress, can trigger suberization in the endodermis (Kreszies et al., 2019; Grünhofer et al., 2022). Similarly, suberization in response to toxic environments appears to be a common plant defense mechanism, suggesting that suberization helps block the entry of harmful elements (Degenhardt, 2000; Vaculík et al., 2012). Furthermore, this plasticity of endodermal suberin is thought also to be influenced by nutrient stress. For example, excess boron induced suberization in soybean roots (Ghanati et al., 2005). Similarly, early and enhanced suberization is induced by nitrogen deficiency in barley roots (Melino et al., 2021). Additionally, calcium-related increases in suberization were observed in *Sedum alfredii* roots (Liu et al., 2020). Collectively, these studies demonstrate that suberin deposition exhibits considerable plasticity, enabling plants to adapt to environmental stresses dynamically. Moreover, studies suggest that this suberization plasticity is believed to be regulated by the hormones abscisic acid (ABA) and ethylene (Barberon et al., 2016).

1.7 Suberin biosynthesis

Suberin is a complex polyester composed of aliphatic and aromatic compounds, typically deposited as a thin layer on the inner surfaces of endodermal and exodermal cell walls, acting as an apoplastic barrier (Ranathunge et al., 2011). Common aliphatic

components include primary alcohols, fatty acids, α-ω dicarboxylic acids (diacids), and ω-hydroxy acids (ω-OH acids), while ferulic acid, caffeic acid, and coumaric acid are the major aromatic compounds (Franke et al., 2005). Although the full mechanism of suberin synthesis remains unclear, the discovery of several genes involved in the production of suberin components, such as primary alcohols, fatty acids, diacids, and ω-OH acids, through mutant studies has significantly expanded the understanding of this process (**Figure 1. 3**) (Vishwanath et al., 2015; Nomberg et al., 2022).

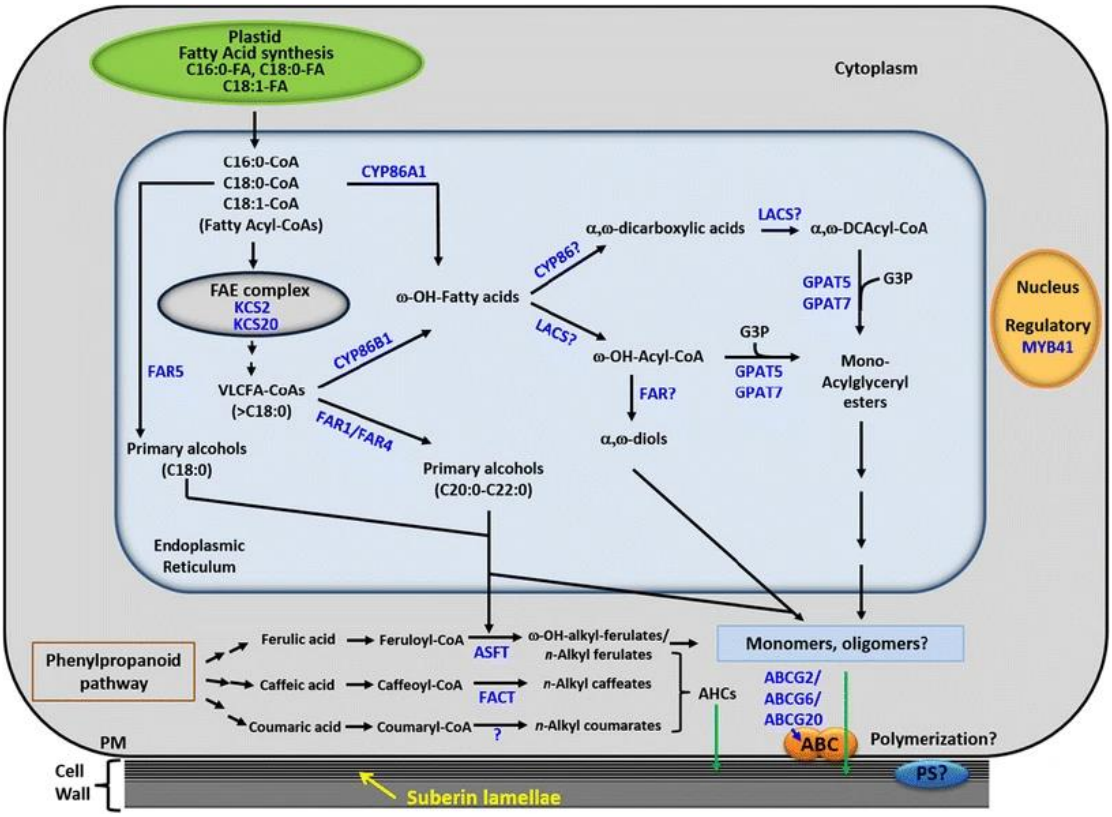

Figure 1. 3 Schematic representation of the biosynthetic pathway of suberin in plants. Cited from (Vishwanath et al., 2015).

Suberin synthesis begins with the formation of C16:0-CoA, C18:0-CoA, and C18:1-CoA in plastids, which are then transported to the endoplasmic reticulum by long-chain acyl-CoA synthetase (LACS). These substrates are elongated to form very long-chain fatty acyl-CoA by the fatty acid elongation (FAE) complex, composed of four enzymes

(Samuels et al., 2008). The rate-limiting enzyme in this complex, β-ketoacyl-CoA synthase (encoded by *KCS2* and *KCS20*), is responsible for synthesizing C22 and C24 fatty acids found in suberin monomers (Lee et al., 2009). Recent studies have also identified *KCS17* as an enzyme that catalyzes the elongation of C22-C24 very long chain fatty acids (VLCFAs), required for seed coat suberin synthesis (Kim et al., 2024). Primary alcohols, another key suberin component, are derived from fatty acids through the activity of fatty acyl reductase (FAR) (Franke et al., 2005). Saturated primary fatty alcohols with chain lengths of C18, C20, and C22 are common in suberin, comprising about 6% of its aliphatic content (Schreiber et al., 2005). The ω-hydroxy acids in suberin are formed by the hydroxylation of terminal methyl groups of fatty acids, catalyzed by cytochrome P450 monooxygenases from the CYP86 subfamily (Molina, 2010). Some ω-hydroxy acids are further oxidized to α-ω dicarboxylic acids by ω-hydroxy fatty acid dehydrogenases. Specifically, *CYP86A1* synthesizes C12-C18 ω-hydroxy acids (Höfer et al., 2008), while *CYP86B1* produces C22-C24 ω-hydroxy acids (Compagnon et al., 2009). Glycerol serves as the backbone for suberin polyesters. *GPAT5*, the first gene identified as essential for suberin synthesis, is thought to facilitate the esterification of glycerol with ω-hydroxy acyl-CoA and α-ω dicarboxylic acids, forming monoacyl glycerides (Li et al., 2007). The aromatic components of suberin, mainly ferulic acid, caffeic acid, and coumaric acid, are derived from precursors in the phenylpropanoid pathway. Arabidopsis *ASFT*/*HHT* catalyzes the transfer of feruloyl-CoA to ω-hydroxy fatty acids and fatty alcohols (Gou et al., 2009), while caffeoyl-CoA acyltransferase (FACT) catalyzes the synthesis of alkyl hydroxycinnamate waxes (Kosma et al., 2012). Suberin monomers are synthesized in the endoplasmic reticulum and transported to the apoplast via vesicles mediated by the Golgi apparatus. Their transport across the plasma membrane into the cell wall is facilitated by ATP-binding cassette (ABC) transporters and possibly lipid transfer proteins (LTPs). In Arabidopsis, *ABCG2*, *ABCG6*, and *ABCG20* have been implicated in suberin metabolism in roots and seed coats (Yadav et al., 2014). Additionally, *AtLTPI4* and *AtLTPG15* are believed

to be involved in suberin monomer transport (Deeken et al., 2016; Lee and Suh, 2018). After transport to the apoplast, suberin monomers will be polymerized into polyesters and deposited in the cell wall. GDSL-type esterase/lipase proteins (GELPs) are thought to be involved in suberin polymerization in Arabidopsis roots (Shukla and Barberon, 2021). The expression of five genes, *GELP22*, *GELP38*, *GELP49*, *GELP51*, and *GELP96*, has been closely associated with endodermal suberization (Ursache et al., 2021).

1.8 Objectives

Cu contamination, primarily resulting from anthropogenic activities, is a critical environmental stress that adversely affects plant growth and development. Barley (*Hordeum vulgare* L.), a globally important cereal crop, is recognized for its relative tolerance to heavy metals, including Cu, Zn, and Cd. Suberin deposition in root endodermis is considered an essential protective mechanism against environmental stress. However, the mechanisms underlying barley's tolerance to Cu stress, particularly the specific role of suberin deposition, remain unclear. Therefore, this study aims to investigate the mechanisms of Cu toxicity in barley, with a particular focus on the impact of Cu stress on suberin biosynthesis and its role in mitigating Cu toxicity. To achieve this, the morphological, physiological, biochemical, and molecular responses of barley (cv. Scarlett) seedlings subjected to 50 μM and 100 μM Cu treatments for six days were investigated. Moreover, to elucidate suberin's protective function under Cu stress, the Cu toxicity effect and suberin biosynthesis in wild-type and suberin-defective mutant (*cyp86b1-1* and *cyp86b1-2*) barley (cv. Golden Promise Fast) seedlings under 50 μM Cu treatment for 6 days were also evaluated. The findings of this study will contribute to a deeper understanding of the interplay between Cu stress and suberin biosynthesis, providing insights into potential mechanisms of Cu tolerance in barley.

2. Materials and Methods

2.1 Plant material and treatments

Barley (*Hordeum vulgare* L.) seeds from the two cultivars, Scarlett and Golden Promise Fast, were stratified at 4 °C for 2-3 days and then germinated on wet filter paper for 3 days in darkness. The 3-day-old seedlings were transferred to an aerated hydroponic system containing half-strength Hoagland solution (Hoagland and Arnon, 1950) and placed in a climate-controlled chamber under long-day conditions (16 h light/8 h dark) with day/night temperatures of 23 °C/20 °C. After 3 days of hydroponic growth, the 6-day-old seedlings were subjected to 6 days of stress treatment. At this stage, each barley seedling had two leaves and five to six seminal roots. Six-day-old seedlings were subjected to Cu stress by transferring them to Cu treatment solutions for 6 days. The treatments included (i) control (no excess Cu), (ii) 50 µM Cu ($CuSO_4 \cdot 5H_2O$), and (iii) 100 µM Cu ($CuSO_4 \cdot 5H_2O$). The pH of all solutions was adjusted to 5.8 using HCl to prevent Cu precipitation (**Figure 2. 1A**). After 12 days of growth, seedlings were harvested, and root and shoot lengths were recorded. "Shoot" refers to all aboveground plant material, including leaves (**Figure 2. 1B**). Seminal roots were segmented into three distinct zones based on suberin deposition, following the method described by Kreszies et al. (2019) (**Figure 2. 1C**). The segmented roots were then used for histochemical analysis, chemical analysis, and real-time quantitative PCR (RT-qPCR) analysis.

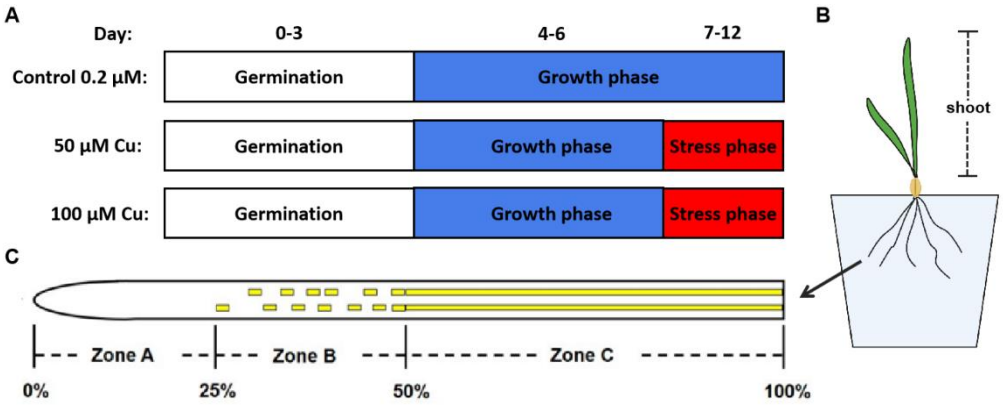

Figure 2. 1 Experimental overview of Cu stress. (A) Schematic diagram of growth conditions. (B) Schematic diagram of barley grown in hydroponic pots. (C) Schematic diagram showing the different root zones that were harvested. The seminal roots of barley grown in nutrient solution at pH 5.8 were divided into three zones based on the development of suberin lamellae. Modified from (Hongjun Meng, 2023).

2.2 Physiological parameters

After six days of Cu treatment, chlorophyll fluorescence parameters were measured in fully expanded mature leaves from 9 plants per treatment using a Junior-PAM modulation fluorometer (Walz® GmbH, Effeltrich, Germany). Dark-adapted leaves were subjected to induction curves to obtain the following chlorophyll fluorescence parameters: maximum quantum yield of PSII (Fv/Fm), effective photochemical quantum yield of PSII (ΔF/Fm'), photochemical quenching coefficient (qP and qL), and non-photochemical quenching coefficients (qN and NPQ). After conducting the induction curve, the light response curves were conducted to obtain the following chlorophyll fluorescence parameters: the maximum electron transport rate (ETRmax), indicative of overall photosynthetic capacity; the initial slope of the electron transport rate curve (α_ETR), indicative of photosynthetic light-use efficiency; and the saturating irradiance level for electron transport (Ek), representing the plant's ability to utilize light energy.

2.3 Histochemical detection of $O_2^{\bullet-}$ and H_2O_2 in roots

In situ detection of H_2O_2 and $O_2^{\bullet-}$ in barley leaves and roots was performed using 3,3′-diaminobenzidine (DAB) and nitro blue tetrazolium chloride (NBT) staining, following modified methods from Jambunathan (2010) and Kumar et al. (2014). For H_2O_2 detection, tissues were incubated in 1 mg/mL DAB solution (pH 3.8) for 5-6 hours until brown precipitates formed. Chlorophyll was removed by repeated ethanol washes at 60°C until tissues became clear. Stained tissues were fixed in a 3:1:1 solution of ethanol, lactic acid, and glycerol before imaging. For $O_2^{\bullet-}$ detection, tissues were stained with 0.1% NBT for 15 minutes, and the reaction was terminated by immersion in 95% ethanol. Chlorophyll removal followed the same ethanol-washing procedure. Leaf staining images were captured using a CanoScan LiDE 400 scanner (Canon), while root staining images were acquired with a Nikon DXM1200 digital camera using ACT-1 software. The average staining intensities in barley root tips and leaves were quantified by ImageJ/Fiji software.

2.4 Lipid peroxidation and proline determination

Lipid peroxidation levels were quantified as MDA content. MDA content was determined by the thiobarbituric acid (TBA) method of Liu et al. (2022) with slight modifications. Barley tissue samples (100 mg fresh weight) were homogenized and extracted in 2 ml of 10% trichloroacetic acid (TCA) solution. After centrifugation at 4000 rpm for 10 min, equal volumes of supernatant and 0.6% TBA in 10% TCA solution (freshly prepared) were added into a new tube. The mixture was incubated at 95°C for 30 min, followed by quick cooling on ice, and then centrifuged at 10,000×g for 10 min. The absorbance under 450, 532, and 600 nm was measured. MDA concentration was calculated using the following formula: MDA [nmol/g FW] = [6.45 × (D532 − D600) − 0.56 × D450] × V_T / FW, where V_T represents the volume of extraction solution and FW represents the fresh weight of the sample.

Proline was analyzed in the leaves and roots of the control and the Cu-treated seedlings of the two barley cultivars following the modified method of Bates et al. (1973). Briefly, barley tissue samples (100 mg fresh weight) were homogenized and extracted in 2 ml of 3% sulphosalicylic acid. The extract was centrifuged at 12 000×g for 5 min (4 °C). Then, 1 ml of the extract was mixed with 1 ml of glacial acetic acid and 1 ml of ninhydrin reagent (1.25 g ninhydrin in 20 ml 6 M phosphoric acid and 30 ml glacial acetic acid) and thoroughly mixed. After 1 h of incubation at 100 °C, the tubes were cooled, and the proline-ninhydrin reaction product was extracted with 2 ml toluene. The absorbance of chromatophore-containing toluene was measured at 520 nm. The proline content was calculated by generating the standard curve. The concentration of proline in the samples was expressed in units of μg/g fresh weight (FW).

2.5 Histochemical analysis of suberin lamellae

Histochemical analysis was conducted to detect suberin lamellae along the length of barley roots. Harvested roots were fixed in fixation solution (3.7% formaldehyde in 1× PBS solution) to preserve tissue integrity (**Table 2. 1**). Segments of seminal roots, 1 cm long, were cut into 30 μm thick cross-sections using a cryostat microtome (Microm HM 500 M, Microm International GmbH). Suberin lamellae were stained with 0.01% (w/v) fluorol yellow 088 in ethanol for 1 hour (Brundrett et al., 1991). Cross-sections were examined using epifluorescence microscopy (Zeiss AxioPlan, Carl Zeiss, Germany) with an ultraviolet (UV) filter set. Images were captured with a Canon EOS 600D camera at ISO 400 and 1/4 s exposure.

Table 2. 1 Fixation solution (pH 7.4)

Compound	Concentration
NaCl	137 mM
KCl	2.7 mM
Na_2HPO_4	10 mM
KH_2PO_4	1.8 mM
Formaldehyde	3.7% (v/v)

2.6 Chemical analytics of suberin in roots

The chemical composition of suberin in barley seminal roots was quantified by relating suberin amounts (µg) to endodermal surface area (cm^2). Endodermal areas were calculated using the formula $A=2\pi rL$ (where r is the endodermis radius and L is the root zone length), with the radius measured using ImageJ software. For each treatment, 10 segments per zone were pooled, and three biological replicates were analyzed. The root samples were enzymatically digested and analyzed via gas chromatography.

2.6.1 Sample preparation and suberin extraction

Enzymatic digestion and solvent extraction were performed to obtain cell wall samples for suberin analysis (Zeier and Schreiber, 1997). Roots were treated with an enzyme solution at pH 3 containing 0.5% (w/v) cellulase and pectinase, along with 1 mM sodium azide to inhibit microbial growth (**Table 2. 2**). This process occurred at room temperature on a rotary shaker (100 rpm) for three weeks, with enzyme solution replaced every 2-3 days. After enzyme digestion, the roots were washed with a borax buffer (0.01 M sodium tetraborate, pH 9) for two days to remove phenolic compounds, then treated with a chloroform/methanol mixture (1:1) for a week to extract soluble

lipids, with solution changes every two or three days. The samples were dried on PTFE and stored in a desiccator with silica gel for subsequent suberin analysis.

Table 2. 2 Enzyme solution

Compound	Concentration
Citric acid	10 mM
Adjust pH to 3	
Cellulase	0.5%, w/v
Pectinase	0.5%, w/v
Sodium azide	1 mM

2.6.2 Transesterification and derivatization

Dried root samples (up to 5 mg) were weighed using a precision balance (Sartorius, Germany). For suberin analysis, the samples were subjected to transesterification in 4-9 ml vials with 2 ml BF_3/MeOH for 16 hours at 70 °C in a heating block. This process released suberin monomers, including aromatic compounds and esterified long-chain fatty acids such as ω-hydroxy acids and α-ω dicarboxylic acids, which are typical components of suberin (Zeier and Schreiber, 1997). The reaction involves protonation of esters followed by alcohol substitution. After transesterification, 10 µg of dotriacontane (C32 alkane) was added as an internal standard and vortexed. The reaction was terminated by slowly adding 2 ml of saturated $NaHCO_3/H_2O$ solution to avoid bubble formation. Monomers were extracted by adding 2 ml of chloroform three times, and the lipophilic (chloroform) phase was collected in clean glass vials. The extracts were concentrated under nitrogen at 60 °C to about 250 µl. To prepare the samples for gas chromatography, the monomers were derivatized using N, O-bis(trimethylsilyl)-trifluoroacetamide (BSTFA) to convert hydroxyl and carboxyl

groups into trimethylsilyl derivatives. This derivatization, catalyzed by pyridine, improves the thermal stability and volatility of the compounds for analysis. 20 µl of pyridine and BSTFA were added to the vials, followed by incubation at 70 °C for 40 minutes.

2.6.3 Gas chromatography analysis (GC-MS/FID)

Quantitative analysis of suberin monomers was performed by injecting 1 µl of the derivatized sample into a gas chromatograph equipped with a flame ionization detector (GC-FID; GC 6890N with 7683 Series Injector, Agilent Technologies, USA). For qualitative analysis, 1 µl of the sample was injected into a gas chromatograph coupled with a mass spectrometer (GC-MS; GC 7890B with 5977A Mass Selective Detector, Agilent Technologies, USA). GC-MS, utilizing a quadrupole mass analyzer, identified suberin compounds based on their mass-to-charge ratio. For subsequent peak identification, the same temperature profile was used for GC-FID and GC-MS (**Table 2. 3**). Peak identification was based on a reference database from Prof. Schreiber's lab at the Institute of Cellular and Molecular Botany, University of Bonn, Germany. Data analysis was further supported by Agilent software, including Mass Hunter and Classic ChemStation.

Table 2. 3 Temperature profiles of GC-MS and GC-FID for the analysis of suberin

Final temperature (°C)	Temperature rise (°C/min)	Temperature hold (min)
50		2
150	10	1
310	3	20

2.7 ICP element analysis

Plant samples (shoots and roots) from 12-day-old barley seedlings (control and Cu-treated) were dried at 60 °C and homogenized to a fine powder. 100 mg of powdered tissue was digested in Teflon tubes with 4 ml of concentrated HNO_3 and 2 ml of 30% H_2O_2 using a microwave digestion system (Ethos.lab, MLS GmbH) at 200 °C and 15 bar for 75 min. Digested samples were diluted to 25 ml with double-distilled H_2O. Elemental quantification was performed using inductively coupled plasma mass spectrometry (ICP-MS, iCAP TQe, ThermoScientific) and inductively coupled plasma optical emission spectroscopy (ICP-OES, iCAP Pro XP, ThermoScientific). Calibration utilized a multielement standard solution (Bernd Kraft GmbH), with analytical accuracy verified by including certified reference material in each digestion batch. Due to sample amount constraints, only one biological replicate was analyzed for this analysis.

2.8 RNA sequencing

To assess the gene expression patterns of barley under Cu stress, RNA-seq data were obtained from the NCBI SRA database under BioProject PRJNA382490 (Kintlová et al., 2017). The gene expression matrix of whole barley roots exposed to 50 µM Cu treatment for five days, including raw and averaged FPKM values, was downloaded from the Barley Expression Database (BarleyExpDB: http://barleyexp.com/). Principal component analysis (PCA) of the gene expression profiles was conducted using SIMCA-P software (version 13.0, Umetrics, Umea, Sweden). The RNA-seq data were processed and analyzed in R (v4.4.1) using Bioconductor packages (http://www.bioconductor.org/). Differentially expressed genes (DEGs) were identified across normalized datasets for biological replicates using linear modeling in the limma package (Linear Models for Microarray Data) in R. Cu-treated samples were compared with control samples, and pairwise t-tests were adjusted using the Benjamini-Hochberg procedure to control the false discovery rate (FDR) (Benjamini and Hochberg, 1995).

Genes were considered significantly differentially expressed if they met the following criteria: |log2 fold change (FC)| > 1.5, p-value < 0.05, and FDR ≤ 0.1.

2.9 RNA isolation and RT-qPCR analysis

For RNA isolation, root samples were harvested from three root zones after six days of treatment, as well as from whole roots at various time points (0h, 12h, 24h, 48h, and 72h). Barley seminal roots under different treatments were cut using acetone-treated blades and rinsed with diethylpyrocarbonate (DEPC)-treated water. Each zone was collected into 2 ml RNase-free centrifuge tubes, quickly frozen in liquid nitrogen, and stored at -80 °C until RNA extraction. The root samples were ground in liquid nitrogen using a mortar and pestle. Total RNA was extracted using the Quick-RNA Miniprep Kit (Zymo Research, USA) according to the manufacturer's protocol. RNA quality was assessed using a Nanodrop spectrophotometer (Thermo Fisher Scientific, USA) and agarose gel electrophoresis. RNA samples were diluted to the same concentration before cDNA synthesis. Reverse transcription to synthesize cDNA was performed using the RevertAid First Strand cDNA Synthesis Kit (Thermo Fisher Scientific, USA). The PCR amplifications were performed in a final volume of 20 µl containing 4 µl of 5× EvaGreen-qPCR-Mix-II (Bio-Budget, Krefeld, Germany), 1 µl of primers, 1 µl of DNA template and 14 µl of nuclease-free water using a QuantStudio™ 3 Real-Time PCR (Thermo Fisher Scientific). The qPCR cycling protocol was as follows: pre-denaturation at 95 °C for 15 minutes, 40 cycles of denaturation at 95 °C for 10 seconds, annealing at 60 °C for 10 seconds, and extension at 72 °C for 10 seconds. To ensure data reliability, three biological replicates (independent RNA samples from separate plants) and three technical replicates (qPCR reactions for each sample) were performed. Relative expression levels were normalized to zone A of the control group (set as 1), and data were calculated using the $2^{-\Delta\Delta Ct}$ method. *Actin* served as internal reference genes. Primer sequences for RT-qPCR are provided in **Table S1**.

2.10 Statistical analysis

Statistical analyses of chemical analytics and physiological experiments were performed using SPSS Statistics 22.0 software (IBM China Company Ltd., Beijing, China). The mean comparisons were made, and Fischer's least significant difference (LSD) was used to determine significant differences among groups at a 5% probability level. Bar charts, box plots, and line charts were generated using GraphPad Prism version 9.5.1 (GraphPad Software, San Diego, CA, USA).

3. Results

3.1 Effect of copper stress on root and shoot morphology

To evaluate the effect of Cu stress on barley seedling development, the morphological parameters of roots and shoots were examined in 12-day-old barley seedlings subjected to 50 µM or 100 µM Cu treatments, alongside untreated controls **(Figure 3. 1-Figure 3. 2)**. Under Cu stress conditions, the seminal root length of barley seedlings significantly decreased. (**Figure 3. 1A**). Specifically, compared to the control (23.42 ± 2.7 cm), the root lengths were markedly reduced to 12.95 ± 1.8 cm and 11.97 ± 1.7 cm under 50 µM and 100 µM Cu treatments, respectively. A similar trend was observed for root dry weight, where the control group had an average dry weight of 12.36 ± 2.7 mg, significantly decreasing to 9.14 ± 1.5 mg and 8.39 ± 1.6 mg at 50 µM and 100 µM Cu, respectively (**Figure 3. 1B**).

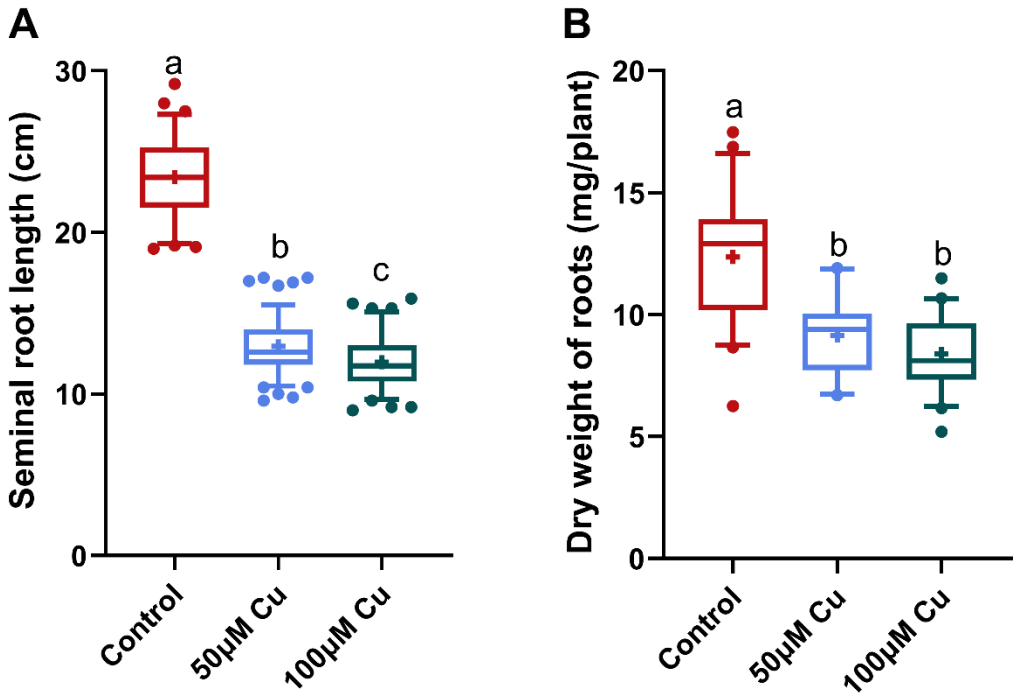

Figure 3. 1 Effect of Cu stress on root length (A) and dry weight (B) in 12-day-old barley plants under control conditions or Cu stress conditions (50 µM or 100 µM Cu). Boxplots represent the 10 to 90 percentiles, with the "+" indicating the mean. The whiskers extend to the

outliers. Data are presented based on at least twenty biological replicates. Different letters indicate significant differences at $p < 0.05$ (One-Way ANOVA, Fisher's LSD).

Similarly, Cu stress also negatively affected shoot development in barley seedlings (**Figure 3. 2**). Compared with the control group (25.78 ± 3.6 cm), shoot lengths were significantly reduced to 18.94 ± 2.4 cm and 18.20 ± 2.2 cm under 50 µM and 100 µM Cu treatments, respectively (**Figure 3. 2A**). Shoot dry weight exhibited a similar decreasing pattern, with the control showing 31.41 ± 5.3 mg, whereas the 50 µM and 100 µM Cu treatments resulted in dry weights of 26.18 ± 4.5 mg and 26.23 ± 6.1 mg, respectively (**Figure 3. 2B**). However, no significant difference in shoot dry weight was observed between the two Cu treatments.

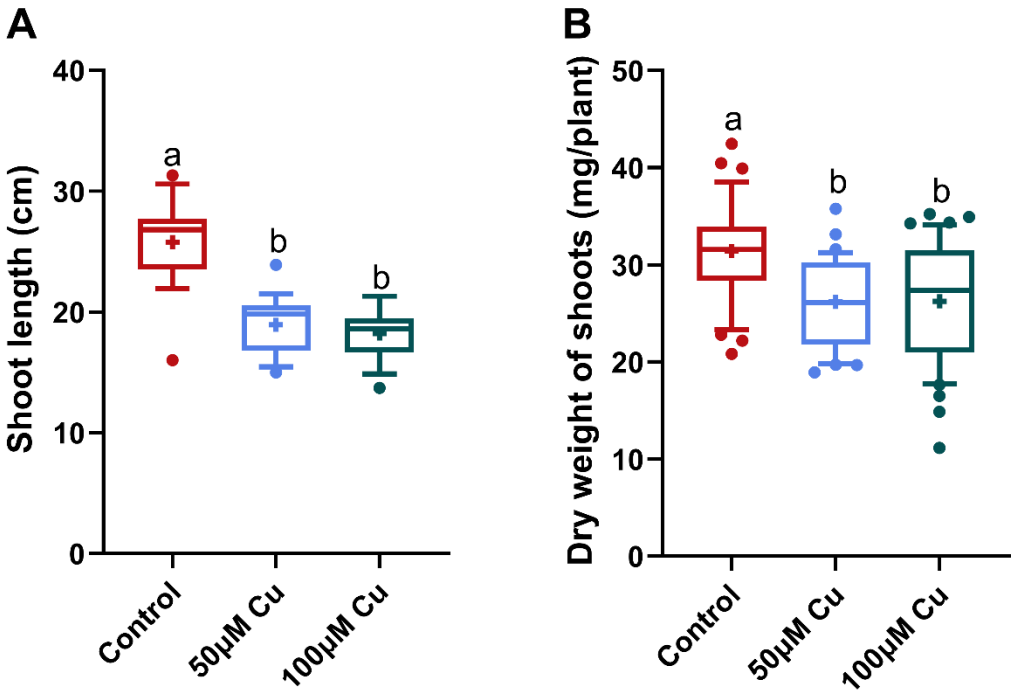

Figure 3. 2 Effect of Cu stress on shoot length (A) and dry weight (B) in 12-d-old barley plants under control conditions or Cu stress conditions (50 µM or 100 µM Cu). Boxplots represent the 10 to 90 percentiles, with the "+" indicating the mean. The whiskers extend to the outliers. Data are presented based on at least twenty biological replicates. Different letters indicate significant differences at $p < 0.05$ (One-Way ANOVA, Fisher's LSD).

Analysis of the variation in root and shoot parameters under Cu stress revealed differential sensitivity between the two plant tissues. Relative to controls, seminal root length reductions under 50 µM and 100 µM Cu treatments were 44.71% and 48.89%, respectively, whereas shoot length reductions were 26.53% and 29.40%, respectively. This difference demonstrates that root growth was more severely inhibited by Cu stress compared to shoot growth. A similar pattern was observed for dry weight, with root dry weight reductions of 26.05% and 32.12% at 50 µM and 100 µM Cu treatments, respectively, compared to smaller shoot dry weight reductions of 16.65% and 16.49%. These findings collectively indicate that barley roots are more sensitive than shoots to Cu toxicity.

3.2 Effect of copper stress on leaf physiological parameters

3.2.1 Leaf pigment content

After six days of Cu exposure, the chlorophyll content, flavonoid index, and anthocyanin index were measured in leaves (**Figure 3. 3**). No significant differences in the levels of chlorophyll, flavonoids, and anthocyanins were observed under either 50 µM or 100 µM Cu treatments compared to the control.

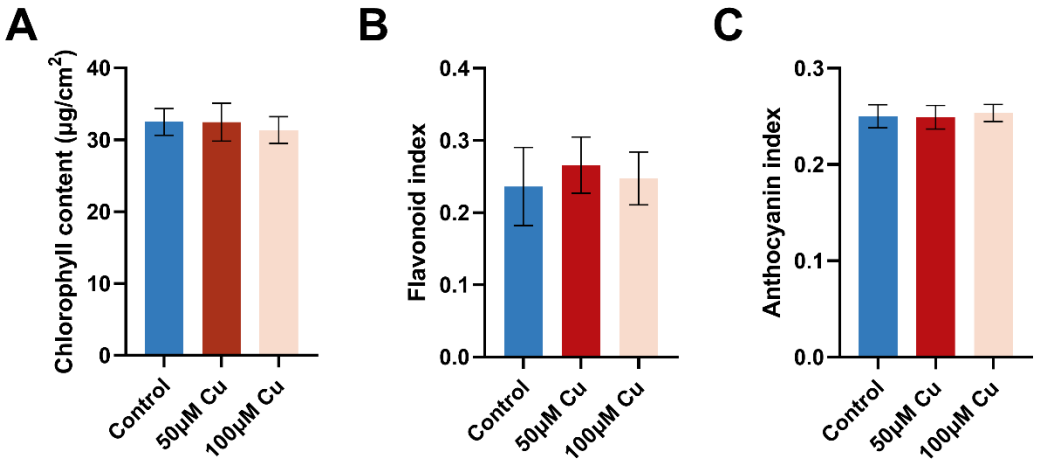

Figure 3. 3 Effect of Cu stress on leaf pigment. Chlorophyll content (A), flavonoid index (B), and anthocyanin index (C) in leaves of barley under control conditions or Cu stress conditions

(50 μM or 100 μM Cu). Data are presented as mean ± SD of nine biological replicates. No significant difference was detected.

3.2.2 Chlorophyll fluorescence parameters

To investigate the impact of Cu stress on barley leaves photosynthetic performance, the basic parameters of Chlorophyll fluorescence in dark-adapted plants were analyzed to assess the PSII photochemical activity (**Figure 3. 4**). Several fluorescence parameters including the maximum quantum yield of PSII (Fv/Fm), the effective quantum yield of PSII (ΔF/Fm'), the photochemical quenching coefficient (qP and qL), the non-photochemical quenching coefficient (qN and NPQ) were measured by the induction curves. Although ΔF/Fm', qP and qL decreased slightly under Cu stress, there were no significant differences in all fluorescence parameters in this study. This result indicated that the Cu treatments applied in this study did not significantly impair PSII activity in barley leaves.

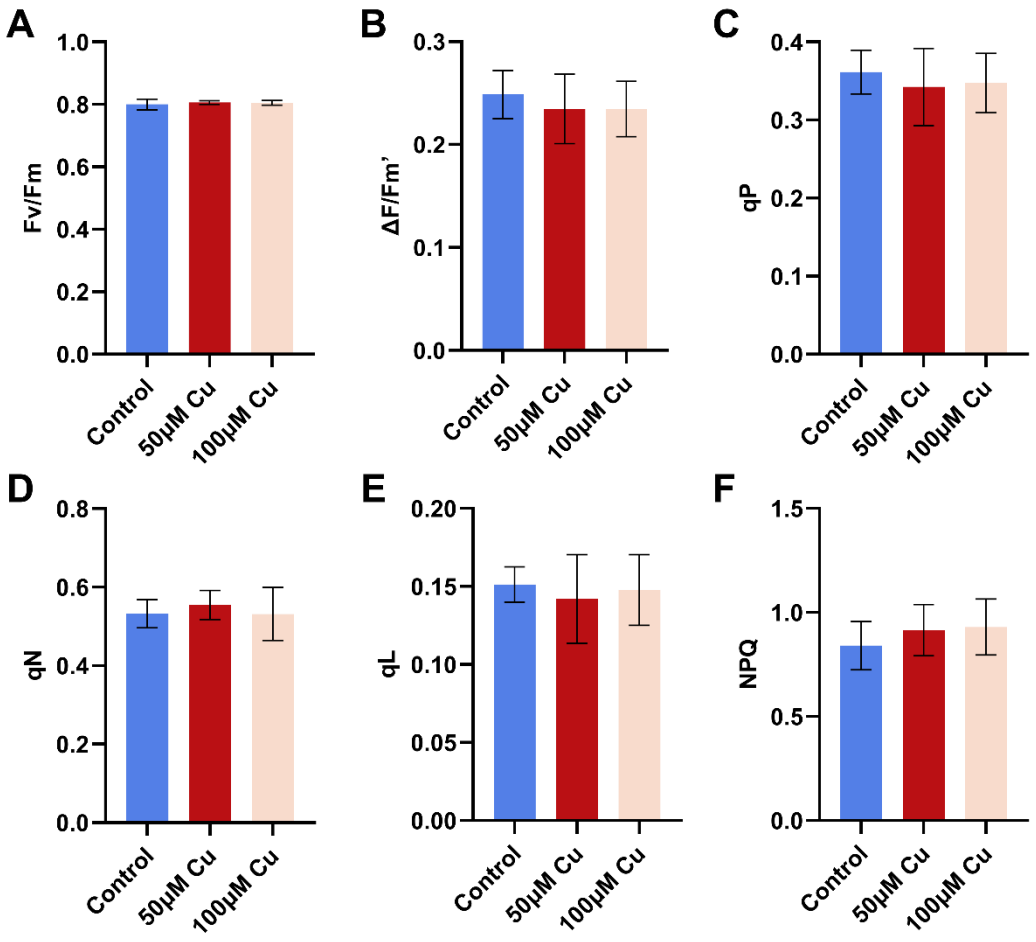

Figure 3. 4 Effect of Cu stress on basic chlorophyll fluorescence parameters. Fv/Fm (A), ΔF/Fm' (B), qP (C), qN (D), qL (E), and NPQ (F) in barley leaves under control conditions or Cu stress conditions (50 μM or 100 μM Cu). Data are presented as mean ± SD of five biological replicates. No significant difference was detected.

To further analyze photosynthetic responses, the maximum electron transport rate (ETRmax), indicative of overall photosynthetic capacity, the initial slope of the electron transport rate curve (α_ETR), indicative of photosynthetic light-use efficiency, and the saturating irradiance level for electron transport (Ek), representing the plant's ability to utilize light energy, were evaluated using rapid light response curves (**Figure 3. 5**). Consistent with the results from the chlorophyll fluorescence induction curves, no significant differences were observed for ETRmax, α_ETR, and Ek between the Cu-treated plants (50 μM and 100 μM Cu) and the control. This result indicated that the Cu

treatments applied in this study did not adversely affect the photosynthetic performance of barley leaves.

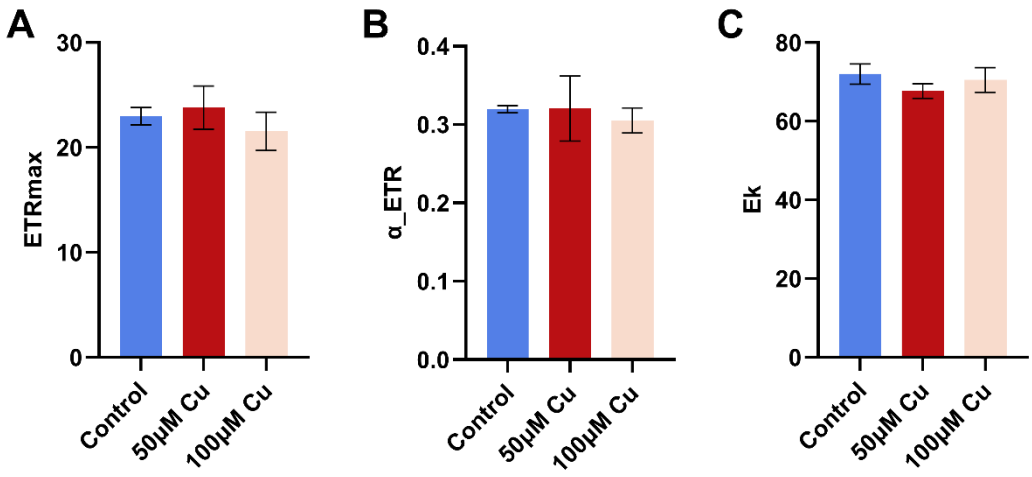

Figure 3. 5 Effect of Cu stress on chlorophyll fluorescence light-response parameters. Maximum electron transport rate (ETRmax) (A), initial slope of the electron transport rate curve (α_ETR) (B), and saturating irradiance level for electron transport (Ek) (C) in barley leaves under control conditions or Cu stress conditions (50 μM or 100 μM Cu). Data are presented as mean ± SD of five biological replicates. No significant difference was detected.

3.3 ROS distribution in apical roots and leaves of barley

To investigate the effect of Cu stress on ROS accumulation, the spatial distribution of $O_2^{\bullet-}$ and H_2O_2 in barley root tips and leaves was analyzed using NBT and DAB staining, respectively (**Figure 3. 6**-**Figure 3. 7**). Under control conditions, $O_2^{\bullet-}$ was broadly distributed throughout the whole root tip but mainly localized in the meristematic zone, gradually decreasing toward the elongation zone (**Figure 3. 6A**). Cu stress significantly reduced $O_2^{\bullet-}$ accumulation, with the 50 μM and 100 μM Cu treatments decreasing the $O_2^{\bullet-}$ content of root tips by 78.3% and 70.2%, respectively, compared to the control (**Figure 3. 6A-D**). In contrast, H_2O_2 was primarily localized to the meristematic in control roots (**Figure 3. 6E-G**), but its levels significantly increased with Cu stress, particularly within the elongation zone. Specifically, 50 μM and 100 μM Cu treatments

increased root H_2O_2 accumulation by approximately 1.6- and 1.7-fold, respectively, compared to the control (**Figure 3. 6H**).

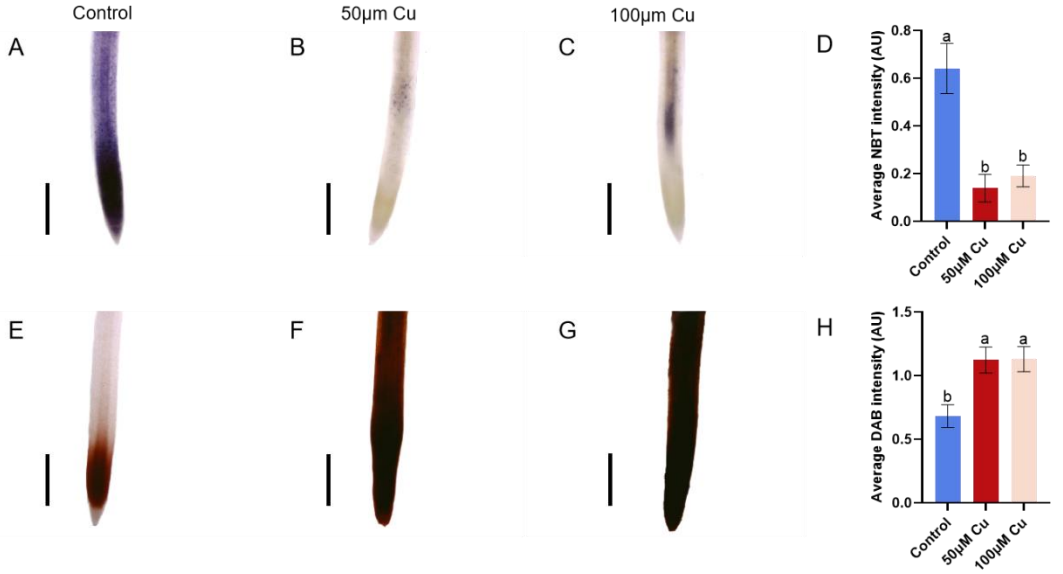

Figure 3. 6 Effect of Cu stress on $O_2^{\bullet-}$, and hydrogen peroxide H_2O_2 accumulation in barley root tips. Histochemical staining of $O_2^{\bullet-}$ (NBT stain, blue) (A-C) and H_2O_2 (DAB stain, brown) (E-G) in barley root tips under control conditions or Cu stress conditions (50 µM or 100 µM Cu). Quantification of NBT staining intensity ($O_2^{\bullet-}$ levels) in root tips (D). Quantification of DAB staining intensity (H_2O_2 levels) in root tips (H). Different letters indicate significant differences at $p < 0.05$ (One-Way ANOVA, Fisher's LSD). The scale bar represents 250 µm.

In leaves, Cu stress induced a marked accumulation of $O_2^{\bullet-}$ in leaves, with 50 µM and 100 µM Cu treatments increasing $O_2^{\bullet-}$ levels by 1.6- and 1.7-fold compared to the control (**Figure 3. 7A-D**). However, no significant differences in H_2O_2 content were observed between Cu-treated and control leaves (**Figure 3. 7E-H**).

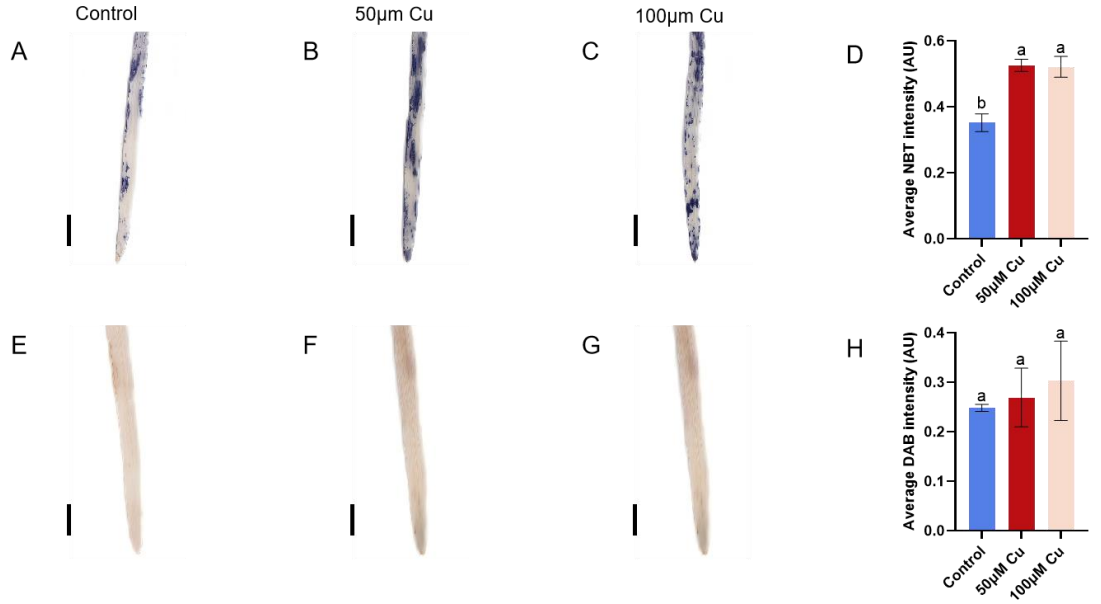

Figure 3. 7 Effect of Cu stress on $O_2^{\bullet-}$, and H_2O_2 accumulation in barley leaves. Histochemical staining of $O_2^{\bullet-}$ (NBT stain, blue) (A-C) and H_2O_2 (DAB stain, brown) (E-G) in barley leaves under control conditions or Cu stress conditions (50 μM or 100 μM Cu). Quantification of NBT staining intensity ($O_2^{\bullet-}$ levels) in leaves (D). Quantification of DAB staining intensity (H_2O_2 levels) in leaves (H). Different letters indicate significant differences at $p < 0.05$ (One-Way ANOVA, Fisher's LSD). The scale bar represents 1cm.

3.4 Lipid peroxidation and proline content

MDA is a commonly used indicator of lipid peroxidation, particularly under stress conditions. In this study, MDA levels were measured to evaluate lipid peroxidation and assess the membrane damage caused by Cu stress. In barley roots, Cu stress significantly increased MDA content (**Figure 3. 8A**). Compared to the control, MDA levels increased by 54.90% and 51.01% following treatment with 50 μM Cu and 100 μM Cu, respectively. A similar trend was observed in the leaves, where MDA levels rose significantly with increasing Cu concentrations (**Figure 3. 8B**). Specifically, MDA content increased by 78.66% and 61.73% in response to 50 μM Cu and 100 μM Cu treatments, respectively, compared to the control. However, no significant difference was detected between the 50 μM and 100 μM Cu treatments in either roots or leaves.

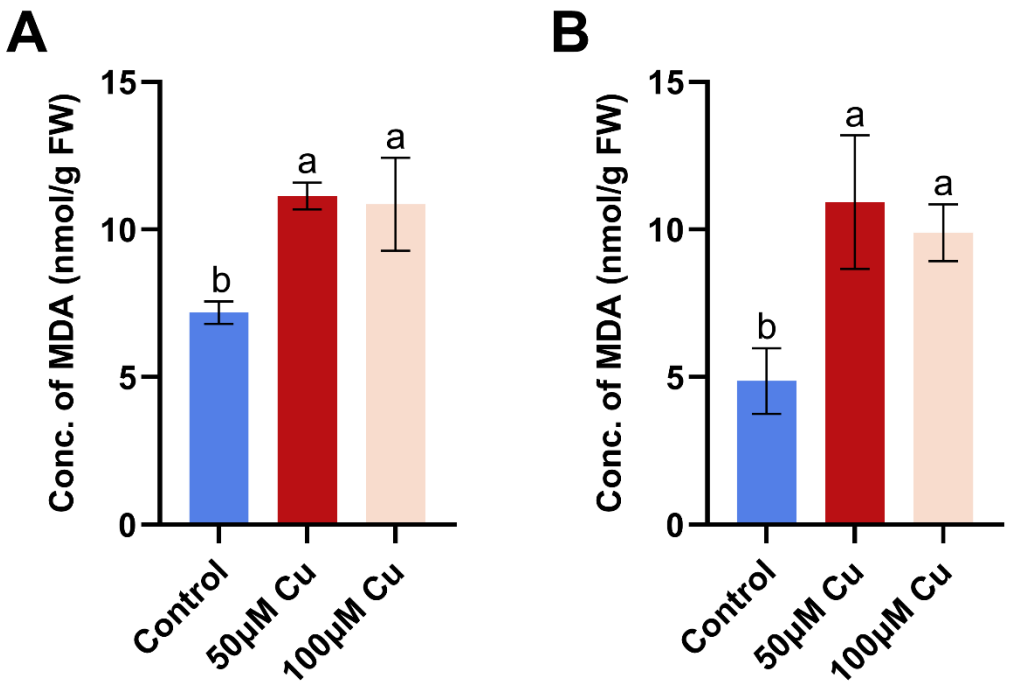

Figure 3. 8 MDA concentration in barley roots (A) and leaves (B) under control conditions or Cu stress conditions (50 µM or 100 µM Cu). Data are presented as mean ± SD of three biological replicates. Different letters indicate significant differences at $p < 0.05$ (One-Way ANOVA, Fisher's LSD).

Proline serves as a notable biomarker in plant responses to Cu stress (Chen et al., 2004). To evaluate its role in barley under Cu stress, proline content in roots and shoots was quantified using the ninhydrin method and expressed as µg/g fresh weight (FW) (**Figure 3. 9**). In roots, Cu treatment induced a significant increase in root proline content. Compared to the control, 50 µM and 100 µM Cu treatments increased proline levels by 2.3-fold, with no significant difference between the two Cu treatments (**Figure 3. 9A**). Similarly, leaves proline content remarkably increased under Cu stress. Relative to the control, 50 µM Cu treatment increased proline by 1.4-fold, while 100 µM Cu treatment caused a more pronounced 3.9-fold increase (**Figure 3. 9B**).

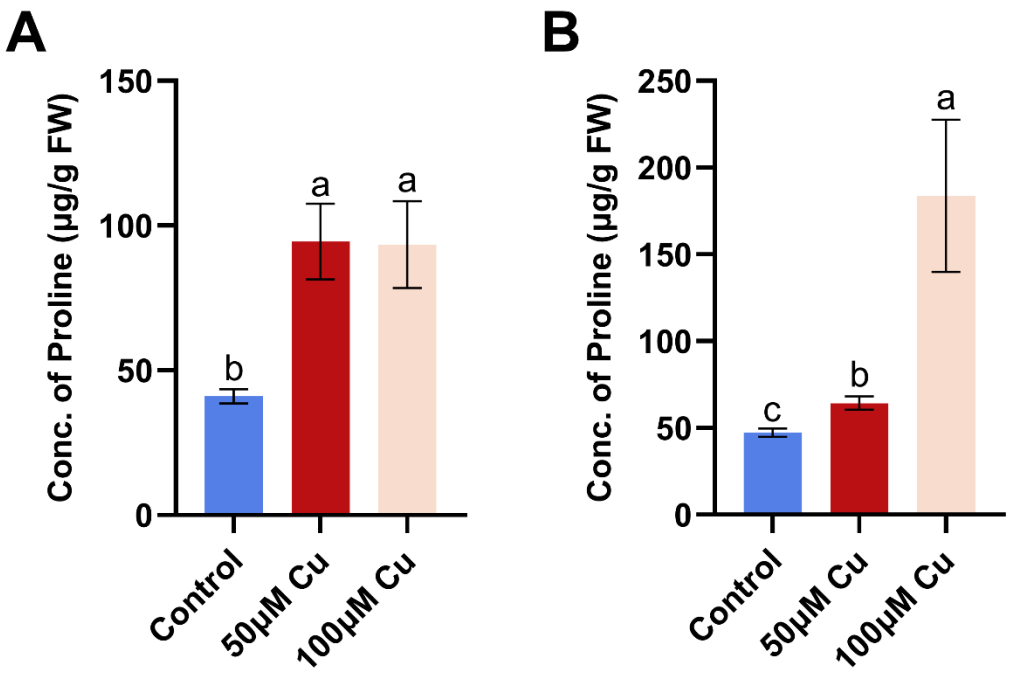

Figure 3. 9 Concentration of proline in barley roots (A) and leaves (B) under control conditions or Cu stress conditions (50 µM or 100 µM Cu). Data are presented as mean ± SD of three biological replicates. Different letters indicate significant differences at $p < 0.05$ (One-Way ANOVA, Fisher's LSD).

3.5 Effect of copper stress on barley endodermal suberization

3.5.1 Suberization of barley roots under different conditions

Histochemical detection of suberin lamellae was performed using fluorol yellow 088, which stains suberin as bright yellow deposits in endodermal cells. In control barley roots, suberin deposition was absent in the youngest root zone (Zone A: 0-25% of root length), except for isolated cells exhibiting suberization at 25% root length. Zone B (25-50%) showed patchy suberization, with only some of the cells exhibiting suberin deposition. Whereas in Zone C (50-100%), corresponding to the mature region near the root base, all endodermal cells displayed continuous suberin deposition (**Figure 3. 10**). Under 50 µM and 100 µM Cu treatments, suberin deposition occurred earlier along the root axis. Specifically, continuous suberization was observed as early as 12.5% of the

root length, with patchy suberization evident between 0-12.5% of the root length (**Figure 3. 10**-**Figure 3. 11**). These findings indicate that Cu stress accelerates suberin barrier formation, which may serve as an adaptive response to restrict toxic Cu entry into the root symplast.

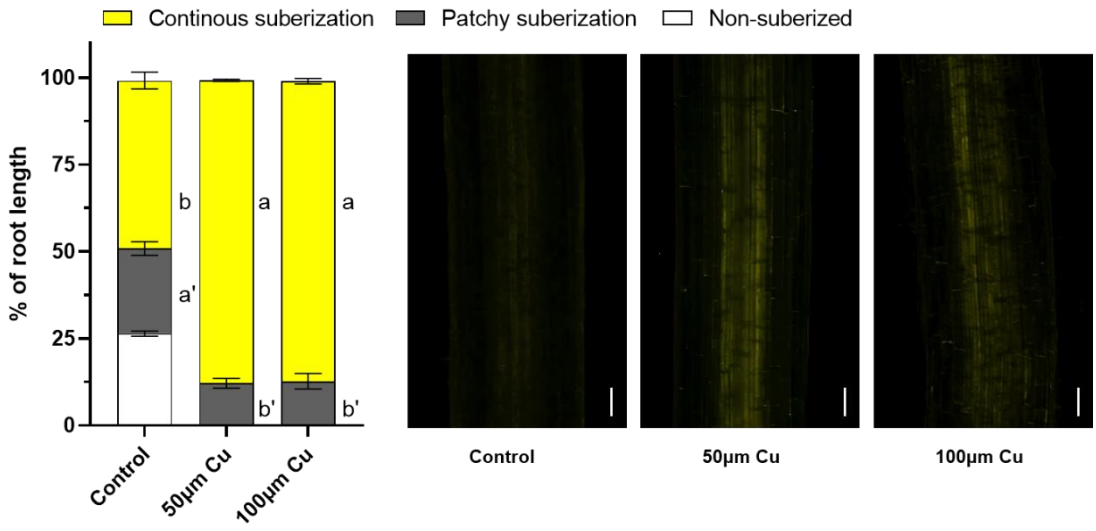

Figure 3. 10 Fluorol yellow 088 staining and suberization of barley roots under different conditions. Pictures were taken at 12.5% length of the roots grown under control conditions or Cu stress conditions (50 µM or 100 µM Cu). The scale bar represents 100 µm. Suberin deposition was quantified along the root axis using three different zones: non-suberized, patchy suberization, and continuous suberization. Data are presented as percentages of root length. Error bars represent SD. Different letters indicate significant differences ($p < 0.05$).

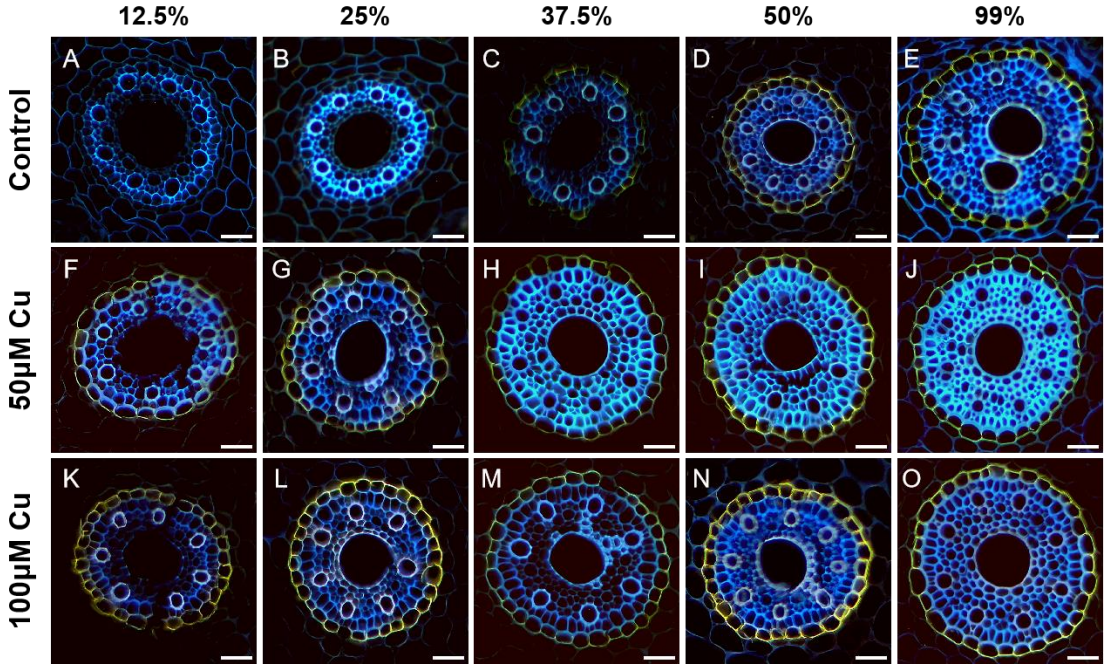

Figure 3. 11 Development of suberin lamellae in the endodermis of barley seminal roots under different conditions. Suberin lamellae in roots grown under control conditions or Cu stress conditions (50 µM or 100 µM Cu) were stained with fluorol yellow 088. A bright yellow fluorescence indicates the presence of suberin lamellae. Numbers represent the percentage of distance from the root tip. Pictures at 12.5% of relative root length (A, F, K), at 25% of relative root length (B, G, L), at 37.5% of relative root length (C, H, M), at 50% of relative root length (D, I, N), and the end of the root (E, J, O) were shown. The scale bar represents 50 µm.

3.5.2 Chemical analysis of suberin in response to Cu stress

To complement the histochemical findings, suberin content in three different root zones (A, B, and C) of barley seminal roots under control and Cu stress conditions was quantified (**Figure 3. 12**-**Figure 3. 14**). Both aliphatic and aromatic suberin levels increased significantly from Zone A (young region) to Zone C (mature region), aligning with the spatial suberization patterns observed in the histochemical analysis (**Figure 3. 12**). In Zone A, total aliphatic suberin content in roots treated with 50 µM and 100 µM Cu reached 4.93 ± 0.81 µg/cm² and 5.54 ± 0.03 µg/cm², respectively, representing 18.3- and 20.5-fold increases relative to control roots. (**Figure 3. 12A**). In Zone B, these treatments led to 5.6- and 6.3-fold increases compared to control levels (1.18 ± 0.08

µg/cm²). In Zone C, aliphatic suberin content reached 8.13 ± 1.09 µg/cm² (50 µM Cu) and 9.25 ± 0.23 µg/cm² (100 µM Cu), corresponding to 1.4- and 1.6-fold increases over control levels (5.80 ± 0.14 µg/cm²). While the 100 µM Cu treatment resulted in slightly higher aliphatic suberin accumulation than 50 µM Cu across all zones, the differences were not statistically significant. A similar pattern was observed for aromatic suberin (**Figure 3. 12B**). In Zone A, 50 µM and 100 µM Cu treatments increased aromatic suberin levels to 6.88 ± 1.64 µg/cm² and 7.26 ± 0.30 µg/cm², corresponding to 7.6- and 8.1-fold increases relative to control levels. In Zone B, aromatic suberin increased by 4.5- and 5.0-fold under 50 µM and 100 µM Cu, respectively, compared to control levels (1.12 ± 0.13 µg/cm²). In Zone C, aromatic suberin content reached 16.42 ± 2.96 µg/cm² (50 µM Cu) and 16.53 ± 1.51 µg/cm² (100 µM Cu), corresponding to 2.5- and 2.5-fold increases over control roots (6.70 ± 0.47 µg/cm²). These results indicate that both aliphatic and aromatic suberin biosynthesis in barley seminal roots are significantly enhanced by Cu stress, with the most pronounced increases occurring in Zone A.

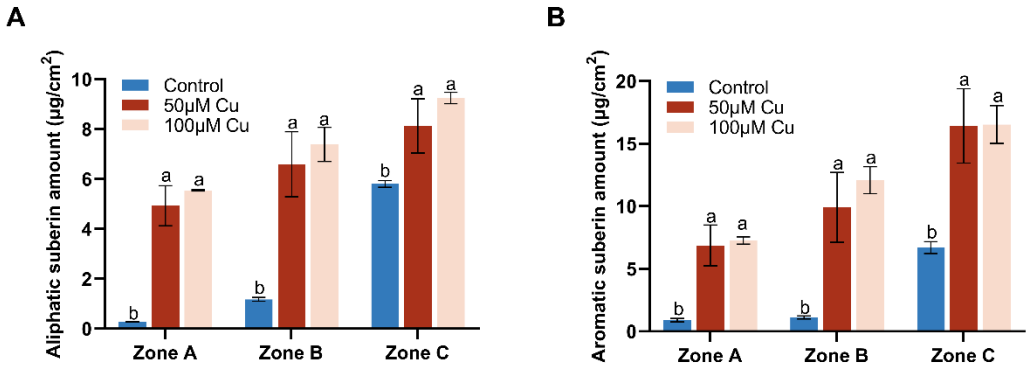

Figure 3. 12 Chemical analysis of suberin content in barley roots under control conditions or Cu stress conditions (50 µM or 100 µM Cu). Aliphatic suberin content (A) and aromatic suberin content (B) in different root zones (Zone A, B, C). Data are presented as mean ± SD of three biological replicates. Different letters indicate significant differences at $p < 0.05$ (One-Way ANOVA, Fisher's LSD).

To further assess the impact of Cu stress on suberin biosynthesis, the composition of aliphatic suberin substance classes in seminal roots of barley grown under control and

Cu stress conditions was analyzed (**Figure 3. 13**). Suberin monomer composition was consistent across conditions, comprising four major substance classes: primary alcohols (alc), fatty acids (fa), α-ω dicarboxylic acids (diacids), and ω-hydroxy acids (ω-OH acids). The content of different classes of aliphatic suberin increased along the root length and in response to Cu stress. Under 50 µM and 100 µM Cu treatments, fatty acids and ω-hydroxy acids exhibited significant accumulation across all root zones compared to the control. In contrast, diacids increased only in Zone A and B, while primary alcohols remained unchanged. Among all root zones, ω-hydroxy acids exhibited the most remarkable upregulation in Zone A under Cu stress, reaching 2.85 ± 0.65 µg/cm² (50 µM Cu) and 3.39 ± 0.05 µg/cm² (100 µM Cu), representing 47.5-fold and 56.5-fold increases, respectively, relative to controls. Similarly, diacid levels increased to 1.02 ± 0.65 µg/cm² (50 µM Cu) and 1.06 ± 0.05 µg/cm² (100 µM Cu) in Zone A, corresponding to 34-fold and 35.3-fold increases. These results suggest that Cu stress primarily upregulates the biosynthesis of ω-hydroxy acids and diacids, particularly in the root apical zone (Zone A).

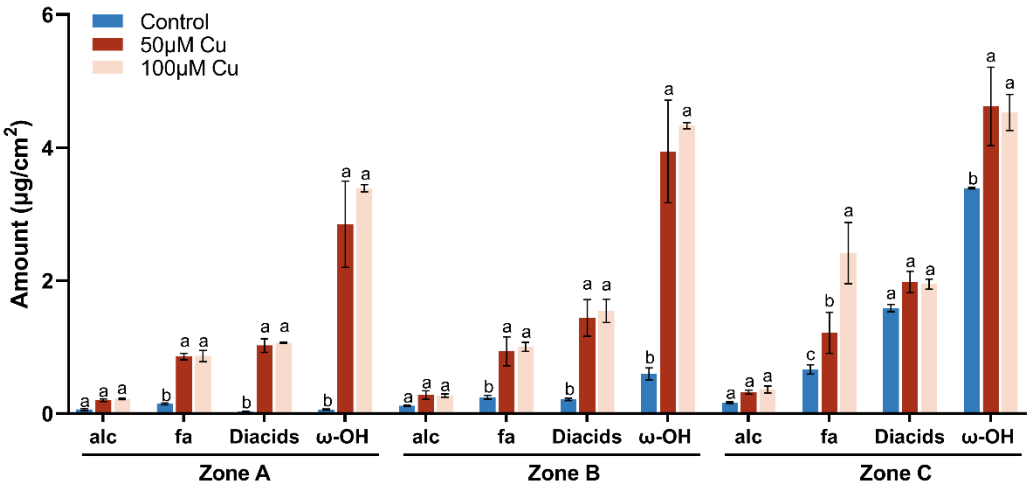

Figure 3. 13 Amounts of substance classes of aliphatic suberin in barley seminal roots grown under control conditions or Cu stress conditions (50 µM or 100 µM Cu). Data are presented as mean ± SD of three biological replicates. Different letters indicate significant differences at p

< 0.05 (One-Way ANOVA, Fisher's LSD). Abbreviations: alc, primary alcohols; fa, fatty acids; diacids, α-ω dicarboxylic acids; ω-OH acids, ω-hydroxy acids.

The chain length distribution of aliphatic suberin monomers in barley seminal roots across the three zones (A, B, and C) was shown in **Figure 3. 14**. Under Cu stress, C18:1 diacids and C18:1 ω-OH acids were the most abundant suberin components in all zones. The majority of ω-OH acids and diacids (including C16 ω-OH acids, C18:1 ω-OH acids, C22 ω-OH acids, C24 ω-OH acids, and C18:1 diacids) exhibited significant increases under both 50 μM and 100 μM Cu treatments. Zone A displayed the most remarkable upregulation of specific suberin monomers, with C18:1 ω-OH acids increasing by 30.6-fold (50 μM Cu) and 31.8-fold (100 μM Cu), while C18:1 diacids increased by 29.4-fold and 30.4-fold under the same treatments. These findings suggest that Cu stress preferentially enhances the synthesis of ω-hydroxy acids and α-ω dicarboxylic acids, particularly in Zone A.

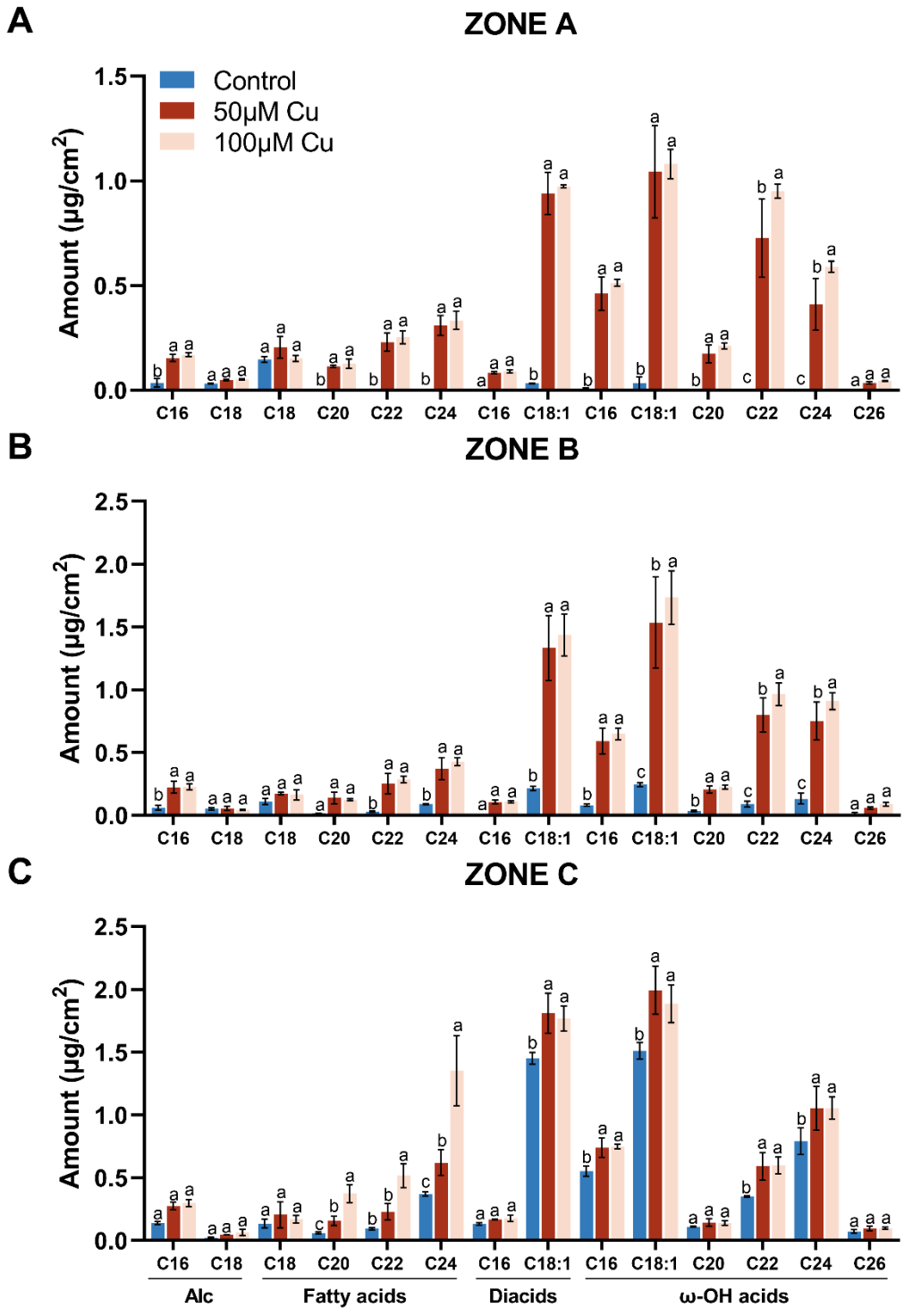

Figure 3. 14 Aliphatic suberin monomers in different zones of barley roots under control conditions or Cu stress conditions (50 μM or 100 μM Cu). Data are presented as mean ± SD of three biological replicates. Different letters indicate significant differences at $p < 0.05$ (One-

Way ANOVA, Fisher's LSD). Abbreviations: alc, primary alcohols; fa, fatty acids; diacids, α-ω dicarboxylic acids; ω-OH acids, ω-hydroxy acids.

3.6 Effect of copper stress on nutrient absorption

To assess the effect of Cu stress on nutrient absorption, the concentrations of essential mineral elements in barley roots and shoots were quantified under both control and Cu stress conditions. The results, presented in **Table 3. 1**, demonstrate that Cu treatment induced tissue-specific and element-specific alterations in nutrient accumulation. It is important to note that these results are based on a single biological replicate and require further validation through repeated experiments. In roots, Cu treatments were associated with reduced concentrations of most essential elements compared to the control, K, Ca, Mg, Fe, Zn, and Mn decreased by 30.8%, 29.1%, 46.9%, 29.2%, 28.8%, and 93.4%, respectively, under 50 μM Cu treatment, with further reductions of 39.8%, 38.2%, 56.3%, 44.3%, 10.8%, and 97.7% at 100 μM Cu treatment. Whereas Cu accumulation exhibited a dose-dependent increase, reaching 4468 mg/kg (50 μM) and 6033 mg/kg (100 μM), representing 15.3- and 20.7-fold increases over the control (291 mg/kg). Moreover, Na concentration showed a non-linear response, increasing by 41.2% at 50 μM Cu but declining to 20.6% above the control at 100 μM Cu. In shoots, Cu accumulation also exhibited a dose-dependent increase, reaching 32 mg/kg at 50 μM Cu and 43 mg/kg at 100 μM Cu, representing 1.5- and 2-fold increases compared to the control (21 mg/kg). However, Cu translocation to shoots increased but remained highly restricted. Compared to the control (7%), shoot Cu concentrations exhibited a lower proportion under 50 μM or 100 μM Cu treatment, which both accounted for only 0.7% of root Cu levels. K, Ca, Mg, Fe, Zn, and Mn displayed dose-dependent declines, with Mn showing the most pronounced reduction (67.8% at 100 μM Cu). Furthermore, Na accumulation increased consistently in shoots (76.9% and 64.7% higher than control at 50 μM and 100 μM Cu, respectively).

Table 3. 1 Mineral element concentrations in barley roots and shoots under different conditions (values expressed in mg/kg dry weight)

Tissue	Treatment	K	Ca	Na	Mg	B	Cu	Fe	Zn	Mn
Root	Control	81700	5500	2097	3200	8	291	3675	139	2413
Root	50μM Cu	56500	3900	2960	1700	6	4468	2603	99	159
Root	100μM Cu	49200	3400	2528	1400	5	6033	2046	124	56
Shoot	Control	80200	5100	566	2300	13	21	66	62	90
Shoot	50μM Cu	69400	4000	1001	2000	14	32	49	44	41
Shoot	100μM Cu	66200	3400	932	1800	13	43	48	42	29

3.7 Subcellular distribution of copper ions in roots

The subcellular distribution of Cu^{2+} in barley root tips was further examined to understand how suberin affects Cu uptake and transport. The subcellular distribution of Cu^{2+} in root tip cross-sections (0-1 cm from the root tip) under different conditions for 6 days was visualized by Rhodamine B hydrazide (RBH), which indicated Cu^{2+} with pink fluorescence (**Figure 3. 15**). In control roots, Cu^{2+} distribution was primarily in the epidermis (ep) cell, followed by cortex (co) cells, with minimal distribution in the endodermis (en) cells and vascular tissues cells (va) (**Figure 3. 15A**). Cu treatment markedly enhanced the accumulation of Cu^{2+}, particularly in cortex and epidermis cell walls (apoplasts) (**Figure 3. 15B**). While Cu^{2+} distribution in the endodermis cell wall (face to cortex side) increased under Cu stress, vascular tissues showed no significant difference between treatments. These results suggest the endodermis suberin likely acts as a barrier limiting Cu^{2+} entry to vascular systems.

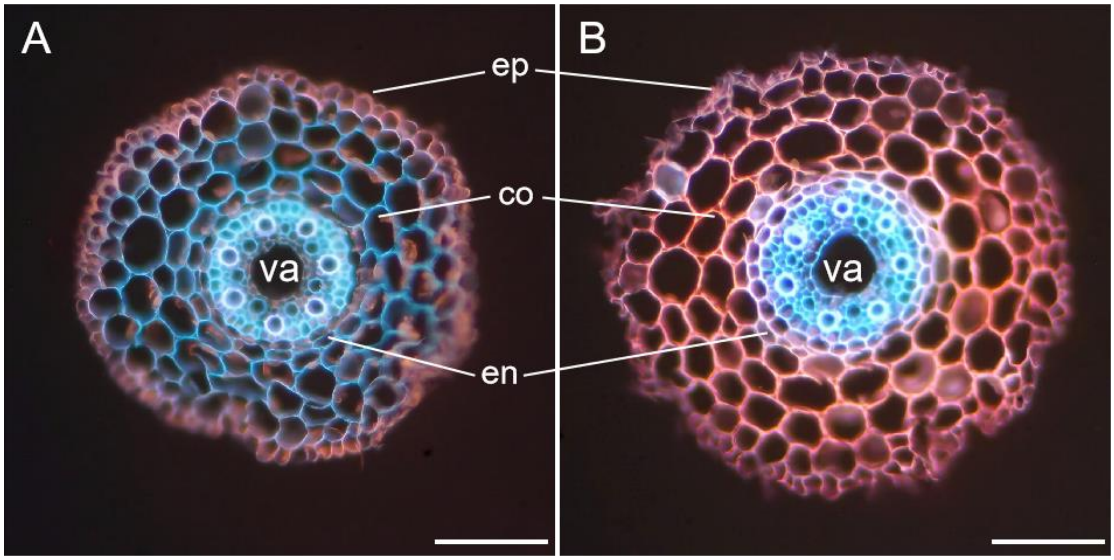

Figure 3. 15 Subcellular Cu^{2+} distribution in barley root tips under control conditions (A) or 50 µM Cu treatment (B). Cu^{2+} distribution appears as pink fluorescence after Rhodamine B hydrazide (RBH) staining of root cross-sections (sections taken 0-1 cm from the root tip). ep, epidermis; co, cortex; en, endodermis; xy, xylem; va, vascular tissues. Scale bar = 100 µm.

3.8 Transcriptome analysis

3.8.1 Differentially regulated genes (DEGs) analysis

To investigate the molecular mechanisms underlying the barley response to Cu stress, RNA sequencing (RNA-seq) datasets obtained from the publicly available BarleyExpDB database (http://barleyexp.com/) were assessed. The RNA-seq data corresponded to 7-day-old barley (cv. Morex) whole root samples which were grown under control conditions or 50 µM Cu treatment for five days. Principal component analysis (PCA) was conducted to assess the variance among RNA-seq samples in an unsupervised manner (**Figure 3. 16**). The PCA score plot visualized the distribution of samples along two principal components: principal component 1 (PC1), which explained 55.3% of the total variance, and principal component 2 (PC2), which explained 18.6% of the total variance. Collectively, these two components explained the majority of transcriptional variation among samples. Despite slight dispersion in one biological replicate from the control group, all replicates clustered tightly,

demonstrating high reproducibility. In contrast, the Cu-treated (Cu) and control (CK) groups were completely separated in the dimension of PC1, indicating substantial transcriptional differences between the two conditions. These results confirm that the dataset is suitable for subsequent identification of differentially expressed genes (DEGs).

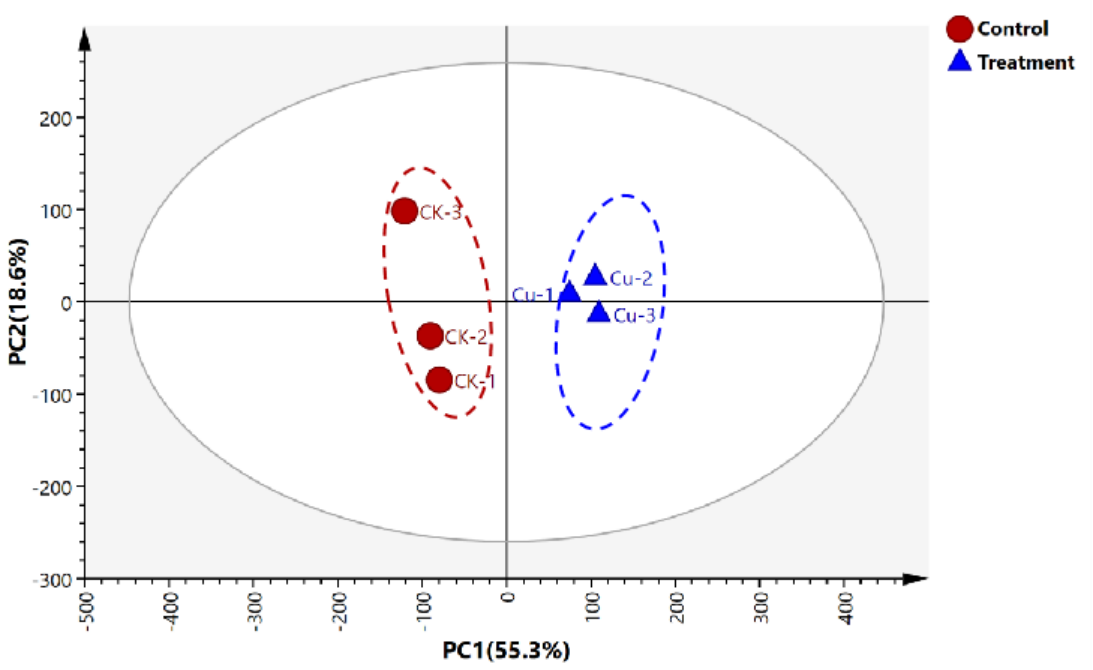

Figure 3. 16 PCA score plot of RNA-seq data in whole barley (cv. Morex) roots under control conditions or 50 μM Cu treatment for five days. Red dots represent control samples, and blue triangles represent 50 μM Cu-treated samples. Three biological replicates were used.

To further explore Cu-induced transcriptional changes, Limma, a widely utilized statistical tool for RNA-seq differential expression analysis, was employed to compare 50 μM Cu-treated samples with controls. Given the limited sample size and the slight variability observed in one control replicate in the PCA plot, lenient filtering criteria were applied (P-value < 0.05, FDR < 10%, $|Log_2FC| > 1.5$). The results, visualized in a volcano plot (**Figure 3. 17**), revealed a total of 2098 DEGs, of which 886 genes were upregulated and 1212 genes were downregulated in response to Cu stress. These differentially expressed genes represent key candidates for further functional analysis to elucidate the molecular mechanisms of Cu toxicity and tolerance in barley.

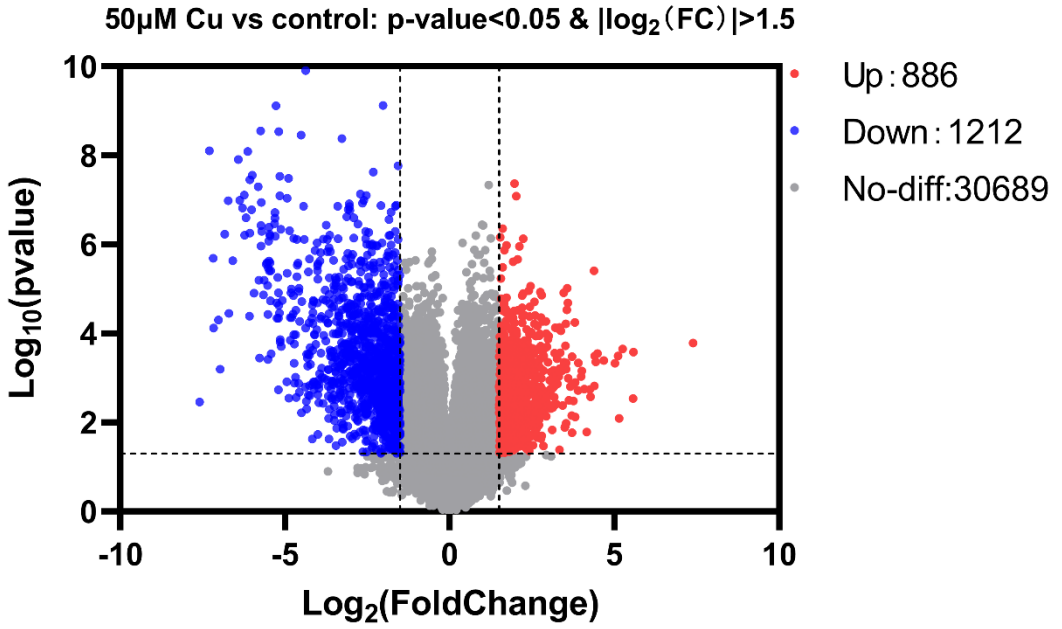

Figure 3. 17 Volcano map of differentially expressed genes (DEGs) in whole barley roots under Cu treatment group relative to the control group. Red dots represent up-regulation genes, blue dots represent down-regulation genes, and grey dots represent stable genes.

3.8.2 KEGG pathway analysis and Gene ontology (GO) enrichment analysis

To identify key metabolic pathways involved in barley's response to Cu stress, Kyoto Encyclopedia of Genes and Genomes (KEGG) pathway enrichment analysis was performed on the DEGs. A total of 123 metabolic pathways were annotated, with the top 25 shown in a bubble plot (**Figure 3. 18**). Among these, the phenylpropanoid biosynthesis pathway, which is closely linked to plant stress responses, was significantly enriched. Given that lignin synthesis is a downstream branch of phenylpropanoid metabolism, it is likely that this pathway is also regulated under Cu stress. This finding suggests that lignin biosynthesis may play a crucial role in Cu tolerance. Similarly, the plant hormone signal transduction pathway, which is involved in both growth regulation and stress responses, was significantly enriched. This indicates its potential role in barley's adaptive response to Cu toxicity. Moreover, consistent with histochemical and chemical analyses (**Section 3.5**), the cutin, suberin,

and wax biosynthesis pathway was significantly enriched. This suggests that suberin biosynthesis serves as a key protective mechanism in barley roots under Cu stress.

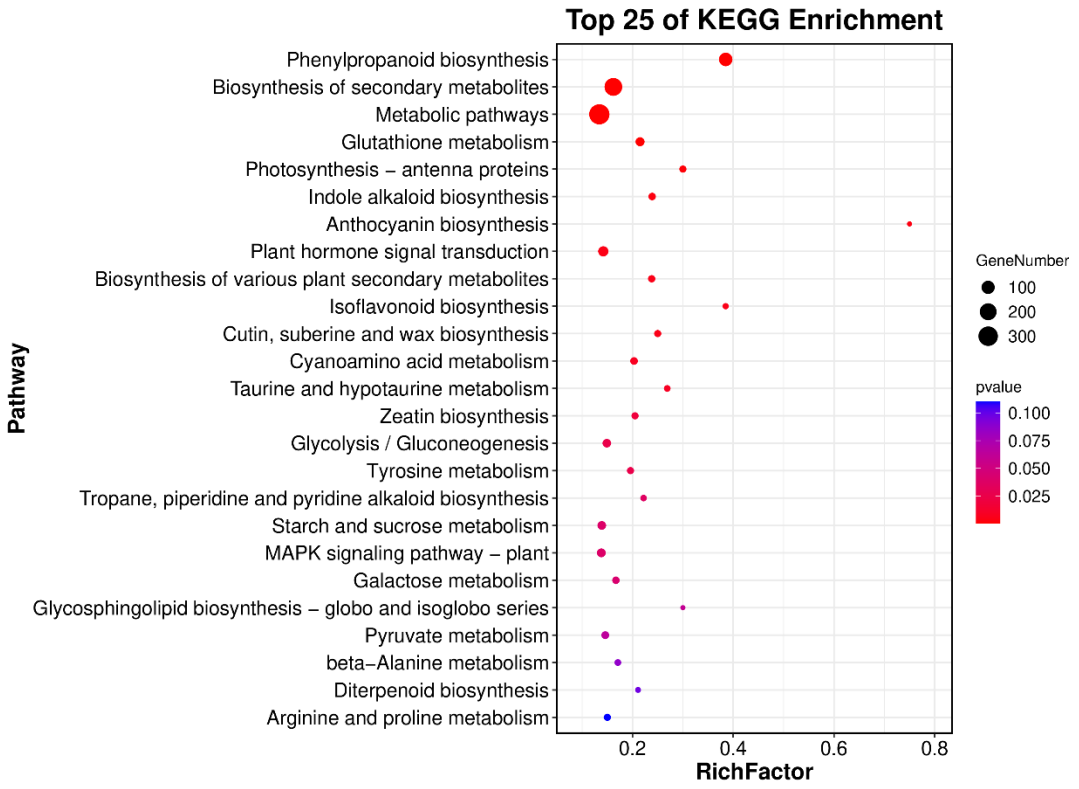

Figure. 18 KEGG enrichment analysis of DEGs in whole barley roots under the Cu treatment group relative to the control group. The bubble plot displays the top 25 pathways, ranked by p-value.

To further investigate Cu-induced transcriptional responses, Gene Ontology (GO) enrichment analysis was conducted, categorizing DEGs into three functional groups: biological process (BP), molecular function (MF), and cellular component (CC). The top 10 enriched GO terms (q-value < 0.05), ranked by gene ratio, are displayed in **Figure. 19**. In the BP category, significant enrichment was observed in phenylpropanoid metabolic and biosynthetic processes, lignin metabolic and biosynthetic processes, and detoxification-related pathways, such as cellular oxidant detoxification, detoxification, and response to toxic substances. This finding highlights the importance of lignin biosynthesis and detoxification mechanisms under Cu stress. The cell wall modification-related terms, including the plant-type cell wall, cell wall,

and apoplast, were significantly enriched in the CC category, aligning with observed suberin deposition in root endodermis (**Section 3.5**). In the MF category, the GO terms peroxidase activity, oxidoreductase activity, and antioxidant activity were remarkably enriched, indicating an enhanced antioxidant defense system against Cu-induced oxidative stress. Furthermore, transmembrane transporter activity was enriched in the MF category, indicating that Cu transport was regulated in response to Cu stress. Collectively, the GO analysis highlighted that Cu tolerance in barley is primarily mediated through cell wall modifications (lignin and suberin biosynthesis), detoxification, antioxidant defense and Cu transport.

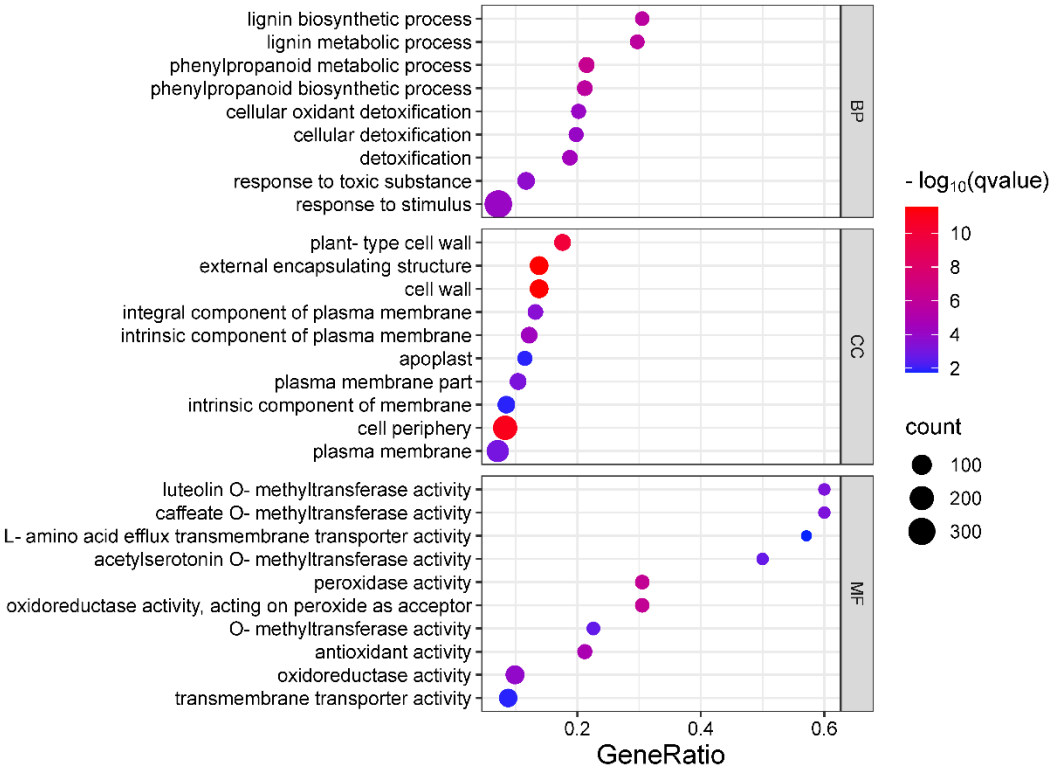

Figure 3. 19 Gene ontology (GO) enrichment analysis of DEGs in whole barley roots under the Cu treatment group relative to the control group. The Y-axis represents gene functions, and the X-axis represents gene ratios. Each bar represents a different GO term, with the statistical significance threshold set at q-value < 0.05. BP, biological process; CC, cellular component; MF, molecular function.

3.8.3 Expression profiles analysis

Based on the results of KEGG pathway analysis and GO enrichment analysis, a complex regulatory network was identified in response to Cu stress, involving cell wall modifications (lignin and suberin biosynthesis), detoxification, antioxidant defense, Cu transport, and plant hormone signal transduction. To further explore key genes associated with these biological processes, the expression profiles of DEGs were analyzed (**Figure 3. 20, Table S2**). Gene expression levels were represented as $\log_2$ fold changes ($\log_2$FC) with a significance threshold of p-value < 0.05. After five days of exposure to 50 μM Cu, transcriptomic analysis revealed Cu-induced alterations in cell wall-associated gene expression. For instance, five cell wall-associated receptor kinase genes (*WAK*, $\log_2$FC +1.6 to +2.0) and two pectin methylesterase genes *(PME41/4*, $\log_2$FC +1.7/+2.2) were upregulated. Conversely, most lignin biosynthesis genes ($\log_2$FC −5.5 to −1.5) and most suberin biosynthesis genes (e.g., *CYP86A1*, $\log_2$FC −2.6; *CYP86B*1, $\log_2$FC −1.7) were downregulated. Interestingly, the downregulation of *CYP86A1* and *CYP86B1* in transcriptomic data contrasts with the increase in suberin content observed in histochemical and chemical analyses after six days of Cu treatment (**Section 3.5**). This discrepancy necessitates further validation of suberin biosynthesis gene expression via RT-qPCR analysis (**Section 3.8.4**). Transcriptomic data indicated that most genes encoding Cu-dependent enzymes, including copper oxidase and plastocyanin, were significantly downregulated. Whereas Cu transporter genes, including *ZIP2* ($\log_2$FC −3.5), *YSL4/6* ($\log_2$FC −2.1/−3.2), and *HMA2* ($\log_2$FC −4.0), were significantly downregulated. Similarly, Cu transport-related genes, including the Cu chaperone gene (*ATX1*, $\log_2$FC −3.3) and three Cu chelate genes (*NAS1/2/3*, $\log_2$FC −3.5 to −1.9), were significantly downregulated. However, the cellular detoxification-related genes, including the type 2 metallothionein-like gene (*MT2*, $\log_2$FC +3.1), fourteen heat shock protein genes (*HSP*, $\log_2$FC +1.5 to +3.2), and seven heavy-metal-associated isoprenylated plant protein genes (*HIPP*, $\log_2$FC +1.7 to +3.2), were significantly upregulated. Likewise, key antioxidant defense genes in

barley roots were upregulated, including two Cu/Zn superoxide dismutase genes (*CSD1/2*, log_2FC +0.6/+1.0), eleven glutathione S-transferase genes (*GST*, log_2FC +1.7 to +4.4), and the catalase gene (*CAT2*, log_2FC +3.1), suggesting an enhanced oxidative stress response. Plant hormonal signaling pathways also exhibited significant transcriptional changes under Cu stress. Most genes associated with growth and cytokinin signaling pathways were downregulated, whereas genes involved in ABA and ethylene signaling pathways, such as *PP2C4* (log_2FC +1.9), *SnRK2* (log_2FC +2.0), and *EIN3* (log_2FC +2.0), were significantly upregulated.

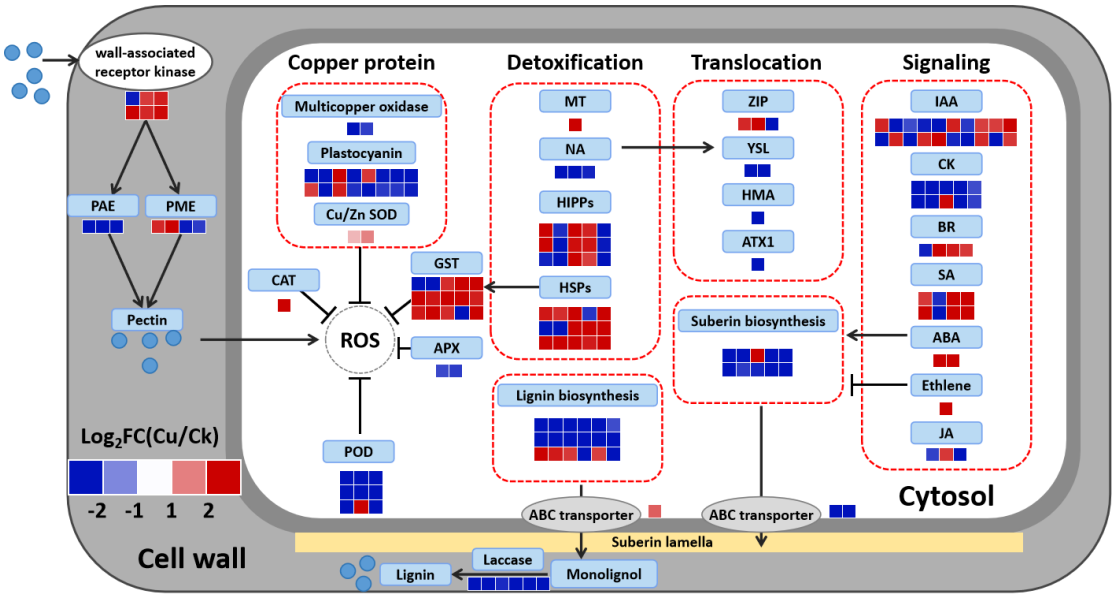

Figure 3. 20 Expression profiles of DEGs in whole barley roots under control conditions or 50 μM Cu treatment for five days. The expression profile of each gene ($p < 0.05$) is displayed as log_2FC. Note: PAE, pectin acetylesterase; PME, pectin methylesterase; GST, glutathione S-transferase; APX, ascorbate peroxidase; CAT, catalase; Cu/Zn SOD, Cu/Zn superoxide dismutase; POD, peroxidase; MT, metallothionein; NA, nicotianamine; HIPPs, heavy-metal-associated isoprenylated plant proteins; HSPs, heat shock proteins; ZIP, Zrt-/Irt-like protein; YSL, yellow stripe-like protein; HMA, heavy metal ATPase; ATX, antioxidant protein.

3.8.4 Expression pattern analysis of suberin genes and ABA genes

To clarify the discrepancy between transcriptomic data (which showed downregulation of *CYP86A1* and *CYP86B1* after five days of 50 μM Cu treatment) and histochemical

and chemical analysis (which demonstrated increased suberin content after six days of 50 µM or 100 µM Cu treatment), the spatial expression patterns of these genes in different root zones after six days of 50 µM or 100 µM Cu treatment were investigated by RT-qPCR (**Figure 3. 21**). Under control conditions, *CYP86A1* and *CYP86B1* exhibited an expression pattern correlated with root maturation, showing the highest expression levels in Zone C (root base) and the lowest in Zone A (young root). However, following 50 µM or 100 µM Cu treatments, the expression pattern was reversed, with the highest gene expression levels detected in Zone A and the lowest in Zone C. Notably, after six days of Cu treatment, *CYP86A1* and *CYP86B1* were strongly upregulated in Zone A, while their expression levels were significantly downregulated in Zones B and C. The zone-specific expression patterns of *CYP86A1* and *CYP86B1* explain their overall downregulation observed in transcriptomic data at five days, highlighting a spatial change in suberin gene expression under Cu stress.

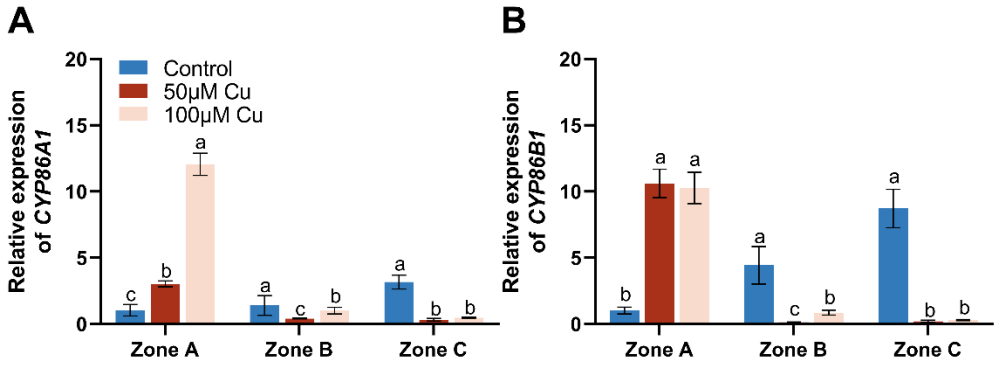

Figure 3. 21 Spatial expression analysis of *CYP86A1* (A) and *CYP86B1* (B) in different barley (cv. Scarlett) root zones under control conditions or Cu stress conditions (50 µM or 100 µM Cu) for 6 days. Data are presented as mean ± SD of three independent experiments. Different letters indicate significant differences at $p < 0.05$ (One-Way ANOVA, Fisher's LSD).

To further investigate the temporal expression dynamics of *CYP86A1* and *CYP86B1*, RT-qPCR analysis was performed in whole barley (cv. Scarlett) roots exposed to 50 µM Cu for 0 h, 12 h, 24 h, 48 h, and 72 h (**Figure 3. 22**). Under Cu stress, both genes exhibited a transient significant increase in expression, peaking at 24 h, followed by a

decline at 48 h and 72 h. The expression levels of Cu treatment at 72 h returned to control levels. These results suggest that *CYP86A1* and *CYP86B1* were primarily upregulated during the early stage (0-3 days) of Cu treatment.

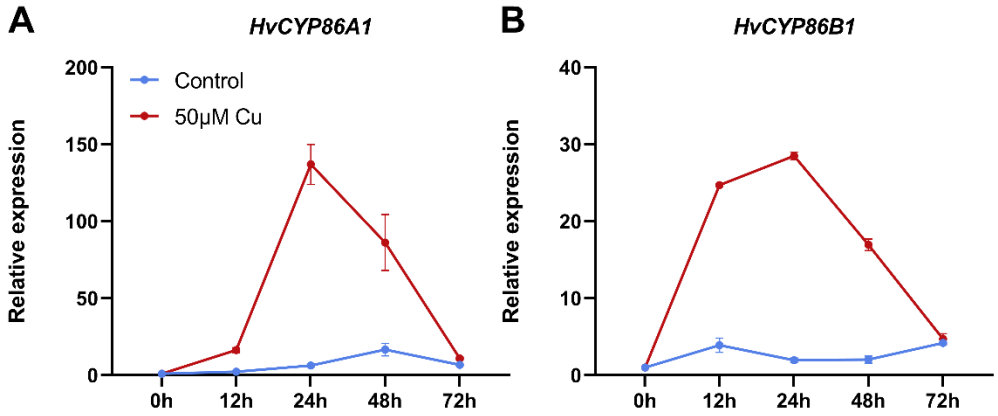

Figure 3. 22 Temporal expression analysis of *CYP86A1* (A) and *CYP86B1* (B) in whole barley (cv. Scarlett) roots under control conditions or 50 μM Cu treatment for 0 h, 12 h, 24 h, 48 h, and 72 h. Data are presented as mean ± SD of three independent experiments.

Considering the role of ABA signaling in suberin biosynthesis and the significant upregulation of ABA pathway genes in RNA-seq data after five days of Cu treatment, the temporal expression patterns of ABA-related genes in whole barley (cv. Scarlett) roots under Cu stress were further examined (**Figure 3. 23**). The expression of ABA biosynthesis genes was significantly induced by Cu treatment, including *nine-cis-epoxycarotenoid dioxygenase* (*NCED1*, *NCED2*) and *abscisic aldehyde oxidase* (*AO5B*), which encodes the final enzyme in the ABA biosynthetic pathway. Specifically, *NCED2* and *AO5B* were upregulated at 12 h, 24 h, 48 h, and 72 h, while *NCED1* was only significantly upregulated at 24 h, 48 h, and 72 h. Similarly, genes involved in ABA signaling, such as *PYR1-like protein* 4 (*PYL4*) and *SNF1-related protein kinase 2* (*SnRK2*), showed a consistent upregulation after 12-72 h of Cu exposure. In contrast, *protein phosphatase type-2C* (*PP2C4*), a negative regulator of ABA signaling, was only upregulated at 24 h and 48 h. The *β-glucosidase 8* (*BG8*) gene, which encodes an enzyme responsible for ABA deconjugation, was also significantly

upregulated. However, the expression of ABA degradation-related genes exhibited differential responses. While *ABA 8′-hydroxylases 1* (*ABA8-OH1*) was upregulated at 24 h but downregulated at other time points, *ABA 8'-hydroxylases 2* (*ABA8-OH2*) did not display a clear expression pattern. Overall, these results indicate that ABA signaling genes were strongly upregulated during the early stages (0-3 days) of Cu exposure, aligning with the expression pattern of suberin biosynthesis genes. This finding suggests that ABA-mediated regulation may contribute to suberin biosynthesis in response to Cu stress.

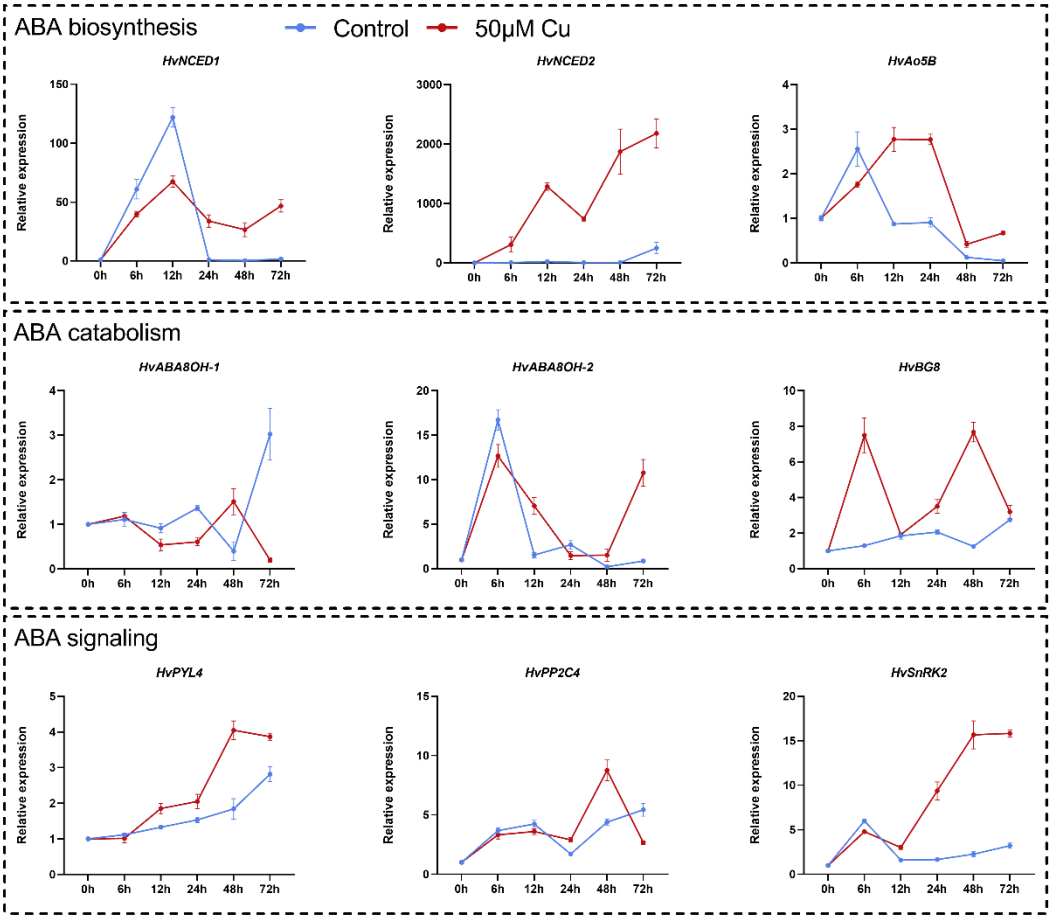

Figure 3. 23 Temporal expression analysis of ABA-related genes in whole barley (cv. Scarlett) roots under control conditions or 50 μM Cu treatment for 0 h, 12 h, 24 h, 48 h, and 72 h. Data are presented as mean ± SD of three independent experiments.

3.9 Effect of copper stress on suberin-defective mutant

Two loss-of-function mutants, *cyp86b1-1* and *cyp86b1-2*, were employed in this study in the background of barley (cv. Golden Promise Fast) (Meng et al., 2024). The *cyp86b1-1* allele contains a 170 bp deletion, whereas the *cyp86b1-2* carries a 168 bp inversion, both resulting in truncated CYP86B1 proteins (**Figure 3. 24**).

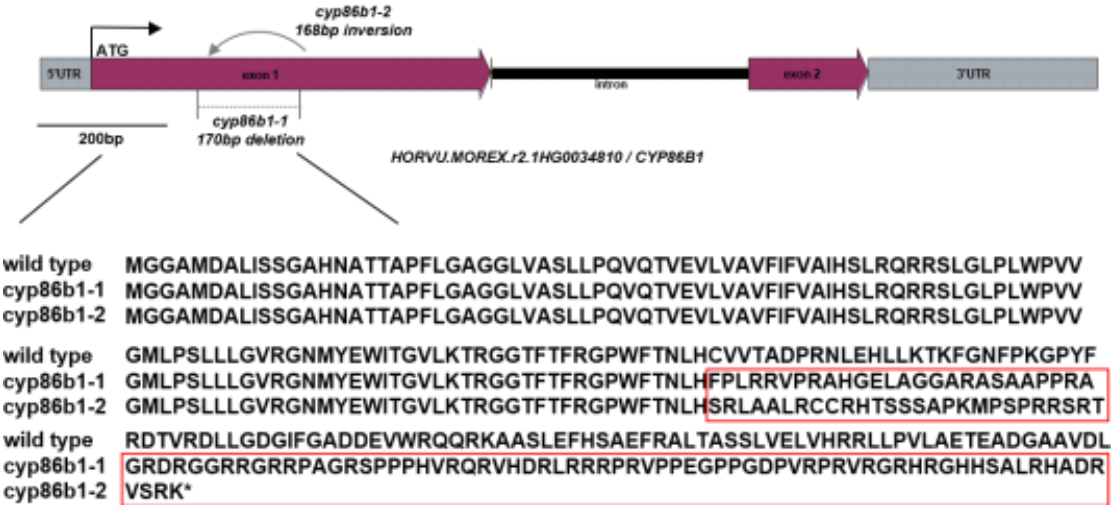

Figure 3. 24 Gene structure and protein sequence of *CYP86B1* mutants. Cited from (Meng et al., 2024).

3.9.1 Morphology parameters of suberin-defective mutant

To investigate the effect of Cu stress on growth, the morphology parameters were examined in wild-type and suberin-defective mutants (*cyp86b1-1* and *cyp86b1-2*) seedlings subjected to control conditions or 50 µM Cu treatment (**Figure 3. 25**-**Figure 3. 26**). Under control conditions, 12-day-old *cyp86b1-1* and *cyp86b1-2* mutants displayed average root lengths of 18.15 ± 3.3 cm and 18.00 ± 3.1 cm, respectively, which were slightly lower (no significant difference) than wild-type (19.76 ± 3.2 cm) (**Figure 3. 25A**). Their average root dry weights (9.18 ± 1.4 mg and 8.90 ± 1.2 mg) also did not significantly differ from wild-type (10.20 ± 1.7 mg) (**Figure 3. 25B**). Following Cu treatment, root growth was significantly inhibited in both wild-type and mutants. Root length was reduced to 15.31 ± 1.9 cm (wild-type), 11.36 ± 2.6 cm (*cyp86b1-1*), and 11.09 ± 1.9 cm (*cyp86b1-2*). Dry weight declined to 8.33 ± 1.7 mg (wild-type),

6.79 ± 1.4 mg (*cyp86b1-1*), and 6.74 ± 1.7 mg (*cyp86b1-2*). Notably, the root length and dry weight of *cyp86b1-1* and *cyp86b1-2* were significantly lower than the wild-type under Cu stress, with no significant difference between the two mutants. This finding suggests that Cu stress exhibits stronger root growth inhibition in suberin-defective mutants than in wild-type.

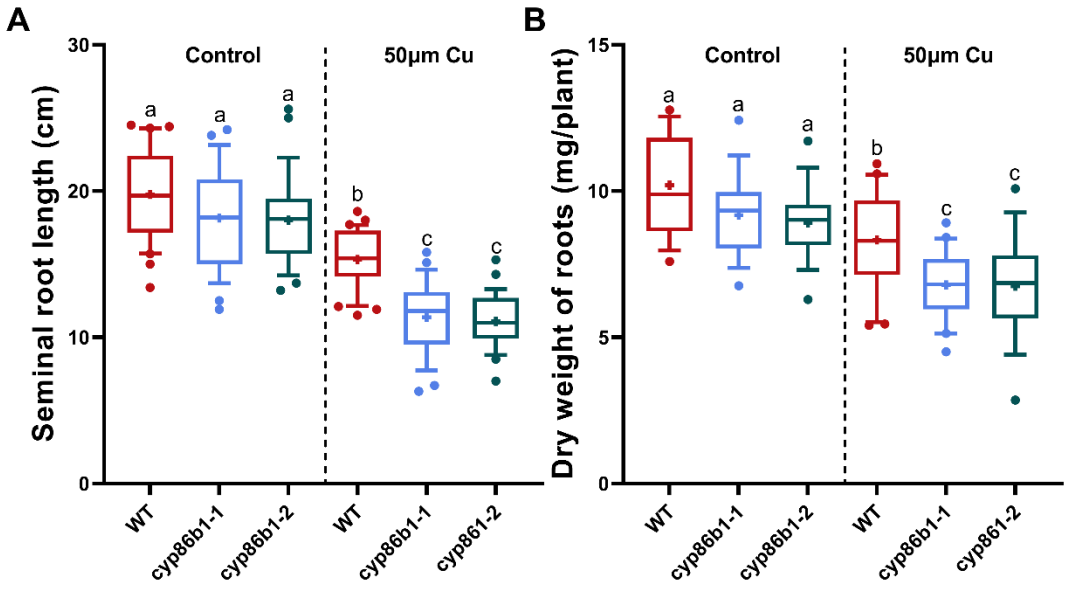

Figure 3. 25 Effect of Cu stress on root length (A) and dry weight (B) in wild-type and suberin-defective mutant (*cyp86b1-1* and *cyp86b1-2*) barley under control conditions or 50 µM Cu treatment. Boxplots represent the 10 to 90 percentiles, with "+" indicating the mean. The whiskers extend to outliers. Data are presented based on at least twenty biological replicates. Different letters indicate significant differences at $p < 0.05$ (One-Way ANOVA, Fisher's LSD).

Shoot growth was similarly affected by Cu treatment (**Figure 3. 26**). Under control conditions, the average shoot lengths of *cyp86b1-1* and *cyp86b1-2* mutants were 18.90 ± 1.7 cm and 18.89 ± 1.6 cm, respectively, comparable to wild-type (19.90 ± 2.1 cm). However, their shoot dry weights (23.20 ± 5.1 mg and 23.08 ± 2.6 mg) were significantly lower than wild-type (27.24 ± 6.5 mg). Under Cu stress, shoot lengths were significantly reduced to 17.10 ± 2.5 cm (wild-type), 15.04 ± 2.4 cm (*cyp86b1-1*), and 14.52 ± 2.8 cm (*cyp86b1-2*), respectively. Correspondingly, shoot dry weight

declined to 22.53 ± 4.2 mg (wild-type), 18.66 ± 2.7 mg (*cyp86b1-1*), and 17.35 ± 4.4 mg (*cyp86b1-2*), respectively. Both mutant lines had significantly lower shoot lengths and dry weights than wild-type under Cu stress, indicating that Cu stress has a more pronounced inhibitory effect on shoot growth in suberin-defective mutants.

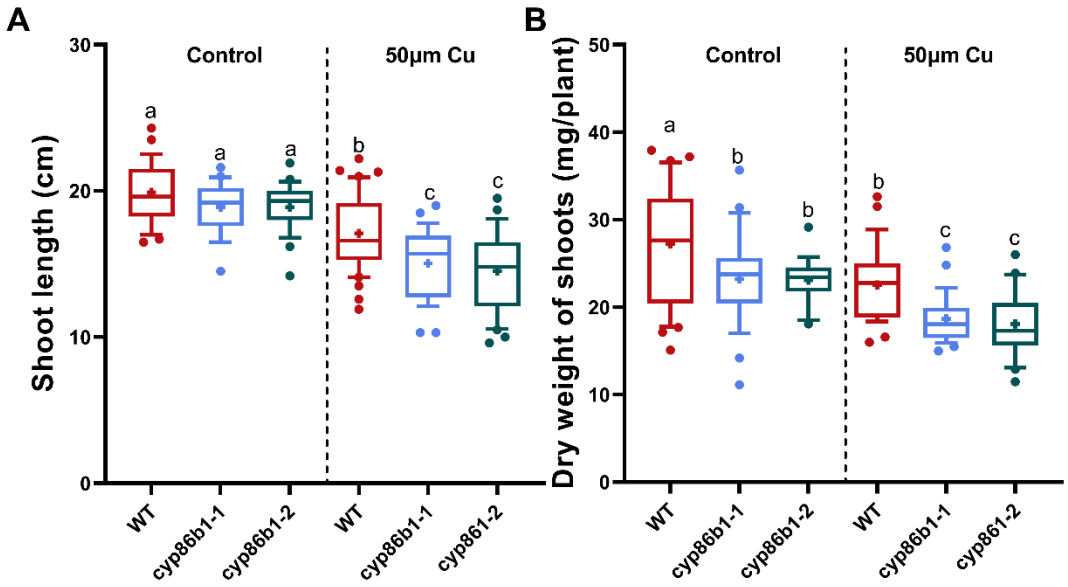

Figure 3. 26 Effect of Cu stress on shoot length (A) and dry weight (B) in wild-type and suberin-defective mutant (*cyp86b1-1* and *cyp86b1-2*) barley under control conditions or 50 µM Cu treatment. Boxplots represent the 10th to 90th percentiles, with "+" indicating the mean. The whiskers extend to outliers. Data are presented based on at least twenty biological replicates. Different letters indicate significant differences at $p < 0.05$ (One-Way ANOVA, Fisher's LSD).

Under Cu stress, all genotypes exhibited significant reductions in root and shoot growth compared to the control. Root length decreased by 22.52% in wild-type, 37.41% in *cyp86b1-1*, and 38.39% in *cyp86b1-2*, while shoot length was reduced by 14.07%, 20.42%, and 23.13%, respectively. Similarly, root dry weight declined by 18.33% (wild-type), 26.03% (*cyp86b1-1*), and 24.27% (*cyp86b1-2*), while shoot dry weight decreased by 17.29%, 19.57%, and 21.69%, respectively. These findings indicate that Cu stress had a stronger inhibitory effect on root growth across all genotypes, with

suberin-defective mutants (*cyp86b1-1* and *cyp86b1-2*) displaying greater susceptibility to Cu-induced growth inhibition than wild-type.

3.9.2 Physiological parameters of suberin-defective mutant

3.9.2.1 Leaf pigment content in suberin-defective mutants

To evaluate the impact of Cu stress on the photosynthetic physiology of barley leaves, the chlorophyll content, flavonoid index, and anthocyanin index in both wild-type and suberin-defective mutant (*cyp86b1-1* and *cyp86b1-2*) leaves after six days of exposure to 50 µM Cu were measured. The results showed that Cu treatment had no significant effect on any of these physiological parameters in either the wild-type or the suberin-defective mutants (**Figure 3. 27**).

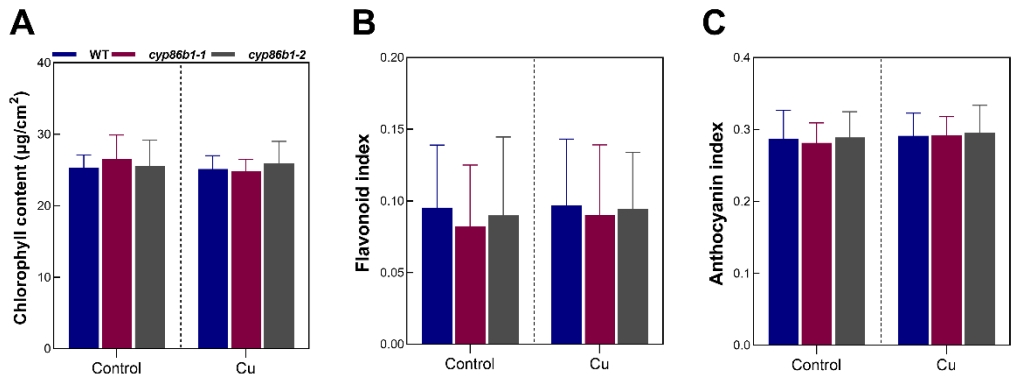

Figure 3. 27 Effect of Cu stress on leaf pigment. Chlorophyll content (A), flavonoid index (B), and anthocyanin index (C) in wild-type and suberin-defective mutants (*cyp86b1-1* and *cyp86b1-2*) leaves under control conditions or 50 µM Cu treatment. Data are presented as mean ± SD of three biological replicates. No significant differences were detected.

3.9.2.2 Chlorophyll fluorescence parameters in suberin-defective mutant

To further investigate the effect of Cu stress on photosynthetic performance, the basic chlorophyll fluorescence parameters (Fv/Fm, ΔF/Fm', qP, qL, qN and NPQ) in dark-adapted wild-type and suberin-defective mutants (*cyp86b1-1* and *cyp86b1-2*) leaves were analyzed by the induction curves. The results indicated no significant differences

between Cu-treated and control plants in any of these parameters for both the wild-type and the suberin-defective mutants (**Figure 3. 28**).

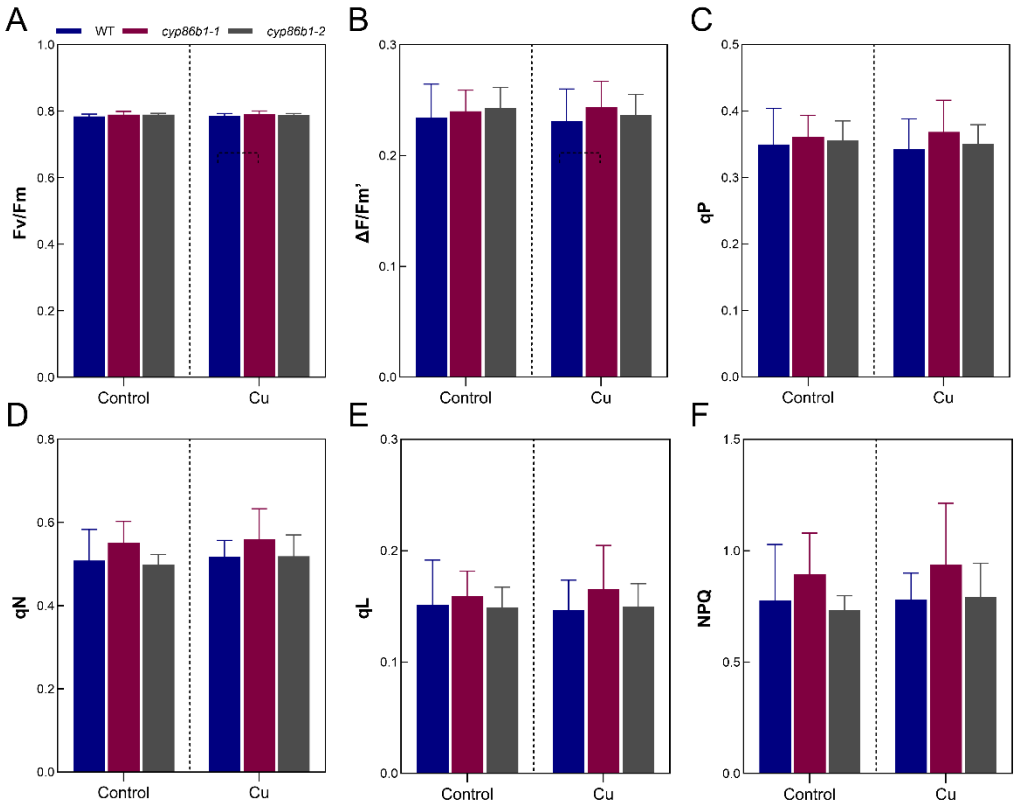

Figure 3. 28 Effect of Cu stress on basic chlorophyll fluorescence parameters. Fv/Fm (A), ΔF/Fm' (B), qP (C), qN (D), qL (E), and NPQ (F) in wild-type and suberin-defective mutants (*cyp86b1-1* and *cyp86b1-2*) leaves under control conditions or 50 μM Cu treatment. Data are presented as mean ± SD of three biological replicates. No significant differences were detected.

To further evaluate photosynthetic performance, the chlorophyll fluorescence light-response parameters (ETRmax, α_ETR, Ek) in wild-type and suberin-defective mutants (*cyp86b1-1* and *cyp86b1-2*) leaves were analyzed. Similar to the basic fluorescence parameters, ETRmax, α_ETR, and Ek showed no significant differences between Cu-treated and control plants in both wild-type and suberin-defective mutants (**Figure 3. 29**).

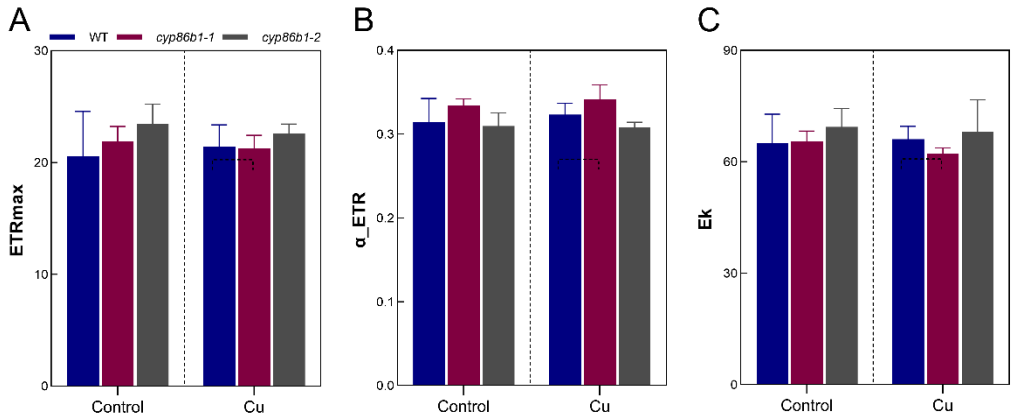

Figure 3. 29 Effect of Cu stress on chlorophyll fluorescence light-response parameters. Maximum electron transport rate (ETRmax) (A), initial slope of the electron transport rate curve (α_ETR) (B), and saturating irradiance level for electron transport (Ek) (C) in wild-type and suberin-defective mutants (*cyp86b1-1* and *cyp86b1-2*) leaves under control conditions or 50 μM Cu treatment. Data are presented as mean ± SD of three biological replicates. No significant differences were detected.

3.9.3 ROS distribution in apical roots and leaves of suberin-defective mutant

To evaluate the effects of Cu stress on ROS accumulation, the distribution of $O_2^{\bullet-}$ and H_2O_2 in root tips and leaves of wild-type and suberin-defective mutants (*cyp86b1-1* and *cyp86b1-2*) was examined using NBT and DAB staining, respectively (**Figure 3. 30**-**Figure 3. 31**). Under control conditions, $O_2^{\bullet-}$ levels in the root tips of *cyp86b1-1* and *cyp86b1-2* mutants were significantly lower compared to the wild-type (**Figure 3. 30**). After six days of exposure to 50 μM Cu, $O_2^{\bullet-}$ levels decreased markedly in all genotypes relative to their respective control levels. Notably, Cu treatment eliminated initial genotype differences, as both wild-type and suberin-defective mutants exhibited similarly reduced $O_2^{\bullet-}$ accumulation under Cu stress. In contrast, H_2O_2 accumulation showed no significant differences between wild-type and mutant plants under control conditions. Under 50 μM Cu treatment, while H_2O_2 levels significantly increased in the root tips of all genotypes, the magnitude of this increase was comparable between wild-

type and suberin-defective mutants. These findings indicate the roots of all genotypes exhibit a similar response in ROS accumulation under Cu stress.

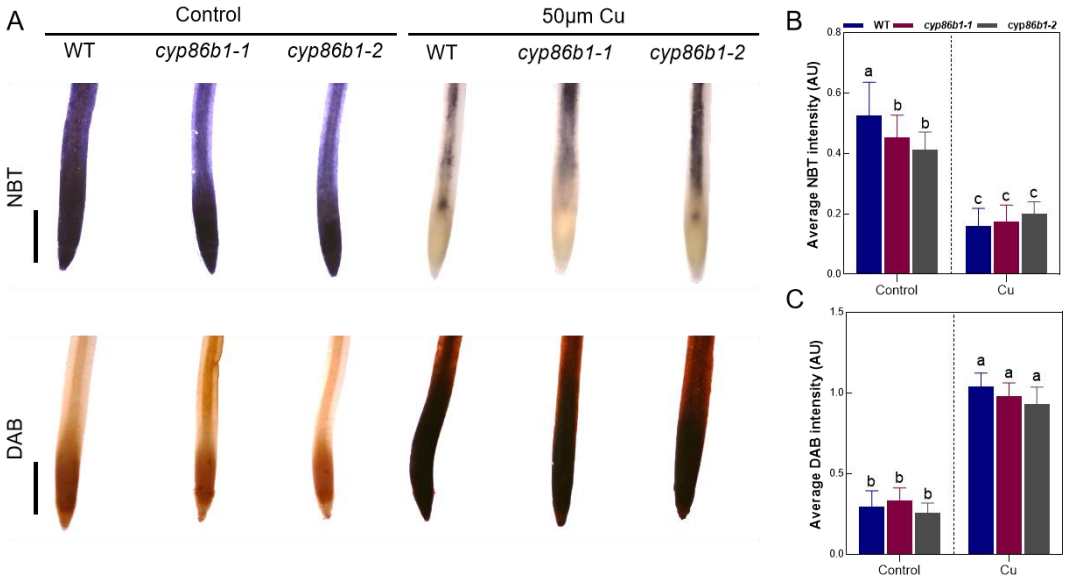

Figure 3. 30 Effect of Cu stress on $O_2^{\bullet-}$ and H_2O_2 accumulation in barley root tips. Histochemical staining of $O_2^{\bullet-}$ (NBT stain, blue) and H_2O_2 (DAB stain, brown) in wild-type and suberin-defective mutants (*cyp86b1-1* and *cyp86b1-2*) barley root tips under control conditions or 50 μM Cu treatment (A). Quantification of NBT staining intensity ($O_2^{\bullet-}$ levels) in root tips (B). Quantification of DAB staining intensity (H_2O_2 levels) in root tips (C). The scale bar represents 250 μm.

Under control conditions, $O_2^{\bullet-}$ levels in the leaves of *cyp86b1-1* and *cyp86b1-2* mutants were significantly lower than those in wild-type plants (**Figure 3. 31**). However, under Cu treatment, $O_2^{\bullet-}$ accumulation in *cyp86b1-1* and *cyp86b1-2* mutant leaves significantly increased, reaching levels comparable to those of wild-type plants. Interestingly, in wild-type leaves, Cu treatment did not significantly alter $O_2^{\bullet-}$ levels, suggesting a genotype-specific response in ROS accumulation under Cu stress. Conversely, H_2O_2 accumulation in leaves remained consistent across all genotypes, with no significant differences observed between wild-type and suberin-defective mutants under both control and Cu stress conditions.

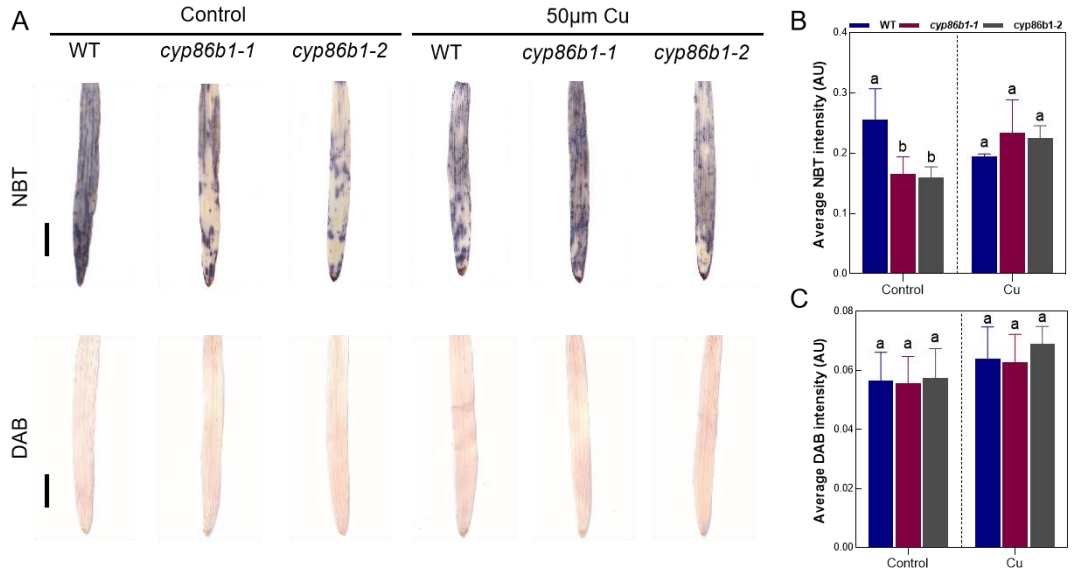

Figure 3. 31 Effect of Cu stress on $O_2^{\bullet-}$ and H_2O_2 accumulation in barley leaves. Histochemical staining of $O_2^{\bullet-}$ (NBT stain, blue) and H_2O_2 (DAB stain, brown) in wild-type and suberin-defective mutants (*cyp86b1-1* and *cyp86b1-2*) barley leaves under control conditions or 50 μM Cu treatment (A). Quantification of NBT staining intensity ($O_2^{\bullet-}$ levels) in leaves (B). Quantification of DAB staining intensity (H_2O_2 levels) in leaves (C). The scale bar represents 1cm.

3.9.4 Lipid peroxidation and proline content a of suberin-defective mutant

To evaluate membrane damage under Cu stress, MDA content in wild-type and suberin-defective mutants (*cyp86b1-1* and *cyp86b1-2*) barley was analyzed as an indicator of lipid peroxidation. In roots, MDA levels were comparable among wild-type and suberin-defective mutants, with no significant difference observed both under control conditions and 50 μM Cu treatment. However, upon Cu treatment, MDA levels in the *cyp86b1-1* and *cyp86b1-2* mutants leaves increased significantly, becoming higher than those in Cu-treated wild-type leaves which remained unchanged (**Figure 3. 32**).

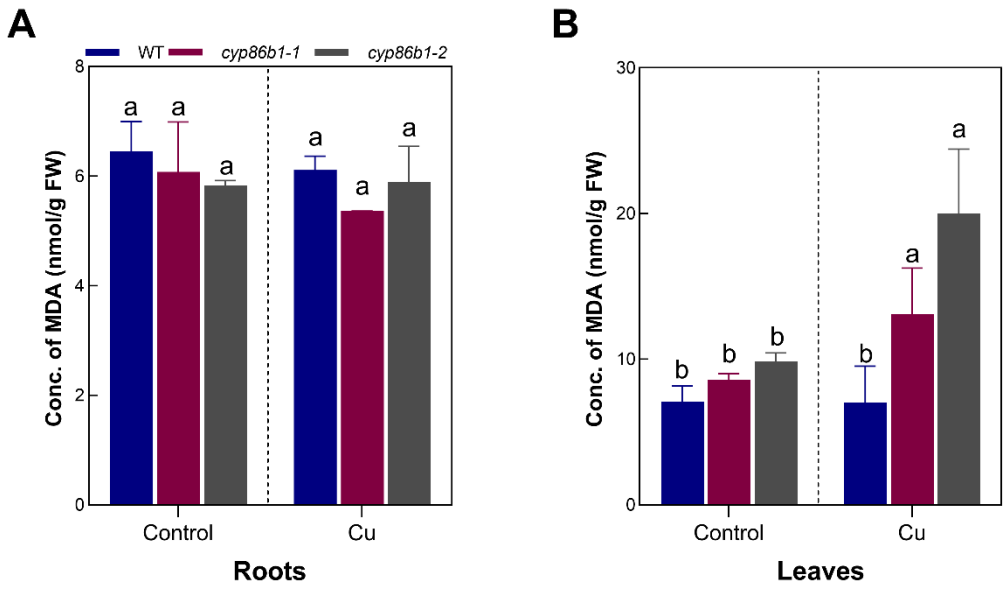

Figure 3. 32 MDA concentration in wild-type and suberin-defective mutants (*cyp86b1-1* and *cyp86b1-2*) barley roots (A) and leaves (B) under control conditions or 50 µM Cu treatment. Data are presented as mean ± SD of three biological replicates. Different letters indicate significant differences at $p < 0.05$ (One-Way ANOVA, Fisher's LSD).

The proline content, a key biomarker for Cu stress response, was measured in wild-type and suberin-defective mutants (*cyp86b1-1* and *cyp86b1-2*) barley. No significant differences in proline content were detected between Cu-treated and control plants in both wild-type and suberin-defective mutants (**Figure 3. 33**).

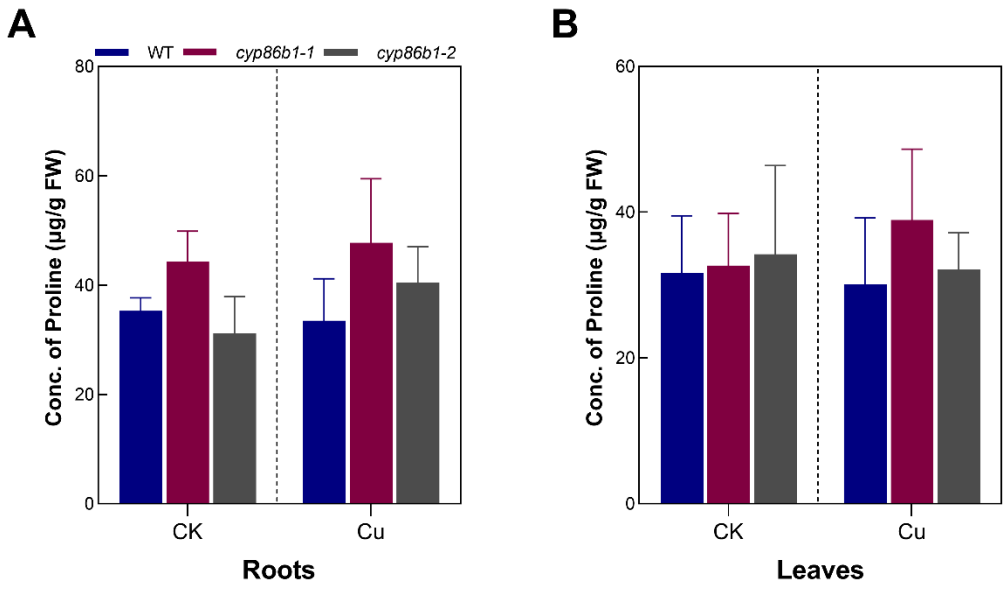

Figure 3. 33 Proline concentration in wild-type and suberin-defective mutants (*cyp86b1-1* and *cyp86b1-2*) barley roots (A) and shoots (B) under control conditions or 50 µM Cu treatment. Data are presented as mean ± SD of three biological replicates. No significant differences were detected.

3.9.5 Suberin lamellae in suberin-defective mutant roots

To examine the formation of suberin lamellae, histochemical analysis was conducted on the endodermis of barley (cv. Golden Promise Fast) wild-type and suberin-defective mutants (*cyp86b1-1* and *cyp86b1-2*) under control conditions or 50 µM Cu treatment (**Figure 3. 34**). Under control conditions, no suberin deposition was detected at 12.5% relative root length in either wild-type or mutant lines. However, under 50 µM Cu stress, earlier and more extensive suberin deposition was observed, leading to complete suberization at 12.5% relative root length. This pattern of accelerated suberization in response to Cu stress was consistent with observations in barley (cv. Scarlett), suggesting a conserved Cu-induced suberin development response in barley. Furthermore, no significant differences in suberin lamellae development were observed between wild-type and suberin-defective mutants (*cyp86b1-1* and *cyp86b1-2*) under

either control conditions or 50 μM Cu treatment, indicating that the mutations did not significantly alter suberin formation in response to Cu stress.

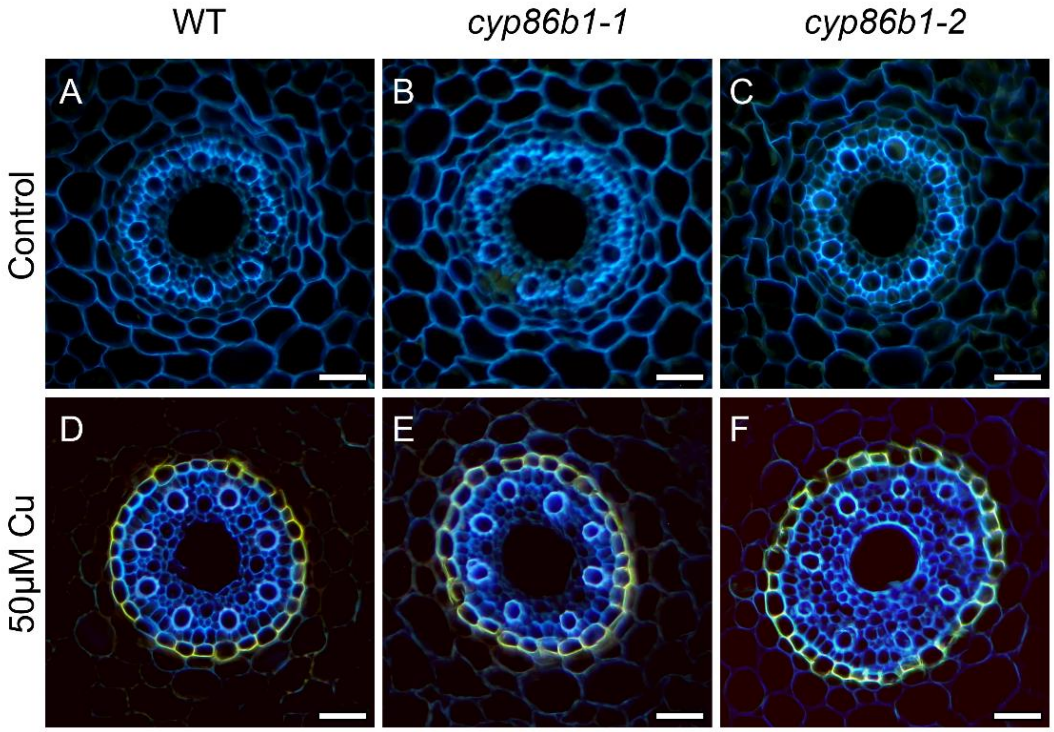

Figure 3. 34 Development of suberin lamellae in the endodermis of wild type and suberin-defective mutants (*cyp86b1-1* and *cyp86b1-2*) barley seminal roots. Suberin lamellae in 12.5% relative length of roots grown under different conditions were stained with fluorol yellow 088. The presence of suberin lamellae is indicated by a bright yellow fluorescence. Suberin lamellae in 12-day-old wild-type (A), *cyp86b1-1* (B) and *cyp86b1-2* (C) roots under control conditions. Suberin lamellae in 12-day-old wild-type (D), *cyp86b1-1* (E) and *cyp86b1-2* (F) roots under 50 μM Cu treatment. The scale bar represents 50 μm.

3.9.6 Chemical analysis of suberin in suberin-defective mutant roots

To further evaluate the impact of Cu stress on suberin biosynthesis, the aliphatic suberin content in roots of wild-type and suberin-defective mutants (*cyp86b1-1* and *cyp86b1-2*) was quantified under control conditions and 50 μM Cu treatment (**Figure 3. 35**). Under control conditions, no significant differences in total aliphatic suberin content

were observed between wild-type and mutants in Zone A and B, whereas Zone C of both mutants exhibited higher suberin content compared to wild-type. Under 50 µM Cu treatment, total aliphatic suberin levels increased significantly in both wild-type and mutants in all root zones. In Zone A, the aliphatic suberin content of wild-type, *cyp86b1-1*, and *cyp86b1-2* increased 9.1-fold, 12.5-fold, and 11.8-fold relative to controls. In Zone B, the aliphatic suberin content of wild-type, *cyp86b1-1*, and *cyp86b1-2* increased 3.7-fold, 6.7-fold, and 9.7-fold relative to controls. In Zone C, the aliphatic suberin content of wild-type, *cyp86b1-1*, and *cyp86b1-2* increased 1.5-fold, 1.6-fold, and 1.6-fold compared to control. These results suggest that Cu stress primarily enhances aliphatic suberin biosynthesis in Zone A, with suberin-defective mutants accumulating significantly higher suberin levels than wild-type in all root zones.

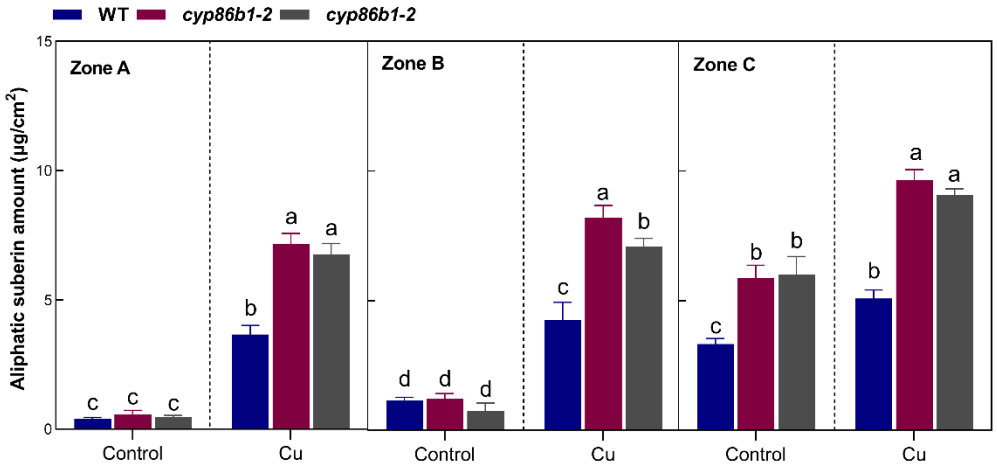

Figure 3. 35 Total amounts of aliphatic suberin in wild-type and suberin-defective mutants (*cyp86b1-1* and *cyp86b1-2*) barley roots under control conditions or 50 µM Cu treatment. Data are presented as mean ± SD of three biological replicates. Different letters indicate significant differences at $p < 0.05$ (One-Way ANOVA, Fisher's LSD).

To further analyze suberin biosynthesis under Cu stress, the four major aliphatic suberin substance classes (primary alcohols, fatty acids, α-ω dicarboxylic acids, and ω-hydroxy acids) were quantified in wild-type and suberin-defective mutants (*cyp86b1-1* and

cyp86b1-2) roots under control and Cu treatment conditions (**Figure 3. 36**). Under control conditions, no significant differences were observed between wild-type and mutants, except for higher fatty acid and diacid levels in Zone C of mutants. However, under Cu treatment, all four suberin substance classes increased significantly in both wild-type and mutants across all root zones. In Zone A, *cyp86b1-1* and *cyp86b1-2* exhibited the highest increase in α-ω dicarboxylic acids and ω-hydroxy acids, suggesting their primary role in suberin biosynthesis under Cu stress. Whereas *cyp86b1-1* and *cyp86b1-2* displayed significantly greater increases in primary alcohols, fatty acids, and diacids than wild-type, with Zone A showing the most pronounced elevation in fatty acids (3.4-fold and 2.8-fold) and diacids (2.4-fold and 2.3-fold) compared to wild-type. Similar trends were also observed in Zones B and C, with *cyp86b1-1* and *cyp86b1-2* accumulating more primary alcohols, fatty acids, and diacids than wild-type. Moreover, although ω-hydroxy acids also increased in the *cyp86b1-1* and *cyp86b1-2* compared to wild-type, they showed the smallest increase among the four suberin components under Cu stress. These findings suggest that Cu stress preferentially enhances the biosynthesis of ω-hydroxy acids and diacids, particularly in the root apical zone (Zone A), which aligns with previous findings in barley (cv. Scarlett). Additionally, suberin-defective mutants displayed significantly higher accumulation of primary alcohols, fatty acids, and diacids than wild-type, suggesting a different regulation in suberin biosynthesis of suberin-defective mutants in response to Cu stress.

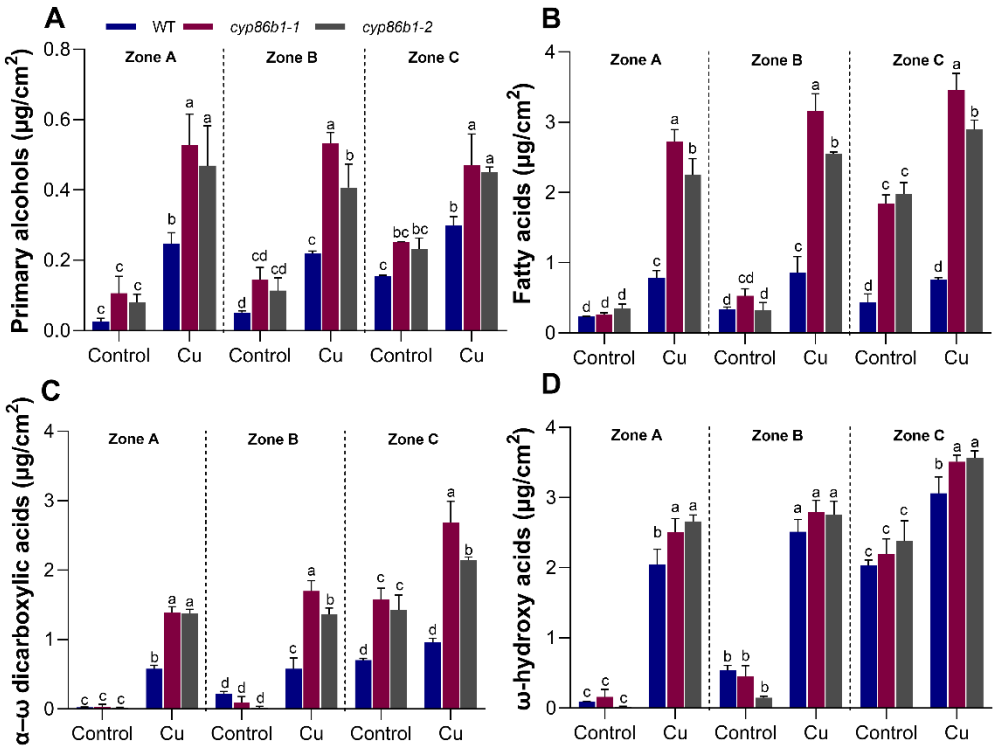

Figure 3. 36 Amounts of substance classes of aliphatic suberin in wild-type and suberin-defective mutants (*cyp86b1-1* and *cyp86b1-2*) barley roots under different conditions. Amounts of primary alcohols (A), fatty acids (B), α-ω dicarboxylic acids (C), and ω-hydroxy acids (D) in different zones of barley roots under control conditions or 50 µM Cu treatment. Data are presented as mean ± SD of three biological replicates. Different letters indicate significant differences at $p < 0.05$ (One-Way ANOVA, Fisher's LSD).

The composition of individual aliphatic suberin monomers was analyzed in roots of 12-day-old wild-type barley and suberin-defective mutants (*cyp86b1-1* and *cyp86b1-2*) under control conditions or 50 µM Cu treatment in three different root zones (**Figure 3. 37**-**Figure 3. 39**). In Zone A, mutants (*cyp86b1-1* and *cyp86b1-2*) lacked detectable levels of C22-C26 ω-OH acids under both control and Cu stress conditions (**Figure 3. 37**). Under control conditions, most monomers showed no significant differences among genotypes, except for significantly higher C18 primary alcohols (alc) and lower C26 ω-OH acids in mutants compared to wild-type. Upon exposure to Cu stress, nearly

all detectable suberin monomers increased significantly in both wild-type and mutants, except for C18 fatty acids, which did not differ significantly. C22-C26 ω-OH acids remained undetectable in mutants even under stress conditions. Notably, *cyp86b1-1* and *cyp86b1-2* mutants exhibited significantly higher levels of most suberin monomers, including C16 alc, C16 ω-OH acids, C18:1 ω-OH acids, C18:1 diacids, and C18-C24 fatty acids, resulting in higher total aliphatic suberin content compared to wild-type under Cu stress.

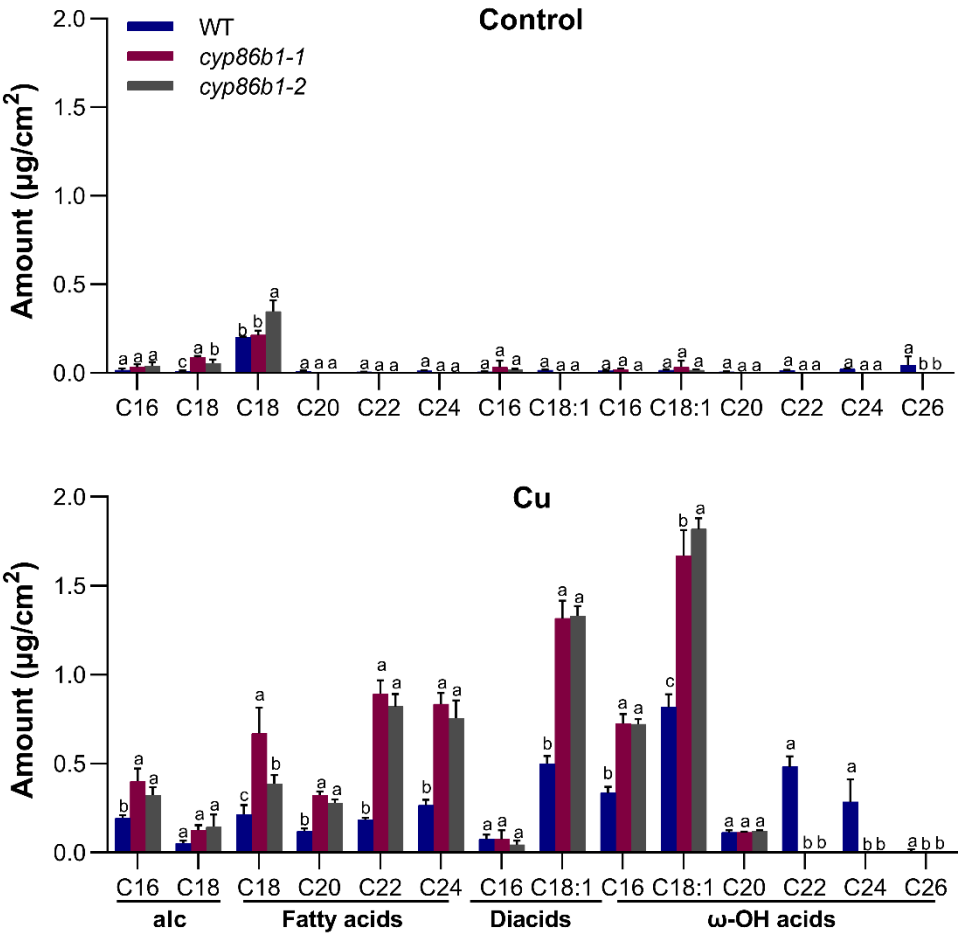

Figure 3. 37 Amounts of monomers of aliphatic suberin in zone A of wild-type and suberin-defective mutants (*cyp86b1-1* and *cyp86b1-2*) barley roots under control conditions or 50 µM Cu treatment. Data are presented as mean ± SD of three biological replicates. Different letters

indicate significant differences at $p < 0.05$ (One-Way ANOVA, Fisher's LSD). Abbreviations: alc, primary alcohols; diacids, α-ω dicarboxylic acids; ω-OH acids, ω-hydroxy acids.

In Zone B, under control conditions, most monomers also showed no significant differences among genotypes, except *cyp86b1-1* and *cyp86b1-2* mutants showed significantly lower levels of C18:1 diacids than wild-type (**Figure 3. 38**). While C22-C26 ω-OH acids were detectable only at low levels in wild-type and remained absent in suberin-defective mutants. Under 50 μM Cu treatment, a general increase in most detectable monomers was observed across all genotypes, consistent with the trends noted in Zone A. Although wild-type exhibited an increase in C22-C26 ω-OH acids under stress, these suberin monomers were still undetectable in *cyp86b1-1* and *cyp86b1-2* mutants. Furthermore, the *cyp86b1-1* and *cyp86b1-2* mutants accumulated significantly higher levels of C16 ω-OH acids, C18:1 ω-OH acids, C18:1 diacids, and C18-C24 fatty acids compared to wild-type, leading to significantly greater total aliphatic suberin content in *cyp86b1-1* and *cyp86b1-2* mutants under Cu stress.

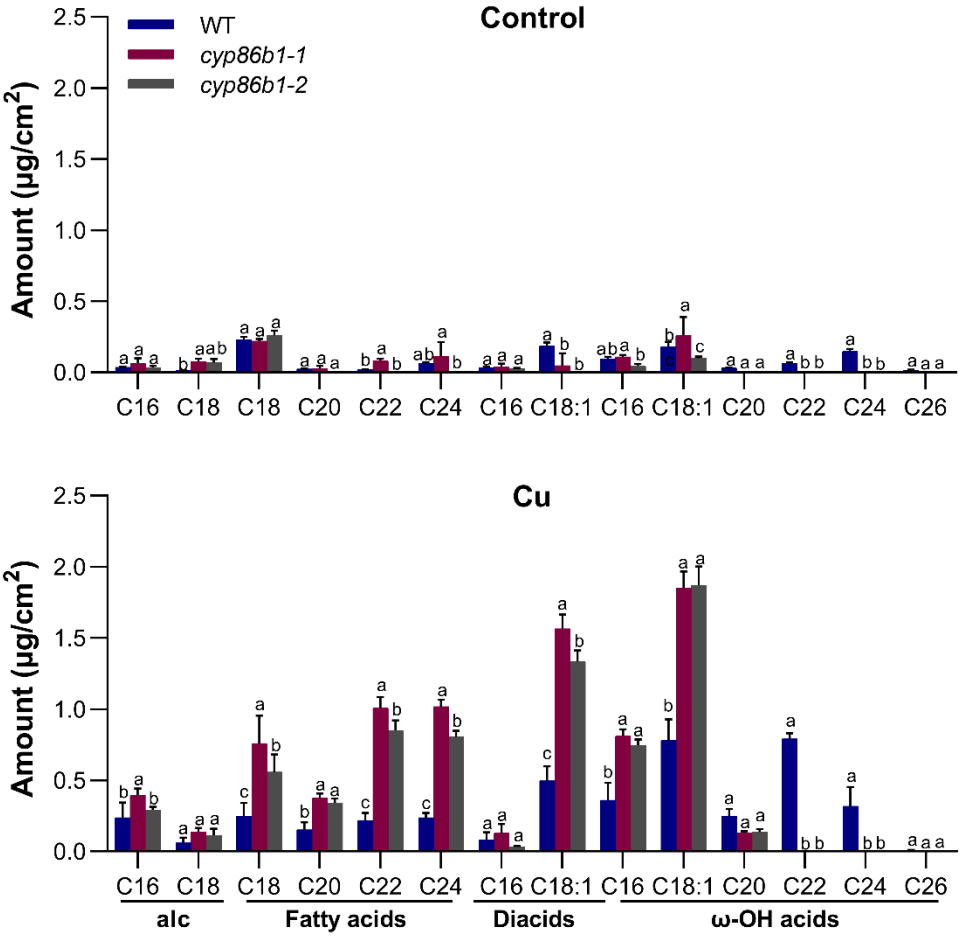

Figure 3. 38 Amounts of monomers of aliphatic suberin in zone B of wild-type and suberin-defective mutants (*cyp86b1-1* and *cyp86b1-2*) barley roots under control conditions or 50 µM Cu treatment. Data are presented as mean ± SD of three biological replicates. Different letters indicate significant differences at $p < 0.05$ (One-Way ANOVA, Fisher's LSD). Abbreviations: alc, primary alcohols; diacids, α-ω dicarboxylic acids; ω-OH acids, ω-hydroxy acids.

In Zone C, under control conditions, *cyp86b1-1* and *cyp86b1-2* mutants continued to lack C22-C26 ω-OH acids, which were present at higher levels in wild-type (**Figure 3. 39**). Conversely, *cyp86b1-1* and *cyp86b1-2* mutants accumulated significantly higher levels of several other monomers, including C16 ω-OH acids, C18:1 ω-OH acids, C18:1 diacids, and C18-C24 fatty acids, leading to increased total aliphatic suberin contents compared to wild-type. Under 50 µM Cu treatment, similar to Zones A and B, significant increases in suberin monomers were observed in all genotypes. Although

wild-type showed upregulation of C22-C26 ω-OH acids, these remained undetectable in the *cyp86b1-1* and *cyp86b1-2* mutants. Nevertheless, *cyp86b1-1* and *cyp86b1-2* mutants consistently accumulated significantly higher amounts of other suberin monomers, including C16 ω-OH acids, C18:1 ω-OH acids, C18:1 α-ω diacids, and C18-C24 fatty acids, relative to wild-type under Cu stress conditions.

Overall, *cyp86b1-1* and *cyp86b1-2* mutants were unable to synthesize C22-C26 ω-OH acids across all root zones under both control and Cu stress conditions. Despite this, both *cyp86b1-1* and *cyp86b1-2* mutants exhibited greater accumulation of alternative suberin monomers (C16 ω-OH acids, C18:1 ω-OH acids, C18:1 diacids, and C18-C24 fatty acids) compared to wild-type under Cu stress. These compensatory changes resulted in increased total aliphatic suberin contents in *cyp86b1-1* and *cyp86b1-2* mutants.

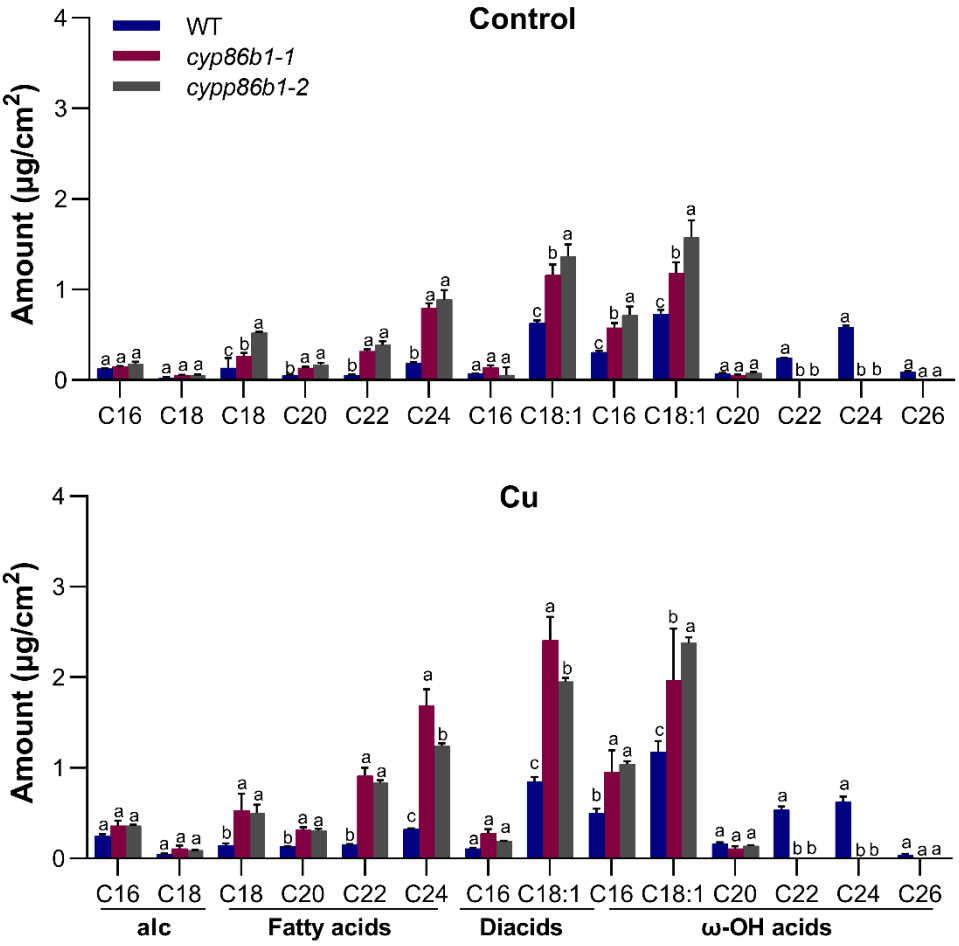

Figure 3. 39 Amounts of monomers of aliphatic suberin in zone C of wild-type and suberin-defective mutants (*cyp86b1-1* and *cyp86b1-2*) barley roots under control conditions or 50 µM Cu treatment. Data are presented as mean ± SD of three biological replicates. Different letters indicate significant differences at $p < 0.05$ (One-Way ANOVA, Fisher's LSD). Abbreviations: alc, primary alcohols; diacids, α-ω dicarboxylic acids; ω-OH acids, ω-hydroxy acids.

3.9.7 Subcellular distribution of copper ions in suberin-defective mutant roots

The subcellular distribution of Cu^{2+} in barley root tips was further examined to understand how suberin deficiency affects Cu^{2+} uptake and transport. The distribution of Cu^{2+} in wild-type and suberin-defective mutants (*cyp86b1-1* and *cyp86b1-2*) root tip cross-sections (0-1 cm from the root tip) was visualized by RBH staining (**Figure 3. 40**). In wild-type root tips after 6 days of 50 µM Cu treatment, copper ions were mainly

sequestered in the cell walls (apoplast) of the outer cell layers, especially epidermal and cortex cells. Only a small amount of Cu^{2+} entered into the inner of the stele (e.g., within the pericycle and xylem vessels) in the wild type. In contrast, *cyp86b1-1* and *cyp86b1-2* mutant root tips accumulated markedly less Cu^{2+} in the apoplast of the epidermis and cortex while showing a strongly increased accumulation of Cu^{2+} in the xylem relative to wild-type. These differences indicate that an intact suberin barrier in endodermal cell walls likely restricts the entry of Cu^{2+} into the xylem vessels.

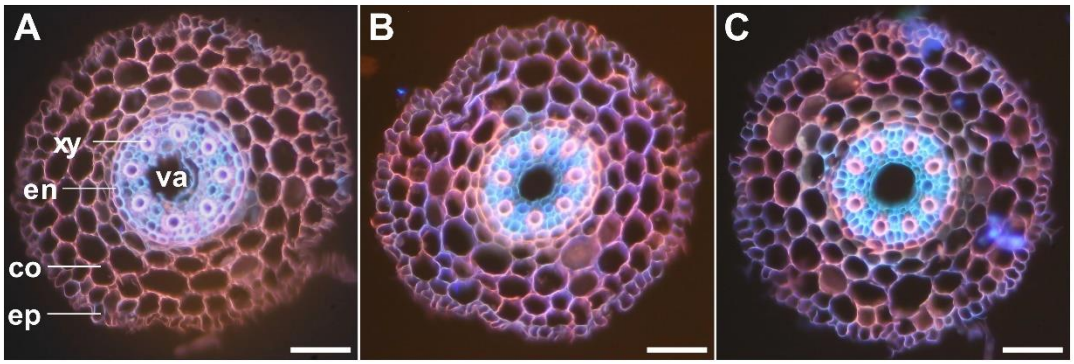

Figure 3. 40 Subcellular distribution of Cu^{2+} in root tips of wild-type (A), *cyp86b1-1* (B), and *cyp86b1-2* (C) barley under 50 μM Cu treatment. Cu^{2+} distribution appears as pink fluorescence after Rhodamine B hydrazide (RBH) staining of root cross-sections (sections taken 0-1 cm from the root tip). ep, epidermis; co, cortex; en, endodermis; xy, xylem; va, vascular tissues. Scale bar = 100 μm.

4. Discussion

4.1 Effect of copper stress on barley morphology

Previous numerous studies have reported that Cu toxicity induced growth inhibition in many species (Zhang et al., 2018c; Reckova et al., 2019; Cao et al., 2023). Align with these results, the results of this study indicated barley exhibited significant inhibition in root growth (root length and root dry weight) and shoot growth (shoot length and shoot dry weight) under 50 μM or 100 μM Cu treatment (**Figure 3. 1**-**Figure 3. 2**). These findings are consistent with previous studies that have demonstrated Cu-induced growth inhibition through the disruption of cell division and elongation (Madejón et al., 2009; Lequeux et al., 2010). The results of this study indicated that roots were more sensitive to Cu than shoots, with root length reductions (44.71-48.89%) exceeding shoot reductions (26.53-29.40%) and root dry weight reductions (26.05-32.12%) exceeding shoot dry weight reductions (16.49-16.65%) (**Figure 3. 1**-**Figure 3. 2**). This differential sensitivity is likely due to Cu tends to accumulate in roots, causing toxicity that first affects root structure and function before impacting aboveground physiological processes (Cambrollé et al., 2013).

4.2 Physiological responses to copper stress in barley

Cu toxicity is well known to inhibit photosynthetic processes through chlorophyll degradation and photosystem II (PSII) impairment across plant species (Pätsikkä et al., 2002; Li et al., 2019a). In contrast, the results of this study indicated that there were no significant changes in the level of leaf pigment including chlorophyll, flavonoid, and anthocyanin of barley leaves under 50 μM or 100 μM Cu treatments for six days (**Figure 3. 3**). Similarly, the results of this study showed there were no significant changes in photochemical efficiency (Fv/Fm, ΔF/Fm', qP, qN, qL, NPQ) and electron transport parameters (ETRmax, α_ETR, Ek) of barley leaves under 50 μM or 100 μM Cu treatments for six days (**Figure 3. 4**-**Figure 3. 5**). However, some studies have shown that many species have less tolerance of short-term 50-100 μM Cu stress

regarding photosynthetic performance (Shabbir et al., 2020). For instance, in some rice or wheat cultivars, short-term 100 μM Cu treatment can trigger significant chlorophyll loss (leaf chlorosis) and a marked decrease in PSII photochemical efficiency (Mostofa et al., 2014; Li et al., 2023). The strong contrast between those outcomes and the present results in barley suggested that as a relative metal-tolerant crop, barley can better tolerate moderate concentrations of Cu treatment in the short term and maintain stable photosynthetic performance. A similar good tolerance of barley photosynthetic performance was also reported in barley under 28 mg/kg cadmium treatment (Vassilev et al., 2004). Considering that barley maintained normal photosynthetic activity under Cu stress, it is likely that the growth inhibition observed in Cu-treated barley may primarily result from root-specific toxicity effects and impaired nutrient absorption rather than direct leaf photosynthetic damage.

4.3 Excess copper induced oxidative stress

Copper is a redox-active metal that catalyzes reactive oxygen species (ROS) production through Haber-Weiss and Fenton reactions, leading to oxidative stress and cellular damage (Kanti Das et al., 2014). Excess Cu triggers ROS bursts, disrupting cellular homeostasis and inhibiting plant growth (Adrees et al., 2015). The results of this study demonstrated that Cu treatment significantly increased H_2O_2 levels in barley root tips while decreasing $O_2^{\bullet-}$ content in roots but increasing $O_2^{\bullet-}$ accumulation in leaves (**Figure 3. 6**-**Figure 3. 7**). ROS plays a dual role in root growth regulation, acting as both signaling molecules and oxidative stress inducers (Tsukagoshi, 2016). A high $O_2^{\bullet-}/H_2O_2$ ratio in root tips promotes cell proliferation, while a low ratio promotes differentiation, leading to meristem exhaustion and root growth inhibition (Eljebbawi et al., 2021). The results of this study align with this model, Cu-induced H_2O_2 accumulation, coupled with reduced $O_2^{\bullet-}$ levels, likely disrupted the root redox balance, prematurely triggering differentiation and limiting elongation. Similar effects have been reported in Arabidopsis, where excessive H_2O_2 suppresses meristematic activity, leading to reduced root growth (Tsukagoshi et al., 2010). Thus, Cu-induced ROS

imbalances in root tips appear to be a major driver of growth suppression in barley. While Cu increased $O_2^{\bullet -}$ content in leaves, the results of this study showed no significant impairment of photosynthetic function. This suggests that barley's antioxidant defense system effectively scavenges ROS to prevent photodamage. Excess Cu disrupts electron transport in chloroplasts, leading to superoxide formation (Karimi et al., 2012), but plants with strong antioxidant capacity can mitigate oxidative stress (Farid et al., 2021). In barley, the stability of photosynthetic parameters under Cu stress indicates efficient ROS detoxification, likely through superoxide dismutase and other enzymatic mechanisms (Karimi et al., 2012). These findings highlight the differential impact of Cu-induced ROS accumulation in roots and leaves. In roots, increased H_2O_2 and a reduced $O_2^{\bullet -}/H_2O_2$ ratio disrupt developmental signaling, inhibiting root growth. In contrast, leaves tolerate ROS accumulation without photosynthetic impairment due to efficient antioxidant defenses.

Excess Cu generates ROS, leading to oxidative stress and cellular damage (Wang et al., 2022). One major consequence is the peroxidation of membrane lipids, which compromises cell integrity. MDA, as a well-known end product of lipid peroxidation, is widely used as a biomarker of ROS-induced oxidative stress (Shulaev and Oliver, 2006). Consistent with the increased production of ROS, the results of this study indicated that Cu stress caused a significant increase in MDA content in barley roots and leaves relative to controls (**Figure 3. 8**). This increase in MDA content indicated enhanced lipid peroxidation and confirms that Cu-generated ROS caused membrane damage in barley cells. To protect against ROS damage, plants have evolved various mechanisms, including proline accumulation, which prevents membrane deformation and scavenges hydroxyl radicals (Tripathi and Gaur, 2004; Tripathi et al., 2006). The results of this study demonstrated that Cu stress induced a marked accumulation of proline in barley roots and leaves (**Figure 3. 9**), suggesting that barley activates proline-mediated defense against Cu toxicity. The increased proline likely helps maintain membrane integrity and detoxify ROS under Cu stress (Mir et al., 2022). Similar

findings have been reported in other species. For example, Cu-exposed chickpea plants with higher proline levels showed lower MDA and improved Cu tolerance (Singh et al., 2010). Moreover, exogenous proline application has been shown to alleviate Cu-induced oxidative damage and growth inhibition in stressed plants, further demonstrating proline's protective role (Noreen et al., 2018). These findings support that proline accumulation is an important adaptive response in barley, helping to mitigate ROS-induced lipid peroxidation and thus reducing cellular damage under Cu stress.

4.4 Suberin biosynthesis and its role under copper stress

Long-term evolution has enabled plants to adapt to environmental stress through plastic endodermal suberin lamellae (Barberon et al., 2016; Doblas et al., 2017; Peralta Ogorek et al., 2023). Histochemical staining results showed that the Cu-treated roots formed suberin lamellae earlier and more intensely in the endodermis (**Figure 3. 10**-**Figure 3. 11**). This suggests that barley roots respond to excessive Cu by rapidly strengthening their endodermis barrier. Similar phenomena have been reported in other species; for example, radish roots exposed to toxic concentrations of Cu formed a large number of suberin/lignin deposits near the root tip (Kováč et al., 2018). The fact that Cu stress induces root suberization in this study highlights that this is a major adaptive response to Cu stress. This finding is also consistent with the common strategy of plants to cope with toxic environments, namely, toxic environment-induced suberization to prevent the entry of toxic elements (Degenhardt, 2000; Vaculík et al., 2012; Líška et al., 2016). Based on these results, this study proposes a hypothesis that under Cu stress, suberin acts as a protective barrier to restrict Cu uptake into the symplast, thereby enhancing the sequestration of Cu in the root apoplast and reducing Cu translocation to shoots.

Since histochemical staining can only qualitatively describe the development of suberin lamellae in response to Cu stress, chemical analysis (gas chromatography and mass spectrometry) was used in this study to directly quantify the suberin content (Kreszies

et al., 2019). The results of chemical analysis showed that barley aliphatic suberin monomers were mainly composed of primary alcohols, fatty acids, α-ω dicarboxylic acids, and ω-hydroxy acids (**Figure 3. 13**-**Figure 3. 14**). This result is consistent with the composition of suberin monomers in barley reported in previous studies (Kreszies et al., 2018). The further chemical analysis results indicated that the increase in aliphatic suberin content under Cu stress may be due to the preferential upregulation of ω-hydroxy acids and α-ω dicarboxylic acids by Cu stress, especially in the root tip (zone A; **Figure 3. 12**-**Figure 3. 14**). ω-hydroxy acids and α-ω dicarboxylic acids, as the main components of the suberin polyester backbone, are crucial for the hydrophobicity of suberin (Graça and Pereira, 2000; Graça, 2015). Therefore, the preferential upregulation of these monomers also implies an enhanced barrier effect in response to Cu stress, which is more hydrophobic and impermeable to Cu ions. The root apex is the main site of Cu absorption and accumulation (Song et al., 2013). In the root apex, under control conditions, since the Casparian strip and the suberin lamellae have not yet been fully formed, Cu ions can be radially transported to the vascular tissue through the apoplast pathway without restriction and then transported to the aerial part through the xylem (Lu et al., 2017). Therefore, the specific accumulation of suberin in the root tips induced by Cu stress in present results is consistent with the universal strategy of plants to limit the entry of toxic substances (Degenhardt, 2000; Vaculík et al., 2012; Líška et al., 2016), and also strengthens the hypothesis proposed in this study that suberin acts as a protective barrier to restrict Cu uptake into the symplast, thereby enhancing the sequestration of Cu in the root apoplast and reducing Cu translocation to shoots.

4.5 Excess copper induced nutrient imbalance

A key defense strategy observed in hyperaccumulators is that plants utilize metal sequestration in roots to minimize heavy metal toxicity in aerial tissues (Emamverdian et al., 2015). In this study, Cu content in barley roots increased proportionally with external Cu concentration. While shoot Cu levels increased under Cu stress, they accounted for only 0.7% of root Cu concentration, which is even lower than the control

(**Table 3. 1**). A similar result was also reported in mustard under Cu stress (Sharma et al., 2019), suggesting that restricted Cu translocation is a common protective mechanism in plants. Cell wall (apoplast) sequestration plays a crucial role in Cu resistance (Kholodova et al., 2011). The results of Cu staining in root tip cross-sections revealed that under control conditions, Cu was primarily localized in epidermal and cortex cells, with minimal distribution in the endodermis and vascular tissues (**Figure 3. 15**). However, Cu treatment significantly increased Cu accumulation in the cell walls (apoplasts) of epidermal and cortex cells. Notably, Cu also accumulated in the facing cortex-side apoplast of the endoderm. In contrast, xylem tissues, which are responsible for Cu translocation to shoots, did not exhibit a significant increase in Cu content. These findings suggest that apoplastic sequestration in roots prevents excessive Cu entry into the symplast, limiting xylem loading and shoot translocation. This supports the hypothesis of this study that suberin functions as a key protective barrier restricting Cu uptake into vascular tissues. Excess Cu also disrupts nutrient uptake, which contributes substantially to the overall phytotoxic effects observed in plants (Lequeux et al., 2010; Li et al., 2019b). In this study, Cu stress strongly reduced K, Ca, Mg, Fe, Zn, and Mn concentrations in both roots and leaves. High Cu levels have been shown to interfere with the absorption of these essential minerals, resulting in nutrient imbalances and deficiencies in aboveground tissues (Zhao et al., 2012). The observed decline in nutrient content aligns with previous reports demonstrating that excess Cu alters root morphology and competes with other metal ions at root transport sites, thereby impairing their uptake and homeostasis (Roy et al., 2017; Feil et al., 2020). Considering that photosynthetic parameters remained stable under Cu stress conditions, it is likely that the growth inhibition observed in barley was primarily due to root impairment and subsequent limitations in nutrient acquisition (Bouazizi et al., 2010a; Zhao et al., 2012). Notably, since only a single biological replicate sample was used for the elemental analysis, this part of the discussion can only draw limited conclusions based on

preliminary results. And suggest follow-up studies with multiple biological replicates to validate the initial observations.

4.6 Transcriptomic responses of barley roots to copper stress

The results of transcriptomic analysis identified extensive transcriptional changes in barley roots under Cu stress, including 886 upregulated and 1212 downregulated genes (**Figure 3. 17**). These marked changes indicate a strong transcriptional response consistent with previous studies reporting significant transcriptomic reprogramming in plants exposed to heavy metal stress (Dubey et al., 2014; Wa Lwalaba et al., 2021). Further functional analyses using KEGG pathway and GO enrichment revealed a complex regulatory network involving cell wall modification (lignin and suberin biosynthesis), detoxification mechanisms, antioxidant defenses, Cu transport, and hormone signaling pathways (**Figure 3. 18**-**Figure 3. 19**). Similar transcriptional patterns have also been observed in other species under heavy metal stress (Lin et al., 2013; Luo et al., 2024), indicating conserved molecular mechanisms across plant species for metal tolerance. Notably, transcriptome analysis identified a unique enrichment of the suberin biosynthetic pathway, distinguishing the findings in this study from previous studies and highlighting the key role of suberin in mediating Cu tolerance in barley.

The results of transcriptomic data presented here further clarify the molecular response pathways activated by Cu stress (**Figure 3. 20**, **Table S2**). Among these, cell wall modification was particularly remarkable. The plant cell wall is recognized as a primary defensive barrier, limiting metal entry into cellular compartments (Krzesłowska, 2011). The results of this study revealed that Cu stress significantly upregulated the expression of *WAK* genes and *PME* genes. *WAK* regulates *PME* activity, modulating pectin methyl esterification to enhance the cell wall's capacity for metal sequestration (Xia et al., 2018). This highlights the role of cell wall modification in Cu tolerance, reducing Cu entry into the symplast.

Despite observed increases in suberin content through histochemical and chemical analyses, the results of transcriptomic data indicated downregulation of the key suberin biosynthesis genes *CYP86A1* and *CYP86B1* throughout the root after five days of exposure to 50 μM Cu. The results of spatial and temporal expression analyses explained this discrepancy by showing that *CYP86A1* and *CYP86B1* expression initially increased (0-3 days) throughout the root but was later downregulated in the complete suberized root zone (Zone B and Zone C) after six days of exposure to 50 μM Cu, except in the youngest root zone (Zone A, incompletely suberized root zone) (**Figure 3. 21**-**Figure 3. 22**). Suberin deposition has been reported to restrict metal entry, but excessive accumulation can impair water and nutrient transport (Ranathunge et al., 2011). Thus, initial induction of suberin synthesis in the incompletely suberized root zone likely enhanced early-stage Cu tolerance, while subsequent gene downregulation in the completely suberized root zone avoided excessive deposition to maintain root functions. This spatiotemporal-specific regulation of suberin synthesis is also consistent with a general strategy of plant growth-defense trade-offs (Karasov et al., 2017; He et al., 2022).

Lignin biosynthesis also contributes to the strengthening of root cell walls, effectively reducing Cu mobility and translocation (Bouazizi et al., 2010b; Tugbaeva et al., 2022). Contrary to previous reports of lignin gene upregulation under metal stress (Ren et al., 2022), the results of transcriptomic analysis revealed that lignin biosynthesis genes were downregulated after five days of exposure to 50 μM Cu. Early lignin deposition likely contributes to Cu sequestration, but prolonged synthesis may be downregulated to prevent excessive rigidity and lignification, ensuring continued root growth (Nair and Chung, 2014). This finding explained the discrepancy between this study and previous studies and indicated that lignin biosynthesis likely exhibits a similar spatiotemporal-specific regulation observed in suberin biosynthesis. However, this hypothesis needs to be validated by further lignin staining analysis, chemical analysis and gene expression analysis.

Reducing Cu uptake and enhancing cellular detoxification represent two primary strategies plants employ to mitigate Cu toxicity (Adrees et al., 2015). The results of transcriptomic analysis revealed that Cu stress significantly downregulated the expression of metal transporter genes (*ZIP2, YSL4/6, HMA2*), the Cu chaperone gene (*ATX1*), and the Cu chelator genes (*NAS1/2/3*), thereby limiting Cu absorption and translocation. In contrast, genes associated with cellular detoxification mechanisms, including *MT2*, *HIPP* genes, and *HSP* genes, were markedly upregulated. Their coded proteins function by intracellularly sequestering excess Cu and enhancing antioxidant activity, thereby minimizing oxidative damage and enhancing tolerance (Liu et al., 2015; Cui et al., 2019; Xiong et al., 2023). These findings highlight a dual adaptive strategy involving restricted Cu uptake and active cellular detoxification (Clemens, 2001; Kosakivska et al., 2021).

Excess Cu generates ROS, resulting in a strong antioxidant response (Mir et al., 2021). The results of transcriptomic analysis revealed that Cu stress upregulated the expression of antioxidant enzyme genes, including *CSD1/2*, *GST* genes, and *CAT2*, which help scavenge ROS and mitigate oxidative stress (Cao et al., 2019; Tiwari et al., 2022). This reinforced antioxidant defense system is crucial for Cu tolerance, alleviating cellular damage caused by Cu-induced oxidative stress (Boojar and Goodarzi, 2007; Madejón et al., 2009).

Multiple hormone signaling pathways are involved in plant responses to Cu stress (Wang et al., 2024). The results of transcriptomic analysis indicated that Cu stress downregulated the related genes in auxin and cytokinin signaling pathways, likely suppressing root growth to conserve energy for stress adaptation. In contrast, genes related to ABA and ethylene signaling pathways, including *PP2C4*, *SnRK2*, and *EIN3*, involved in regulating suberin biosynthesis, were significantly upregulated (Barberon et al., 2016). RT-qPCR analysis further confirmed Cu-induced upregulation of ABA pathway genes at early stages (0-3 days) (**Figure 3. 23**), supporting its role in early suberin induction (Wei et al., 2020). Ethylene, known to antagonize suberin synthesis,

may contribute to feedback inhibition, preventing excessive suberin accumulation (Chen et al., 2025). This hormonal crosstalk optimizes growth-defense trade-offs, balancing Cu tolerance with root development.

4.7 Effect of copper stress on suberin-defective mutant

Biochemical and molecular data in this study indicated that suberin plays a critical role in Cu tolerance in barley, and the *CYP86B1* gene is involved in suberin biosynthesis under Cu stress. To further investigate this, the effects of Cu stress on the morphology, physiology, biochemistry, and suberin biosynthesis of the barley (cv. Golden Promise Fast) wild-type and its suberin-defective mutants (*cyp86b1-1* and *cyp86b1-2*) were analyzed. The results of this study demonstrated that suberin-defective mutants (*cyp86b1-1* and *cyp86b1-2*) exhibited significantly stronger inhibition of root and shoot growth under 50 μM Cu treatment compared to wild-type plants (**Figure 3. 25**-**Figure 3. 26**). These results indicated that suberin-defective mutants with impaired suberin biosynthesis are more susceptible to Cu-induced toxicity, highlighting the protective role of suberin as a barrier against heavy metal uptake. This conclusion aligns with previous studies emphasizing the general importance of suberin in plant defense against metal stress (Cheng et al., 2014; Cheng et al., 2015).

Interestingly, despite significant growth inhibition, the results of this study indicated that leaf pigment composition and chlorophyll fluorescence parameters (including PSII efficiency) were not significantly affected by Cu treatment in either wild-type or suberin-defective mutants (**Figure 3. 27**-**Figure 3. 29**). This outcome aligns with earlier observations in the barley (cv. Scarlett), confirming the tolerance of barley photosynthetic apparatus under moderate metal toxicity (Vassilev et al., 2004). The stable photosynthetic parameters suggest that growth inhibition in barley likely results from root-specific damage or impaired water and nutrient transport rather than from direct leaf photosynthetic impairment.

Furthermore, different genotype-dependent oxidative stress responses under Cu treatment were observed. Specifically, the results of this study indicated that Cu-induced increases in leaf $O_2^{\bullet -}$ and MDA levels only occurred in suberin-defective mutants, whereas these parameters remained unchanged in wild-type plants (**Figure 3. 31**-**Figure 3. 32**). While this increased oxidative stress in suberin-defective mutants is likely due to the absence of effective suberin barriers, resulting in increased Cu accumulation in shoots. Notably, despite increased oxidative stress in leaves, the results of this study indicated that root MDA content remained unaffected by Cu stress in all genotypes. This discrepancy indicates that Cu-induced oxidative stress responses differ in various plant tissues, likely due to differences in tissue-specific metal distribution mechanisms or antioxidant responses. Moreover, contrary to the results of this study in barley (cv. Scarlett) and some previous findings (Chen et al., 2001; Singh et al., 2010), Cu stress did not induce significant changes in proline accumulation in either wild-type or suberin-defective mutants barley (cv. Golden Promise Fast) leaves or roots under experimental conditions in this study (**Figure 3. 33**). These results suggest that Cu-induced proline responses in barley may be cultivar-specific or more relevant under severe Cu stress conditions (Schat et al., 1997; Szafrańska et al., 2011).

Histochemical analysis results demonstrated rapid and complete suberin deposition in the root endodermis of all genotypes under Cu stress (**Figure 3. 34**). Despite the mutations, *cyp86b1-1* and *cyp86b1-2* mutants exhibited similar suberin lamellae formation patterns compared to wild-type, consistent with previous findings in Arabidopsis that suberin deposition pattern was unaltered in suberin-defective mutants (Calvo-Polanco et al., 2021). These findings suggest that while *CYP86B1* mutation alters suberin chemical composition, it does not alter the formation pattern of suberin barriers in roots under Cu stress.

Chemical analysis results revealed marked increases in total aliphatic suberin content of wild-type and suberin-defective mutants under Cu treatment across all root zones (**Figure 3. 35**). Suberin-defective mutants showed notably greater accumulation of

aliphatic suberin content compared to wild-type, particularly in zone A (the youngest root zone). Detailed analysis of suberin compositions indicated a marked increase in α-ω dicarboxylic acids and ω-hydroxy acids in all genotypes under Cu treatment, highlighting their primary role in Cu-induced suberin synthesis (**Figure 3. 36**) (Graça and Pereira, 2000; Graça, 2015). However, suberin-defective mutants exhibited a specific lack of C22-C26 very long chain (C > 20) ω-hydroxy acids across all conditions and zones (**Figure 3. 37**-**Figure 3. 39**). This is consistent with the function of the *CYP86B1* gene reported in Arabidopsis, which is responsible for the synthesis of very long chain (C > 20) ω-hydroxy acids (Compagnon et al., 2009). Interestingly, this deficiency in suberin-defective mutants activated compensatory increases of other suberin monomers, including ω-hydroxy acids, fatty acids, and α-ω dicarboxylic acids, contributing to the higher aliphatic suberin content. This altered composition suggests compensatory biosynthesis pathways are activated in the absence of functional *CYP86B1* enzyme activity, consistent with previous findings in Arabidopsis (Compagnon et al., 2009; Yadav et al., 2014). The increased suberin levels in *cyp86b1* mutants may be a compensatory mechanism to maintain barrier integrity and function. ω-Hydroxy acids and α-ω dicarboxylic acids, as the main components of aliphatic suberin, are mainly synthesized by two genes, *CYP86A1* and *CYP86B1* (Franke et al., 2005; Nomberg et al., 2022). Fatty acids are components of suberin and are used as precursors for the synthesis of ω-hydroxy acids and α-ω dicarboxylic acids. The results of this study showed that this metabolic compensation specifically increased the production of C16 and C18:1 ω-hydroxy acids and C18:1 diacids synthesized by *CYP86A1*, as well as the content of fatty acids as precursors for suberin synthesis. Therefore, this metabolic compensation seems to involve redirecting metabolic flux to other suberin synthesis branches and upstream precursors. The study on *CYP86B1* mutants in Arabidopsis has also observed similar metabolic compensation mediated by metabolic flux redirection (Compagnon et al., 2009). Despite increased suberin deposition, *cyp86b1* mutants remained more sensitive to Cu stress. This indicates that

Cu tolerance depends not only on suberin quantity but also critically on its chemical composition. Studies in Arabidopsis demonstrate that suberin monomer composition is essential for barrier integrity, with specific monomers contributing significantly to suberin functionality and overall barrier properties (Ranathunge and Schreiber, 2011). Specifically, very long chain ω-hydroxy acids (C22-C26 ω-OH acids) likely enhance hydrophobicity and impermeability of suberin polymers, critical features for restricting metal uptake and transport within roots (Graça, 2015). This was further confirmed by the study on *CYP86B1* mutants in Arabidopsis, which exhibited enhanced root hydraulic conductivity (Calvo-Polanco et al., 2021). Thus, their absence in *cyp86b1-1* and *cyp86b1-2* mutants likely disrupts polymer integrity, resulting in increased permeability to Cu ions. Cu ions staining results further demonstrated the functional significance of suberin composition in limiting Cu translocation into inner root tissues (**Figure 3. 40**). Under Cu stress, in wild-type plants, Cu was mainly restricted to apoplastic regions of epidermal and cortex cells, whereas *cyp86b1-1* and *cyp86b1-2* mutants showed significantly enhanced Cu accumulation within xylem vessels. Such increased Cu entry into vascular tissues in mutants indicates that compromised suberin barriers allow increased Cu transport into the shoot, worsening toxicity effects and explaining the observed heightened susceptibility in mutants. These results highlight the important role of specific very long chain ω-hydroxy acids in suberin barrier integrity and function.

5. Conclusion

Cu contamination, primarily resulting from anthropogenic activities, is a critical environmental stress that adversely affects plant growth and development. Suberin deposition in root endodermal cells is considered an essential protective mechanism against environmental stress. However, the specific role of suberin under Cu stress remains unclear. This study aimed to clarify Cu-induced phytotoxicity and elucidate the protective role of suberin biosynthesis in barley under Cu stress.

In this study, the morphological, physiological, biochemical, and molecular responses of 12-day-old barley (cv. Scarlett) seedlings subjected to 50 μM or 100 μM Cu treatments for six days were investigated. The results of this study demonstrated that Cu stress significantly inhibited barley growth, with roots exhibiting greater sensitivity compared to shoots. Despite evident growth inhibition, photosynthetic parameters, including pigment composition and chlorophyll fluorescence parameters, remained stable under Cu treatment. Cu stress triggered oxidative stress in barley, characterized by H_2O_2 accumulation in roots, decreased $O_2^{\bullet -}$ levels in roots, and increased $O_2^{\bullet -}$ content in leaves. As a result, barley plants accumulated proline in both roots and leaves, likely mitigating oxidative stress. The results of histochemical and chemical analyses demonstrated that Cu stress accelerated suberin deposition in barley roots, especially through increased synthesis of aliphatic suberin monomers (ω-hydroxy acids and α-ω dicarboxylic acids), particularly at the root apex (Zone A, 0-25% root length). Additionally, Cu stress affected the uptake of essential mineral nutrients, disrupting nutrient homeostasis. Histochemical analysis of Cu distribution in root cross-sections and mineral nutrition analysis indicated that suberin served as an effective endodermis barrier, limiting the xylem loading of Cu ions. Consequently, Cu primarily accumulated in root apoplastic regions, significantly reducing its translocation to shoots and alleviating shoot toxicity. Transcriptomic analysis revealed a complex regulatory

network involving cell wall modifications (lignin and suberin biosynthesis), detoxification pathways, antioxidant defense mechanisms, Cu transport regulation, and hormone signaling pathways in response to Cu stress. Transcriptome analysis and RT-qPCR analysis further revealed that Cu-induced spatiotemporal-specific regulation of key suberin biosynthesis genes, *CYP86A1* and *CYP86B1*, was up-regulated throughout the roots during the early Cu exposure stage (0-3 days), possibly mediated by ABA signaling. However, the expression of these genes decreased throughout the roots during later stages (5-6 days), except in the youngest root zone (Zone A).

Moreover, the Cu stress effect on wild-type and suberin-defective mutant (*cyp86b1-1* and *cyp86b1-2*) barley seedlings was investigated. Compared to wild-type plants, suberin-defective mutants showed enhanced sensitivity to Cu stress, evidenced by stronger growth inhibition and increased oxidative stress (significantly increased $O_2^{\bullet -}$ and MDA content only in mutant leaves). Chemical analysis revealed that mutants lacked very long chain (C22-C26, carbon chain length >20) ω-hydroxy acids under all experimental conditions and root zones. However, this deficiency triggered compensatory increases in other suberin monomers, resulting in increased total aliphatic suberin content under Cu stress. Furthermore, copper ion staining analysis indicated an impaired barrier function in the mutants, with greater Cu accumulation in xylem vessels. These findings highlight the important role of specific very long chain ω-hydroxy acids in suberin barrier integrity and function.

Overall, this study provides comprehensive insights into Cu-induced phytotoxicity and highlights the important protective function of suberin as an endodermis barrier in barley roots. The findings of this study provide new insights into varietal selection and genetic improvement aimed at enhancing Cu tolerance and provide a useful genetic resource for future studies in enhancing Cu tolerance and improving the phytoremediation potential of barley and other crops in Cu-contaminated soil.

6. References

Abdel-Ghany SE (2009) Contribution of plastocyanin isoforms to photosynthesis and copper homeostasis in *Arabidopsis thaliana* grown at different copper regimes. Planta **229**: 767–779

Abdel-Ghany SE, Burkhead JL, Gogolin KA, Andrés-Colás N, Bodecker JR, Puig S, Peñarrubia L, Pilon M (2005) AtCCS is a functional homolog of the yeast copper chaperone Ccs1/Lys7. FEBS Lett **579**: 2307–2312

Adeleke R, Nwangburuka C, Oboirien B (2017) Origins, roles and fate of organic acids in soils: A review. S Afr J Bot **108**: 393–406

Adrees M, Ali S, Rizwan M, Ibrahim M, Abbas F, Farid M, Zia-ur-Rehman M, Irshad MK, Bharwana SA (2015) The effect of excess copper on growth and physiology of important food crops: a review. Environ Sci Pollut Res **22**: 8148–8162

Alengebawy A, Abdelkhalek ST, Qureshi SR, Wang MQ (2021) Heavy metals and pesticides toxicity in agricultural soil and plants: ecological risks and human health implications. Toxics **9**: 42

Al-Hakimi ABM, Hamada AM (2011) Ascorbic acid, thiamine or salicylic acid induced changes in some physiological parameters in wheat grown under copper stress. Plant Prot Sci **47**: 92–108

Aly AA, Mohamed AA (2012) The impact of copper ion on growth, thiol compounds and lipid peroxidation in two maize cultivars ('*Zea mays*' L.) grown'in vitro'. Aust J Crop Sci **6**: 541–549

Andrés-Colás N, Sancenón V, Rodríguez-Navarro S, Mayo S, Thiele DJ, Ecker JR, Puig S, Peñarrubia L (2006) The Arabidopsis heavy metal P-type ATPase HMA5

interacts with metallochaperones and functions in copper detoxification of roots. Plant J **45**: 225–236

Anwar Hossain M, Hoque MdA, Burritt DJ, Fujita M (2014) Chapter 16 - Proline protects plants against abiotic oxidative stress: biochemical and molecular mechanisms. *In* P Ahmad, ed, Oxidative Damage to Plants. Academic Press, San Diego, pp 477–522

Apori OS, Hanyabui E, Asiamah YJ (2018) Remediation technology for copper contaminated soil: a review. Asian J Agric Res **8**: 1–7

Arslan Ö, Çulha Erdal Ş, Ekmekçi Y (2022) Salt pretreatment-mediated alleviation of boron toxicity in safflower cultivars: growth, boron accumulation, photochemical activities, antioxidantdefense response. Plants **11**: 2316

Azeez MO, Adesanwo OO, Adepetu JA (2015) Effect of Copper (Cu) application on soil available nutrients and uptake. Afr J Agric Res **10**: 359–364

Ballabio C, Panagos P, Lugato E, Huang JH, Orgiazzi A, Jones A, Fernández-Ugalde O, Borrelli P, Montanarella L (2018) Copper distribution in European topsoils: An assessment based on LUCAS soil survey. Sci Total Environ **636**: 282–298

Barberon M, Vermeer JEM, De Bellis D, Wang P, Naseer S, Andersen TG, Humbel BM, Nawrath C, Takano J, Salt DE, et al (2016) Adaptation of root function by nutrient-induced plasticity of endodermal differentiation. Cell **164**: 447–459

Bates L, Waldren R, Tears I (1973) Rapid determination of free proline for water-stress studies. Plant Soil **39**: 205–207

Batool R, Hameed M, Ashraf M, Ahmad MSA, Fatima S (2015) Physio-anatomical responses of plants to heavy metals. *In* M Öztürk, M Ashraf, A Aksoy, MSA Ahmad, eds, Phytoremediation for Green Energy. Springer, Netherlands, pp 79–96

Baxter I, Hosmani PS, Rus A, Lahner B, Borevitz JO, Muthukumar B, Mickelbart MV, Schreiber L, Franke RB, Salt DE (2009) Root suberin forms an extracellular

barrier that affects water relations and mineral nutrition in Arabidopsis. PLoS Genet **5**: e1000492

Benjamini Y, Hochberg Y (1995) Controlling the false discovery rate: a practical and powerful approach to multiple testing. J R Stat Soc B **57**: 289–300

Bernal M, Casero D, Singh V, Wilson GT, Grande A, Yang H, Dodani SC, Pellegrini M, Huijser P, Connolly EL, et al (2012) Transcriptome sequencing identifies *SPL7*-regulated copper acquisition genes *FRO4*/*FRO5* and the copper dependence of iron homeostasis in Arabidopsis. Plant Cell **24**: 738–761

Bernal M, Sánchez-Testillano P, Risueño MDC, Yruela I (2006) Excess copper induces structural changes in cultured photosynthetic soybean cells. Funct Plant Biol **33**: 1001

Blaby-Haas CE, Padilla-Benavides T, Stübe R, Argüello JM, Merchant SS (2014) Evolution of a plant-specific copper chaperone family for chloroplast copper homeostasis. Proc Natl Acad Sci USA **111**: E5480–E5487

Boden JS, Konhauser KO, Robbins LJ, Sánchez-Baracaldo P (2021) Timing the evolution of antioxidant enzymes in cyanobacteria. Nat Commun **12**: 4742

Boojar MMA, Goodarzi F (2007) The copper tolerance strategies and the role of antioxidative enzymes in three plant species grown on copper mine. Chemosphere **67**: 2138–2147

Bouazizi H, Jouili H, Geitmann A, El Ferjani E (2010a) Copper toxicity in expanding leaves of *Phaseolus vulgaris* L.: antioxidant enzyme response and nutrient element uptake. Ecotox Environ Safe **73**: 1304–1308

Bouazizi H, Jouili H, Geitmann A, El Ferjani E (2010b) Structural changes of cell wall and lignifying enzymes modulations in bean roots in response to copper stress. Biol Trace Elem Res **136**: 232–240

Boutigny S, Sautron E, Finazzi G, Rivasseau C, Frelet-Barrand A, Pilon M, Rolland N, Seigneurin-Berny D (2014) HMA1 and PAA1, two chloroplast-envelope PIB-ATPases, play distinct roles in chloroplast copper homeostasis. J Exp Bot **65**: 1529–1540

Bravin MN, Garnier C, Lenoble V, Gérard F, Dudal Y, Hinsinger P (2012) Root-induced changes in pH and dissolved organic matter binding capacity affect copper dynamic speciation in the rhizosphere. Geochim Cosmochim Ac **84**: 256–268

Brun LA, Maillet J, Richarte J, Herrmann P, Remy JC (1998) Relationships between extractable copper, soil properties and copper uptake by wild plants in vineyard soils. Environ Pollut **102**: 151–161

Brundrett MC, Kendrick B, Peterson CA (1991) Efficient lipid staining in plant material with Sudan red 7B or Fluoral yellow 088 in polyethylene glycol-glycerol. Biotech Histochem **66**: 111–116

Brunetto G, Bastos De Melo GW, Terzano R, Del Buono D, Astolfi S, Tomasi N, Pii Y, Mimmo T, Cesco S (2016) Copper accumulation in vineyard soils: Rhizosphere processes and agronomic practices to limit its toxicity. Chemosphere **162**: 293–307

Buapet P, Mohammadi NS, Pernice M, Kumar M, Kuzhiumparambil U, Ralph PJ (2019) Excess copper promotes photoinhibition and modulates the expression of antioxidant-related genes in *Zostera muelleri*. Aquat Toxicol **207**: 91–100

Burkhead JL, Gogolin Reynolds KA, Abdel-Ghany SE, Cohu CM, Pilon M (2009) Copper homeostasis. New Phytol **182**: 799–816

Calvo J, Jung H, Meloni G (2017) Copper metallothioneins. IUBMB Life **69**: 236–245

Calvo-Polanco M, Ribeyre Z, Dauzat M, Reyt G, Hidalgo-Shrestha C, Diehl P, Frenger M, Simonneau T, Muller B, Salt DE, et al (2021) Physiological roles of

Casparian strips and suberin in the transport of water and solutes. New Phytol **232**: 2295–2307

Cambrollé J, García JL, Ocete R, Figueroa ME, Cantos M (2013) Growth and photosynthetic responses to copper in wild grapevine. Chemosphere **93**: 294–301

Cao H, Chen D, Kuang L, Yan T, Gao F, Wu D (2023) Metabolomic analysis reveals the molecular responses to copper toxicity in rice (*Oryza sativa*). Plant Physiol Biochem **199**: 107727

Cao Y, Ma C, Chen H, Zhang J, White JC, Chen G, Xing B (2020) Xylem-based long-distance transport and phloem remobilization of copper in *Salix integra Thunb*. J Hazard Mater **392**: 122428

Cao YY, Qi CD, Li S tao, Wang Z rong, Wang X oyun, Wang J fang, Ren S xin, Li X sheng, Zhang N, Guo YD (2019) Melatonin alleviates copper toxicity via improving copper sequestration and ROS scavenging in cucumber. Plant Cell Physiol **60**: 562–574

Catty P, Boutigny S, Miras R, Joyard J, Rolland N, Seigneurin-Berny D (2011) Biochemical characterization of AtHMA6/PAA1, a chloroplast envelope Cu(I)-ATPase. J Biol Chem **286**: 36188–36197

Chaignon V, Quesnoit M, Hinsinger P (2009) Copper availability and bioavailability are controlled by rhizosphere pH in rape grown in an acidic Cu-contaminated soil. Environ Pollut **157**: 3363–3369

Chen CT, Chen LM, Lin CC, Kao CH (2001) Regulation of proline accumulation in detached rice leaves exposed to excess copper. Plant Sci **160**: 283–290

Chen CT, Chen TH, Lo KF, Chiu CY (2004) Effects of proline on copper transport in rice seedlings under excess copper stress. Plant Sci **166**: 103–111

Chen G, Li J, Han H, Du R, Wang X (2022a) Physiological and Molecular Mechanisms of Plant Responses to Copper Stress. Int J Mol Sci **23**: 12950

Chen XF, Hua D, Zheng ZC, Zhang J, Huang WT, Chen HH, Huang ZR, Yang LT, Ye X, Chen LS (2022b) Boron-mediated amelioration of copper-toxicity in sweet orange [*Citrus sinensis* (L.) Osbeck cv. Xuegan] seedlings involved reduced damage to roots and improved nutrition and water status. Ecotox Environ Safe **234**: 113423

Chen Y, Wang C, Tian S, Yao L, Zhu N, Yang X, Bai Z, Liu L, Zhang Y, Sun H, et al (2025) Abscisic acid and ethylene antagonistically regulate root endodermal suberization to mitigate nonuniform salt stress in cotton. Plant Cell Environ **48**: 3199–3216

Chen Z, Song S, Wen Y, Zou Y, Liu H (2016) Toxicity of Cu (II) to the green alga *Chlorella vulgaris*: a perspective of photosynthesis and oxidant stress. Environ Sci Pollut Res **23**: 17910–17918

Cheng H, Jiang ZY, Liu Y, Ye ZH, Wu ML, Sun CC, Sun FL, Fei J, Wang YS (2014) Metal (Pb, Zn and Cu) uptake and tolerance by mangroves in relation to root anatomy and lignification/suberization. Tree Physiol **34**: 646–656

Cheng H, Wang YS, Liu Y, Ye ZH, Wu ML, Sun CC (2015) Pb uptake and tolerance in the two selected mangroves with different root lignification and suberization. Ecotoxicology **24**: 1650–1658

Chu HH, Chiecko J, Punshon T, Lanzirotti A, Lahner B, Salt DE, Walker EL (2010) Successful reproduction requires the function of Arabidopsis Yellow Stripe-Like1 and Yellow Stripe-Like3 metal-nicotianamine transporters in both vegetative and reproductive structures. Plant Physiol **154**: 197–210

Clemens S (2001) Molecular mechanisms of plant metal tolerance and homeostasis. Planta **212**: 475–486

Colangelo EP, Guerinot ML (2006) Put the metal to the petal: metal uptake and transport throughout plants. Curr Opin Plant Biol **9**: 322–330

Compagnon V, Diehl P, Benveniste I, Meyer D, Schaller H, Schreiber L, Franke R, Pinot F (2009) CYP86B1 is required for very long chain ω-hydroxyacid and α, ω-dicarboxylic acid synthesis in root and seed suberin polyester. Plant Physiol **150**: 1831–1843

Cui Y, Wang M, Yin X, Xu G, Song S, Li M, Liu K, Xia X (2019) OsMSR3, a small heat shock protein, confers enhanced tolerance to copper stress in *Arabidopsis thaliana*. Int J Mol Sci **20**: 6096

Curie C, Cassin G, Couch D, Divol F, Higuchi K, Le Jean M, Misson J, Schikora A, Czernic P, Mari S (2009) Metal movement within the plant: contribution of nicotianamine and yellow stripe 1-like transporters. Ann Bot (Lond) **103**: 1–11

Curie C, Panaviene Z, Loulergue C, Dellaporta SL, Briat JF, Walker EL (2001) Maize yellow stripe1 encodes a membrane protein directly involved in Fe(III) uptake. Nature **409**: 346–349

De Freitas TA, França MGC, De Almeida AAF, De Oliveira SJR, De Jesus RM, Souza VL, Dos Santos Silva JV, Mangabeira PA (2015) Morphology, ultrastructure and mineral uptake is affected by copper toxicity in young plants of *Inga subnuda* subs. *luschnathiana* (Benth.) T.D. Penn. Environ Sci Pollut Res **22**: 15479–15494

Deeken R, Saupe S, Klinkenberg J, Riedel M, Leide J, Hedrich R, Mueller TD (2016) The nonspecific lipid transfer protein AtltpI-4 is involved in suberin formation of *Arabidopsis thaliana* Crown Galls. Plant Physiol **172**: 1911–1927

Degenhardt B (2000) Cell wall adaptations to multiple environmental stresses in maize roots. J Exp Bot **51**: 595–603

Del Pozo T, Cambiazo V, González M (2010) Gene expression profiling analysis of copper homeostasis in *Arabidopsis thaliana*. Biochem Biophys Res Commun **393**: 248–252

Deng F, Yamaji N, Xia J, Ma JF (2013) A member of the heavy metal P-type ATPase OsHMA5 is involved in xylem loading of copper in rice. Plant Physiol **163**: 1353–1362

DiDonato RJ, Roberts LA, Sanderson T, Eisley RB, Walker EL (2004) Arabidopsis *Yellow Stripe-Like2 (YSL2)*: a metal-regulated gene encoding a plasma membrane transporter of nicotianamine–metal complexes. Plant J **39**: 403–414

Doblas VG, Geldner N, Barberon M (2017) The endodermis, a tightly controlled barrier for nutrients. Curr Opin Plant Biol **39**: 136–143

Dresler S, Hanaka A, Bednarek W, Maksymiec W (2014) Accumulation of low-molecular-weight organic acids in roots and leaf segments of *Zea mays* plants treated with cadmium and copper. Acta Physiol Plant **36**: 1565–1575

Duan L, Yu J, Xu L, Tian P, Hu X, Song X, Pan Y (2019) Functional characterization of a type 4 metallothionein gene (*CsMT4*) in cucumber. Hortic Plant J **5**: 120–128

Dubey S, Shri M, Misra P, Lakhwani D, Bag SK, Asif MH, Trivedi PK, Tripathi RD, Chakrabarty D (2014) Heavy metals induce oxidative stress and genome-wide modulation in transcriptome of rice root. Funct Integr Genom **14**: 401–417

Ebbs SD, Kochian LV (1998) Phytoextraction of zinc by oat (*Avena sativa*), barley (*Hordeum vulgare*), and Indian Mustard (*Brassica juncea*). Environ Sci Technol **32**: 802–806

Eljebbawi A, Del Carmen Rondón Guerrero Y, Dunand C, Estevez JM (2021) Highlighting reactive oxygen species as multitaskers in root development. iScience **24**: 101978

Emamverdian A, Ding Y, Mokhberdoran F, Xie Y (2015) Heavy metal stress and some mechanisms of plant defense response. Sci World J **2015**: 1–18

Farid M, Farooq MA, Fatima A, Abubakar M, Ali S, Raza N, Alhaithloul HAS, Soliman MH (2021) Copper-induced responses in different plant species. *In* M Hasanuzzaman, ed, Approaches to the Remediation of Inorganic Pollutants. Springer, Singapore, pp 259–280

Feil SB, Pii Y, Valentinuzzi F, Tiziani R, Mimmo T, Cesco S (2020) Copper toxicity affects phosphorus uptake mechanisms at molecular and physiological levels in *Cucumis sativus* plants. Plant Physiol Biochem **157**: 138–147

Fernández-Calviño D, Rodríguez-Suárez JA, López-Periago E, Arias-Estévez M, Simal-Gándara J (2008) Copper content of soils and river sediments in a winegrowing area, and its distribution among soil or sediment components. Geoderma **145**: 91–97

Florence TM (1984) The production of hydroxyl radical from hydrogen peroxide. J Inorg Biochem **22**: 221–230

Franke R, Briesen I, Wojciechowski T, Faust A, Yephremov A, Nawrath C, Schreiber L (2005) Apoplastic polyesters in Arabidopsis surface tissues: a typical suberin and a particular cutin. Phytochemistry **66**: 2643–2658

Gaetke LM, Chow-Johnson HS, Chow CK (2014) Copper: toxicological relevance and mechanisms. Arch Toxicol **88**: 1929–1938

Garcia L, Welchen E, Gey U, Arce AL, Steinebrunner I, Gonzalez DH (2016) The cytochrome c oxidase biogenesis factor AtCOX17 modulates stress responses in Arabidopsis. Plant Cell Environ **39**: 628–644

Garcia-Molina A, Andrés-Colás N, Perea-García A, Del Valle-Tascón S, Peñarrubia L, Puig S (2011) The intracellular Arabidopsis COPT5 transport protein is required for photosynthetic electron transport under severe copper deficiency. Plant J **65**: 848–860

Ghanati F, Morita A, Yokota H (2005) Deposition of suberin in roots of soybean induced by excess boron. Plant Sci **168**: 397–405

Gong Q, Wang L, Dai T, Zhou J, Kang Q, Chen H, Li K, Li Z (2019) Effects of copper on the growth, antioxidant enzymes and photosynthesis of spinach seedlings. Ecotox Environ Safe **171**: 771–780

Gou JY, Yu XH, Liu CJ (2009) A hydroxycinnamoyltransferase responsible for synthesizing suberin aromatics in Arabidopsis. Proc Natl Acad Sci USA **106**: 18855–18860

Graça J (2015) Suberin: the biopolyester at the frontier of plants. Front Chem **3**: 62

Graça J, Pereira H (2000) Suberin structure in potato periderm: glycerol, long-chain monomers, and glyceryl and feruroyl dimers. J Agric Food Chem **48**: 5476–5483

Grünhofer P, Stöcker T, Guo Y, Li R, Lin J, Ranathunge K, Schoof H, Schreiber L (2022) *Populus* × *canescens* root suberization in reaction to osmotic and salt stress is limited to the developing younger root tip region. Physiol Plantarum **174**: e13765

Gupta DK, Huang HG, Corpas FJ (2013) Lead tolerance in plants: strategies for phytoremediation. Environ Sci Pollut Res **20**: 2150–2161

He LY, Zhang YF, Ma HY, Su LN, Chen ZJ, Wang QY, Qian M, Sheng XF (2010) Characterization of copper-resistant bacteria and assessment of bacterial communities in rhizosphere soils of copper-tolerant plants. Appl Soil Ecol **44**: 49–55

He Z, Webster S, He SY (2022) Growth–defense trade-offs in plants. Current Biology **32**: R634–R639

Hinsinger P, Bengough AG, Vetterlein D, Young IM (2009) Rhizosphere: biophysics, biogeochemistry and ecological relevance. Plant Soil **321**: 117–152

Hoagland D, Arnon D (1950) The water-culture method for growing plants without soil. Calif Agric Exp Stat Circ **347**: 1–32

Hoegger PJ, Kilaru S, James TY, Thacker JR, Kües U (2006) Phylogenetic comparison and classification of laccase and related multicopper oxidase protein sequences. FEBS J **273**: 2308–2326

Höfer R, Briesen I, Beck M, Pinot F, Schreiber L, Franke R (2008) The Arabidopsis cytochrome P450 CYP86A1 encodes a fatty acid ω-hydroxylase involved in suberin monomer biosynthesis. J Exp Bot **59**: 2347–2360

Hongjun Meng (2023) Aluminum Stress on Suberin Biosynthesis in Barley (*Hordeum vulgare*) Roots. PhD Thesis. Rheinische Friedrich-Wilhelms-Universität Bonn

Hoppen C, Müller L, Hänsch S, Uzun B, Milić D, Meyer AJ, Weidtkamp-Peters S, Groth G (2019) Soluble and membrane-bound protein carrier mediate direct copper transport to the ethylene receptor family. Sci Rep **9**: 10715

Hossain MS, Abdelrahman M, Tran CD, Nguyen KH, Chu HD, Watanabe Y, Hasanuzzaman M, Mohsin SM, Fujita M, Tran L-SP (2020) Insights into acetate-mediated copper homeostasis and antioxidant defense in lentil under excessive copper stress. Environ Pollut **258**: 113544

Htwe T, Onthong J, Duangpan S, Techato K, Chotikarn P, Sinutok S (2020) Effect of copper concentration on plant growth and metal contents in rice plant (*Oryza Sativa* L.). Commun Soil Sci Plan **51**: 2349–2360

Huo K, Shangguan X, Xia Y, Shen Z, Chen C (2020) Excess copper inhibits the growth of rice seedlings by decreasing uptake of nitrate. Ecotox Environ Safe **190**: 110105

İşeri ÖD, Körpe DA, Yurtcu E, Sahin FI, Haberal M (2011) Copper-induced oxidative damage, antioxidant response and genotoxicity in *Lycopersicum esculentum* Mill. and *Cucumis sativus* L. Plant Cell Rep **30**: 1713–1721

Ishka MR, Chia JC, Vatamaniuk OK (2022) Advances in understanding of copper function and transport in plants. Cation Transporters in Plants. Academic Press, pp 205–226

Jabeen R, Ahmad A, Iqbal M (2009) Phytoremediation of heavy metals: physiological and molecular mechanisms. Bot Rev **75**: 339–364

Jambunathan N (2010) Determination and detection of reactive oxygen species (ROS), lipid peroxidation, and electrolyte leakage in plants. Methods Mol Biol **639**: 292–298

Jin MF, You MX, Lan QQ, Cai LY, Lin MZ (2021) Effect of copper on the photosynthesis and growth of *Eichhornia crassipes*. Plant Biol **23**: 777–784

Juang KW, Lee YI, Lai HY, Wang C-H, Chen BC (2012) Copper accumulation, translocation, and toxic effects in grapevine cuttings. Environ Sci Pollut Res **19**: 1315–1322

Jun SE, Shim JS, Park HJ (2023) Beyond NPK: mineral nutrient-mediated modulation in orchestrating flowering time. Plants **12**: 3299

Kanti Das T, Wati MR, Fatima-Shad K (2014) Oxidative stress gated by Fenton and Haber weiss reactions and its association with Alzheimer's disease. Arch Neurosci **2**: e20078

Karasov TL, Chae E, Herman JJ, Bergelson J (2017) Mechanisms to mitigate the trade-off between growth and defense. Plant Cell **29**: 666–680

Karimi P, Khavari-Nejad RA, Niknam V, Ghahremaninejad F, Najafi F (2012) The effects of excess copper on antioxidative enzymes, lipid peroxidation, proline, chlorophyll, and concentration of Mn, Fe, and Cu in *Astragalus neo-mobayenii*. Sci World J **2012**: 1–6

Khan IU, Rono JK, Zhang BQ, Liu XS, Wang MQ, Wang LL, Wu XC, Chen X, Cao HW, Yang ZM (2019) Identification of novel rice (*Oryza sativa*) HPP and HIPP genes tolerant to heavy metal toxicity. Ecotox Environ Safe **175**: 8–18

Khatun S, Ali MB, Hahn EJ, Paek KY (2008) Copper toxicity in *Withania somnifera*: growth and antioxidant enzymes responses of in vitro grown plants. Environ Exp Bot **64**: 279–285

Kholodova VP, Ivanova EM, Kuznetsov VV (2011) Initial steps of copper detoxification: outside and inside of the plant cell. *In* I Sherameti, A Varma, eds, Detoxification of Heavy Metals. Springer, Berlin Heidelberg, pp 143–167

Khorashad JS, Rizzo S, Tonks A (2024) Reactive oxygen species and its role in pathogenesis and resistance to therapy in acute myeloid leukemia. Cancer Drug Resist **7**: 5

Kim RJ, Han S, Kim HJ, Hur JH, Suh MC (2024) Tetracosanoic acids produced by 3-ketoacyl-CoA synthase 17 are required for synthesizing seed coat suberin in Arabidopsis. J Exp Bot **75**: 1767–1780

Kintlová M, Blavet N, Cegan R, Hobza R (2017) Transcriptome of barley under three different heavy metal stress reaction. Genom Data **13**: 15–17

Kobayashi T, Nishizawa NK (2012) Iron uptake, translocation, and regulation in higher plants. Annu Rev Plant Biol **63**: 131–152

Kopittke PM, Asher CJ, Blamey FPC, Menzies NW (2009) Toxic effects of Cu^{2+} on growth, nutrition, root morphology, and distribution of Cu in roots of sabi grass. Sci Total Environ **407**: 4616–4621

Kosakivska IV, Babenko LM, Romanenko KO, Korotka IY, Potters G (2021) Molecular mechanisms of plant adaptive responses to heavy metals stress. Cell Biol Int **45**: 258–272

Kosma DK, Molina I, Ohlrogge JB, Pollard M (2012) Identification of an Arabidopsis fatty alcohol:caffeoyl-coenzyme A acyltransferase required for the synthesis of alkyl hydroxycinnamates in root waxes. Plant Physiol **160**: 237–248

Kováč J, Lux A, Vaculík M (2018) Formation of a subero-lignified apical deposit in root tip of radish (*Raphanus sativus*) as a response to copper stress. Ann Bot (Lond) **122**: 823–831

Kreszies T, Schreiber L, Ranathunge K (2018) Suberized transport barriers in Arabidopsis, barley and rice roots: from the model plant to crop species. J Plant Physiol **227**: 75–83

Kreszies T, Shellakkutti N, Osthoff A, Yu P, Baldauf JA, Zeisler-Diehl VV, Ranathunge K, Hochholdinger F, Schreiber L (2019) Osmotic stress enhances suberization of apoplastic barriers in barley seminal roots: analysis of chemical, transcriptomic and physiological responses. New Phytol **221**: 180–194

Krzesłowska M (2011) The cell wall in plant cell response to trace metals: polysaccharide remodeling and its role in defense strategy. Acta Physiol Plant **33**: 35–51

Kumar D, Yusuf M, Singh P, Sardar M, Sarin N (2014) Histochemical detection of superoxide and H_2O_2 accumulation in *Brassica juncea* Seedlings. Bio-protocol **4**: e1008–e1008

Kumar P, Tewari RK, Sharma PN (2008) Modulation of copper toxicity-induced oxidative damage by excess supply of iron in maize plants. Plant Cell Rep **27**: 399–409

Kumar V, Pandita S, Singh Sidhu GP, Sharma A, Khanna K, Kaur P, Bali AS, Setia R (2021) Copper bioavailability, uptake, toxicity and tolerance in plants: A comprehensive review. Chemosphere **262**: 127810

La Torre A, Iovino V, Caradonia F (2018) Copper in plant protection: Current situation and prospects. Phytopathol Mediterr **57**: 201–236

Lacey RF, Binder BM (2014) How plants sense ethylene gas — The ethylene receptors. J Inorg Biochem **133**: 58–62

Lai J, Luo X (2019) High-efficiency antioxidant system, chelating system and stress-responsive genes enhance tolerance to cesium ionotoxicity in Indian mustard (*Brassica juncea* L.). Ecotox Environ Safe **181**: 491–498

Lamichhane JR, Osdaghi E, Behlau F, Köhl J, Jones JB, Aubertot JN (2018) Thirteen decades of antimicrobial copper compounds applied in agriculture. A review. Agron Sustain Dev **38**: 28

Lee S, Jung S, Go Y, Kim H, Kim J, Cho H, Park OK, Suh M (2009) Two Arabidopsis 3-ketoacyl CoA synthase genes, *KCS20* and *KCS2/DAISY*, are functionally redundant in cuticular wax and root suberin biosynthesis, but differentially controlled by osmotic stress. Plant J **60**: 462–475

Lee S, Kim YY, Lee Y, An G (2007) Rice P1B-type heavy-metal ATPase, OsHMA9, is a metal efflux protein. Plant Physiol **145**: 831–842

Lee SB, Suh M (2018) Disruption of glycosylphosphatidylinositol-anchored lipid transfer protein 15 affects seed coat permeability in Arabidopsis. Plant J **96**: 1206–1217

Lequeux H, Hermans C, Lutts S, Verbruggen N (2010) Response to copper excess in *Arabidopsis thaliana*: Impact on the root system architecture, hormone distribution, lignin accumulation and mineral profile. Plant Physiol Biochem **48**: 673–682

Li L, Long M, Islam F, Farooq MA, Wang J, Mwamba TM, Shou J, Zhou W (2019a) Synergistic effects of chromium and copper on photosynthetic inhibition, subcellular distribution, and related gene expression in *Brassica napus* cultivars. Environ Sci Pollut Res **26**: 11827–11845

Li Q, Chen HH, Qi YP, Ye X, Yang LT, Huang ZR, Chen LS (2019b) Excess copper effects on growth, uptake of water and nutrients, carbohydrates, and PSII

photochemistry revealed by OJIP transients in Citrus seedlings. Environ Sci Pollut Res **26**: 30188–30205

Li Y, Beisson F, Koo AJK, Molina I, Pollard M, Ohlrogge J (2007) Identification of acyltransferases required for cutin biosynthesis and production of cutin with suberin-like monomers. Proc Natl Acad Sci USA **104**: 18339–18344

Li Y, Shi S, Zhang Y, Zhang A, Wang Z, Yang Y (2023) Copper stress-induced phytotoxicity associated with photosynthetic characteristics and lignin metabolism in wheat seedlings. Ecotox Environ Safe **254**: 114739

Light KM, Wisniewski JA, Vinyard WA, Kieber-Emmons MT (2016) Perception of the plant hormone ethylene: known-knowns and known-unknowns. J Biol Inorg Chem **21**: 715–728

Lin CY, Trinh NN, Fu SF, Hsiung YC, Chia LC, Lin CW, Huang HJ (2013) Comparison of early transcriptome responses to copper and cadmium in rice roots. Plant Mol Biol **81**: 507–522

Lin X, Dai C yang, Chen Z, Zhang T zuo, Pu X yan (2023) Preliminary screening of biomarkers in HAPE based on quasi-targeted metabolomics. Front Physiol **14**: 1122026

Líška D, Martinka M, Kohanová J, Lux A (2016) Asymmetrical development of root endodermis and exodermis in reaction to abiotic stresses. Ann Bot (Lond) **118**: 667–674

Liu H, Bao G, Dou Z, Liu H, Bai J, Chen Y, Yuan Y, Zhang X, Xi J (2022) Response characteristics of highland barley under freeze-thaw, drought and artemisinin stresses. BMC Plant Biol **22**: 126

Liu J, Shi X, Qian M, Zheng L, Lian C, Xia Y, Shen Z (2015) Copper-induced hydrogen peroxide upregulation of a metallothionein gene, *OsMT2c*, from *Oryza sativa* L. confers copper tolerance in *Arabidopsis thaliana*. J Hazard Mater **294**: 99–108

Liu Y, Tao Q, Guo X, Luo J, Li J, Liang Y, Li T (2020) Low calcium-induced delay in development of root apoplastic barriers enhances Cd uptake and accumulation in *Sedum alfredii*. Sci Total Environ **723**: 137810

Lu L, Xie R, Liu T, Wang H, Hou D, Du Y, He Z, Yang X, Sun H, Tian S (2017) Spatial imaging and speciation of Cu in rice (*Oryza sativa* L.) roots using synchrotron-based X-ray microfluorescence and X-ray absorption spectroscopy. Chemosphere **175**: 356–364

Luo T, Sheng Z, Chen M, Qin M, Tu Y, Khan MN, Khan Z, Liu L, Wang B, Kuai J, et al (2024) Phytoremediation of copper-contaminated soils by rapeseed (*Brassica napus* L.) and underlying molecular mechanisms for copper absorption and sequestration. Ecotox Environ Safe **273**: 116123

Mackie KA, Müller T, Kandeler E (2012) Remediation of copper in vineyards – A mini review. Environ Pollut **167**: 16–26

Madejón P, Ramírez-Benítez JE, Corrales I, Barceló J, Poschenrieder C (2009) Copper-induced oxidative damage and enhanced antioxidant defenses in the root apex of maize cultivars differing in Cu tolerance. Environ Exp Bot **67**: 415–420

Markossian KA, Kurganov BI (2003) Copper chaperones, intracellular copper trafficking proteins. Function, structure, and mechanism of action. Biochemistry **68**: 827–837

Marschner H (1995) Mineral nutrition of higher plants. 2nd (eds). Academic Press, New York, p 889

Melino VJ, Plett DC, Bendre P, Thomsen HC, Zeisler-Diehl VV, Schreiber L, Kronzucker HJ (2021) Nitrogen depletion enhances endodermal suberization without restricting transporter-mediated root NO_3^- influx. J Plant Physiol **257**: 153334

Memon AR, Schröder P (2009) Implications of metal accumulation mechanisms to phytoremediation. Environ Sci Pollut Res **16**: 162–175

Meng H, Zhang Q, Kreszies T, Acosta IF, Schreiber L (2024) Aluminium induces suberin biosynthesis in barley roots via ABA. bioRxiv 2024.10.27.620472

Migocka M, Malas K (2018) Plant responses to copper: molecular and regulatory mechanisms of copper uptake, distribution and accumulation in plants. Plant Micronutrient Use Efficiency. Academic Press, pp 71–86

Mihaljevič M, Baieta R, Ettler V, Vaněk A, Kříbek B, Penížek V, Drahota P, Trubač J, Sracek O, Chrastný V, et al (2019) Tracing the metal dynamics in semi-arid soils near mine tailings using stable Cu and Pb isotopes. Chem Geol **515**: 61–76

Milner MJ, Seamon J, Craft E, Kochian LV (2013) Transport properties of members of the ZIP family in plants and their role in Zn and Mn homeostasis. J Exp Bot **64**: 369–381

Mir AR, Alam P, Hayat S (2022) Auxin regulates growth, photosynthetic efficiency and mitigates copper induced toxicity via modulation of nutrient status, sugar metabolism and antioxidant potential in *Brassica juncea*. Plant Physiol Biochem **185**: 244–259

Mir AR, Pichtel J, Hayat S (2021) Copper: uptake, toxicity and tolerance in plants and management of Cu-contaminated soil. Biometals **34**: 737–759

Mishra S, Dubey R (2005) Heavy metal toxicity induced alterations in photosynthetic metabolism in plants. Handbook of photosynthesis **2**: 845–863

Møller IM, Igamberdiev AU, Bykova NV, Finkemeier I, Rasmusson AG, Schwarzländer M (2020) Matrix redox physiology governs the regulation of plant mitochondrial metabolism through posttranslational protein modifications. Plant Cell **32**: 573–594

Moore CA, Bowen HC, Scrase-Field S, Knight MR, White PJ (2002) The deposition of suberin lamellae determines the magnitude of cytosolic Ca^{2+} elevations in root endodermal cells subjected to cooling. Plant J **30**: 457–465

Morel M-C, Spadini L, Brimo K, Martins JMF (2014) Speciation study in the sulfamethoxazole–copper–pH–soil system: implications for retention prediction. Sci Total Environ **481**: 266–273

Mostofa MG, Seraj ZI, Fujita M (2014) Exogenous sodium nitroprusside and glutathione alleviate copper toxicity by reducing copper uptake and oxidative damage in rice (*Oryza sativa* L.) seedlings. Protoplasma **251**: 1373–1386

Nair PMG, Chung IM (2014) A mechanistic study on the toxic effect of copper oxide nanoparticles in soybean (*Glycine max* L.) root development and lignification of root cells. Biol Trace Elem Res **162**: 342–352

Navarrete A, González A, Gómez M, Contreras RA, Díaz P, Lobos G, Brown MT, Sáez CA, Moenne A (2019) Copper excess detoxification is mediated by a coordinated and complementary induction of glutathione, phytochelatins and metallothioneins in the green seaweed *Ulva compressa*. Plant Physiol Biochem **135**: 423–431

Nomberg G, Marinov O, Arya GC, Manasherova E, Cohen H (2022) The key enzymes in the suberin biosynthetic pathway in plants: an update. Plants **11**: 392

Noreen S, Akhter MS, Yaamin T, Arfan M (2018) The ameliorative effects of exogenously applied proline on physiological and biochemical parameters of wheat (*Triticum aestivum* L.) crop under copper stress condition. J Plant Interact **13**: 221–230

Osmolovskaya N, Viet Vu D, Saint Petersburg State University, Kuchaeva L, Saint Petersburg State University (2018) The role of organic acids in heavy metal tolerance in plants. Biological Communications **63**: 9–16

Pai K, Timmons C, Roehm KD, Ngo A, Narayanan SS, Ramachandran A, Jacob JD, Ma LM, Madihally SV (2018) Investigation of the roles of plasma species generated by surface dielectric barrier discharge. Sci Rep **8**: 16674

Parveen A, Saleem MH, Kamran M, Haider MZ, Chen JT, Malik Z, Rana MS, Hassan A, Hur G, Javed MT, et al (2020) Effect of citric acid on growth,

ecophysiology, chloroplast ultrastructure, and phytoremediation potential of jute (*Corchorus capsularis* L.) seedlings exposed to copper stress. Biomolecules **10**: 592

Pätsikkä E, Kairavuo M, Šeršen F, Aro E-M, Tyystjärvi E (2002) Excess copper predisposes photosystem II to photoinhibition in vivo by outcompeting iron and causing decrease in leaf chlorophyll. Plant Physiol **129**: 1359–1367

Peers G, Price NM (2006) Copper-containing plastocyanin used for electron transport by an oceanic diatom. Nature **441**: 341–344

Peñarrubia L, Andrés-Colás N, Moreno J, Puig S (2010) Regulation of copper transport in *Arabidopsis thaliana*: a biochemical oscillator? J Biol Inorg Chem **15**: 29–36

Peralta Ogorek LL, Jiménez JDLC, Visser EJW, Takahashi H, Nakazono M, Shabala S, Pedersen O (2023) Outer apoplastic barriers in roots: prospects for abiotic stress tolerance. Funct Plant Biol **51**: FP23133

Perea-García A, Andrés-Bordería A, Vera-Sirera F, Pérez-Amador MA, Puig S, Peñarrubia L (2020) Deregulated high affinity copper transport alters iron homeostasis in Arabidopsis. Front Plant Sci **11**: 1106

Persson DP, Chen A, Aarts MGM, Salt DE, Schjoerring JK, Husted S (2016) Multi-element bioimaging of *Arabidopsis thaliana* roots. Plant Physiol **172**: 835–847

Pham AN, Xing G, Miller CJ, Waite TD (2013) Fenton-like copper redox chemistry revisited: Hydrogen peroxide and superoxide mediation of copper-catalyzed oxidant production. J Catal **301**: 54–64

Pourrut B, Shahid M, Dumat C, Winterton P, Pinelli E (2011) Lead uptake, toxicity, and detoxification in plants. Rev Environ Contam Toxicol **213**: 113–136

Printz B, Lutts S, Hausman J-F, Sergeant K (2016) Copper trafficking in plants and its implication on cell wall dynamics. Front Plant Sci **7**: 601

Puig S (2014) Function and regulation of the plant COPT family of high-affinity copper transport proteins. Adv Bot **2014**: 1–9

Qu M, Wang Y, Huang B, Zhao Y (2018) Spatial uncertainty assessment of the environmental risk of soil copper using auxiliary portable X-ray fluorescence spectrometry data and soil pH. Environ Pollut **240**: 184–190

Ranathunge K, Schreiber L (2011) Water and solute permeabilities of Arabidopsis roots in relation to the amount and composition of aliphatic suberin. J Exp Bot **62**: 1961–1974

Ranathunge K, Schreiber L, Franke R (2011) Suberin research in the genomics era—new interest for an old polymer. Plant Sci **180**: 399–413

Rashid A, Schutte BJ, Ulery A, Deyholos MK, Sanogo S, Lehnhoff EA, Beck L (2023) Heavy metal contamination in agricultural soil: environmental pollutants affecting crop health. Agronomy **13**: 1521

Reckova S, Tuma J, Dobrev P, Vankova R (2019) Influence of copper on hormone content and selected morphological, physiological and biochemical parameters of hydroponically grown *Zea mays* plants. Plant Growth Regul **89**: 191–201

Rehman M, Liu L, Wang Q, Saleem MH, Bashir S, Ullah S, Peng D (2019) Copper environmental toxicology, recent advances, and future outlook: a review. Environ Sci Pollut Res **26**: 18003–18016

Ren QQ, Huang ZR, Huang WL, Huang WT, Chen HH, Yang LT, Ye X, Chen LS (2022) Physiological and molecular adaptations of *Citrus grandis* roots to long-term copper excess revealed by physiology, metabolome and transcriptome. Environ Exp Bot **203**: 105049

Robbins NE, Trontin C, Duan L, Dinneny JR (2014) Beyond the barrier: communication in the root through the endodermis. Plant Physiol **166**: 551–559

Roncarati F, Sáez CA, Greco M, Gledhill M, Bitonti MB, Brown MT (2015) Response differences between *Ectocarpus siliculosus* populations to copper stress involve cellular exclusion and induction of the phytochelatin biosynthetic pathway. Aquat Toxicol **159**: 167–175

Roy SK, Cho S-W, Kwon SJ, Kamal AHM, Lee D-G, Sarker K, Lee M-S, Xin Z, Woo S-H (2017) Proteome characterization of copper stress responses in the roots of sorghum. Biometals **30**: 765–785

Ruiz LM, Libedinsky A, Elorza AA (2021) Role of copper on mitochondrial function and metabolism. Front Mol Biosci **8**: 711227

Ryan BM, Kirby JK, Degryse F, Harris H, McLaughlin MJ, Scheiderich K (2013) Copper speciation and isotopic fractionation in plants: uptake and translocation mechanisms. New Phytol **199**: 367–378

Samuels L, Kunst L, Jetter R (2008) Sealing plant surfaces: cuticular wax formation by epidermal cells. Annu Rev Plant Biol **59**: 683–707

Sancenón V, Puig S, Mateu-Andrés I, Dorcey E, Thiele DJ, Peñarrubia L (2004) The Arabidopsis copper transporter COPT1 functions in root elongation and pollen development. J Biol Chem **279**: 15348–15355

Sanz A, Pike S, Khan MA, Carrió-Seguí À, Mendoza-Cózatl DG, Peñarrubia L, Gassmann W (2019) Copper uptake mechanism of *Arabidopsis thaliana* high-affinity COPT transporters. Protoplasma **256**: 161–170

Schat H, Sharma SS, Vooijs R (1997) Heavy metal-induced accumulation of free proline in a metal-tolerant and a nontolerant ecotype of *Silene vulgaris*. Physiol Plantarum **101**: 477–482

Schreiber L, Franke R, Hartmann K (2005) Wax and suberin development of native and wound periderm of potato (*Solanum tuberosum* L.) and its relation to peridermal transpiration. Planta **220**: 520–530

Shabbir Z, Sardar A, Shabbir A, Abbas G, Shamshad S, Khalid S, Natasha, Murtaza G, Dumat C, Shahid M (2020) Copper uptake, essentiality, toxicity, detoxification and risk assessment in soil-plant environment. Chemosphere **259**: 127436

Sharaff M, Kamat S, Archana G (2017) Analysis of copper tolerant rhizobacteria from the industrial belt of Gujarat, western India for plant growth promotion in metal polluted agriculture soils. Ecotox Environ Safe **138**: 113–121

Sharma R, Bhardwaj R, Handa N, Gautam V, Kohli SK, Bali S, Kaur P, Thukral AK, Arora S, Ohri P, et al (2016) Responses of phytochelatins and metallothioneins in alleviation of heavy metal stress in plants: an overview. Plant Metal Interaction **pp**: 263–283

Sharma R, Bhardwaj R, Thukral AK, Al-Huqail AA, Siddiqui MH, Ahmad P (2019) Oxidative stress mitigation and initiation of antioxidant and osmoprotectant responses mediated by ascorbic acid in *Brassica juncea* L. subjected to copper (II) stress. Ecotox Environ Safe **182**: 109436

Sharma SS, Dietz KJ (2006) The significance of amino acids and amino acid-derived molecules in plant responses and adaptation to heavy metal stress. J Exp Bot **57**: 711–726

Sheng H, Jiang Y, Rahmati M, Chia JC, Dokuchayeva T, Kavulych Y, Zavodna TO, Mendoza PN, Huang R, Smieshka LM, et al (2021) YSL3-mediated copper distribution is required for fertility, seed size and protein accumulation in *Brachypodium*. Plant Physiol **186**: 655–676

Sheng Z, Luo T, Wang L, Chen M, Ma B, Liu L, Wang B, Kuai J, Wang J, Zhao J, et al (2024) Biochar addition enhances remediation efficiency and rapeseed yield in copper-contaminated soil. Front Plant Sci **15**: 1481732

Shukla V, Barberon M (2021) Building and breaking of a barrier: Suberin plasticity and function in the endodermis. Curr Opin Plant Biol **64**: 102153

Shukla V, Han JP, Cléard F, Lefebvre-Legendre L, Gully K, Flis P, Berhin A, Andersen TG, Salt DE, Nawrath C, et al (2021) Suberin plasticity to developmental and exogenous cues is regulated by a set of MYB transcription factors. Proc Natl Acad Sci USA **118**: e2101730118

Shulaev V, Oliver DJ (2006) Metabolic and Proteomic Markers for Oxidative Stress. New Tools for Reactive Oxygen Species Research. Plant Physiol **141**: 367–372

Sierra Aragón M, Nakamaru YM, García-Carmona M, Martínez Garzón FJ, Martín Peinado FJ (2019) The role of organic amendment in soils affected by residual pollution of potentially harmful elements. Chemosphere **237**: 124549

Singh V, Bhatt I, Aggarwal A, Tripathi BN, Munjal AK, Sharma V (2010) Proline improves copper tolerance in chickpea (*Cicer arietinum*). Protoplasma **245**: 173–181

Song J, Yang YQ, Zhu SH, Chen GC, Yuan XF, Liu TT, Yu XH, Shi JY (2013) Spatial distribution and speciation of copper in root tips of cucumber revealed by μ-XRF and μ-XANES. Biologia plantarum **57**: 581–586

Sun M, Li S, Gong Q, Xiao Y, Peng F (2022) Leucine Contributes to Copper Stress Tolerance in Peach (*Prunus persica*) Seedlings by Enhancing Photosynthesis and the Antioxidant Defense System. Antioxidants **11**: 2455

Szafrańska K, Cvikrová M, Kowalska U, Górecka K, Górecki R, Martincová O, Janas KM (2011) Influence of copper ions on growth, lipid peroxidation, and proline and polyamines content in carrot rosettes obtained from anther culture. Acta Physiol Plant **33**: 851–859

Thounaojam TC, Panda P, Mazumdar P, Kumar D, Sharma GD, Sahoo L, Sanjib P (2012) Excess copper induced oxidative stress and response of antioxidants in rice. Plant Physiol Biochem **53**: 33–39

Timothy N, Tagui Williams E (2019) Environmental pollution by heavy metal: an overview. Int J Environ Chem **3**: 72

Tiwari M, Kidwai M, Dutta P, Narayan S, Gautam N, Chawda K, Shirke PA, Mishra AK, Chakrabarty D (2022) A tau class glutathione-S-transferase (OsGSTU5) confers tolerance against arsenic toxicity in rice by accumulating more arsenic in root. J Hazard Mater **426**: 128100

Tripathi BN, Gaur JP (2004) Relationship between copper- and zinc-induced oxidative stress and proline accumulation in *Scenedesmus* sp. Planta **219**: 397–404

Tripathi BN, Mehta SK, Amar A, Gaur JP (2006) Oxidative stress in Scenedesmus sp. during short- and long-term exposure to Cu^{2+} and Zn^{2+}. Chemosphere **62**: 538–544

Tsukagoshi H (2016) Control of root growth and development by reactive oxygen species. Curr Opin Plant Biol **29**: 57–63

Tsukagoshi H, Busch W, Benfey PN (2010) Transcriptional regulation of ROS controls transition from proliferation to differentiation in the root. Cell **143**: 606–616

Tugbaeva A, Ermoshin A, Wuriyanghan H, Maleva M, Borisova G, Kiseleva I (2022) Copper stress enhances the lignification of axial organs in *Zinnia elegans*. Horticulturae **8**: 558

Tye AM, Young S, Crout NMJ, Zhang H, Preston S, Zhao FJ, McGrath SP (2004) Speciation and solubility of Cu, Ni and Pb in contaminated soils. Eur J Soil Sci **55**: 579–590

Ursache R, De Jesus Vieira Teixeira C, Dénervaud Tendon V, Gully K, De Bellis D, Schmid-Siegert E, Grube Andersen T, Shekhar V, Calderon S, Pradervand S, et al (2021) GDSL-domain proteins have key roles in suberin polymerization and degradation. Nat Plants **7**: 353–364

Vaculík M, Landberg T, Greger M, Luxová M, Stoláriková M, Lux A (2012) Silicon modifies root anatomy, and uptake and subcellular distribution of cadmium in young maize plants. Ann Bot (Lond) **110**: 433–443

Van Hoof NALM, Koevoets PLM, Hakvoort HWJ, Ten Bookum WM, Schat H, Verkleij JAC, Ernst WHO (2001) Enhanced ATP-dependent copper efflux across the root cell plasma membrane in copper-tolerant *Silene vulgaris*. Physiol Plantarum **113**: 225–232

Vassilev A, Lidon FC, Ramalho JC, Matos MDC, Bareiro MG (2004) Shoot cadmium accumulation and photosynthetic performance of barley plants exposed to high cadmium treatments. J Plant Nutr **27**: 775–795

Violante A, Cozzolino V, Perelomov L, Caporale AG, Pigna M (2010) Mobility and bioavailability of heavy metals and metalloids in soil environments. J Soil Sci Plant Nutr **10**: 268–292

Vishwanath SJ, Delude C, Domergue F, Rowland O (2015) Suberin: biosynthesis, regulation, and polymer assembly of a protective extracellular barrier. Plant Cell Rep **34**: 573–586

Vives-Peris V, De Ollas C, Gómez-Cadenas A, Pérez-Clemente RM (2020) Root exudates: from plant to rhizosphere and beyond. Plant Cell Rep **39**: 3–17

Wa Lwalaba JL, Zvobgo G, Gai Y, Issaka JH, Mwamba TM, Louis LT, Fu L, Nazir MM, Ansey Kirika B, Kazadi Tshibangu A, et al (2021) Transcriptome analysis reveals the tolerant mechanisms to cobalt and copper in barley. Ecotox Environ Safe **209**: 111761

Wan X, Lei M, Chen T (2016) Cost–benefit calculation of phytoremediation technology for heavy-metal-contaminated soil. Sci Total Environ **563**: 796–802

Wang J, Moeen-ud-din M, Yin R, Yang S (2022) ROS homeostasis involved in dose-dependent responses of Arabidopsis seedlings to copper toxicity. Genes **14**: 11

Wang P, Calvo-Polanco M, Reyt G, Barberon M, Champeyroux C, Santoni V, Maurel C, Franke RB, Ljung K, Novak O, et al (2019) Surveillance of cell wall diffusion barrier integrity modulates water and solute transport in plants. Sci Rep **9**: 4227

Wang Q, Wei N, Jin X, Min X, Ma Y, Liu W (2021) Molecular characterization of the COPT/Ctr-type copper transporter family under heavy metal stress in alfalfa. Int J Biol Macromol **181**: 644–652

Wang RX, Wang ZH, Sun YD, Wang LL, Li M, Liu YT, Zhang HM, Jing PW, Shi QF, Yu YH (2024) Molecular mechanism of plant response to copper stress: A review. Environ Exp Bot **218**: 105590

Wang SH, Zhang H, Zhang Q, Jin GM, Jiang SJ, Jiang D, He QY, Li ZP (2011) Copper-induced oxidative stress and responses of the antioxidant system in roots of *Medicago sativa*. J Agron Crop Sci **197**: 418–429

Wang Y, Chen X, Chen J (2025) Advances of the mechanism for copper tolerance in plants. Plant Sci **350**: 112299

Wei X, Mao L, Lu W, Wei X, Han X, Guan W, Yang Y, Zha M, Xu C, Luo Z (2020) Three transcription activators of ABA signaling positively regulate suberin monomer synthesis by activating cytochrome P450 *CYP86A1* in Kiwifruit. Front Plant Sci **10**: 1650

Wintz H, Fox T, Wu YY, Feng V, Chen W, Chang HS, Zhu T, Vulpe C (2003) Expression profiles of *Arabidopsis thaliana* in mineral deficiencies reveal novel transporters involved in metal homeostasis. J Biol Chem **278**: 47644–47653

Xia Y, Yin S, Zhang K, Shi X, Lian C, Zhang H, Hu Z, Shen Z (2018) OsWAK11, a rice wall-associated kinase, regulates Cu detoxification by alteration the immobilization of Cu in cell walls. Environ Exp Bot **150**: 99–105

Xiong S, Kong X, Chen G, Tian L, Qian D, Zhu Z, Qu LQ (2023) Metallochaperone OsHIPP9 is involved in the retention of cadmium and copper in rice. Plant Cell Environ **46**: 1946–1961

Xu E, Liu Y, Gu D, Zhan X, Li J, Zhou K, Zhang P, Zou Y (2024) Molecular mechanisms of plant responses to copper: from deficiency to excess. Int J Mol Sci **25**: 6993

Xu J, Yang L, Wang Z, Dong G, Huang J, Wang Y (2006) Toxicity of copper on rice growth and accumulation of copper in rice grain in copper contaminated soil. Chemosphere **62**: 602–607

Xu Q, Qiu H, Chu W, Fu Y, Cai S, Min H, Sha S (2013) Copper ultrastructural localization, subcellular distribution, and phytotoxicity in *Hydrilla verticillata* (L.f.) Royle. Environ Sci Pollut Res **20**: 8672–8679

Xu Y, Yu W, Ma Q, Zhou H, Jiang C (2017) Toxicity of sulfadiazine and copper and their interaction to wheat (*Triticum aestivum* L.) seedlings. Ecotox Environ Safe **142**: 250–256

Yadav V, Molina I, Ranathunge K, Castillo IQ, Rothstein SJ, Reed JW (2014) ABCG transporters are required for suberin and pollen wall extracellular barriers in *Arabidopsis*. Plant Cell **26**: 3569–3588

Yruela I (2009) Copper in plants: acquisition, transport and interactions. Funct Plant Biol **36**: 409

Žaltauskaitė J, Šliumpaitė I (2013) Evaluation of toxic effects and bioaccumulation of cadmium and copper in spring barley (*Hordeum vulgare* L.). Environ Res Eng Manag **64**: 51–58

Zeier J, Schreiber L (1997) Chemical composition of hypodermal and endodermal cell walls and xylem vessels isolated from *Clivia miniata* (Identification of the Biopolymers Lignin and Suberin). Plant Physiol **113**: 1223–1231

Zhang C, Lu W, Yang Y, Shen Z, Ma JF, Zheng L (2018a) OsYSL16 is required for preferential Cu distribution to floral organs in rice. Plant Cell Physiol **59**: 2039–2051

Zhang Q, Wang C (2020) Natural and human factors affect the distribution of soil heavy metal pollution: a review. Water, Air, Soil Pollut **231**: 350

Zhang Y, Chen K, Zhao F-J, Sun C, Jin C, Shi Y, Sun Y, Li Y, Yang M, Jing X, et al (2018b) OsATX1 interacts with heavy metal P1B-type ATPases and affects copper transport and distribution. Plant Physiol **178**: 329–344

Zhang Z, Ke M, Qu Q, Peijnenburg WJGM, Lu T, Zhang Q, Ye Y, Xu P, Du B, Sun L, et al (2018c) Impact of copper nanoparticles and ionic copper exposure on wheat (*Triticum aestivum* L.) root morphology and antioxidant response. Environ Pollut **239**: 689–697

Zhao H, Wu L, Chai T, Zhang Y, Tan J, Ma S (2012) The effects of copper, manganese and zinc on plant growth and elemental accumulation in the manganese-hyperaccumulator *Phytolacca americana*. J Plant Physiol **169**: 1243–1252

Zhou X, Xiong X, Lu F, Shi W, Zhou Y, Lai N, Chen L-S, Huang Z-R (2025) Excessive copper induces lignin biosynthesis in the leaves and roots of two citrus species: Physiological, metabolomic and anatomical aspects. Ecotox Environ Safe **289**: 117692

7. Supplementary data

Table S1 Primer list

Primer name	Sequence 5'-3'
CYP86B1 clone-Forward	ACGGCCATACGTTGCCATCA
CYP86B1 clone-Reverse	TCAGCTTTCTCCTGCAAAGTATCACT
Actin-Forward	GGCACACTGGTGTCATGGT
Actin -Reverse	GCGCCTCATCACCAACATA
CYP86A1-Forward	AGCTTCAGCTGTTGTTACTGG
CYP86A1-Reverse	TCCCTGGATGTTGCGTATGT
CYP86B1-Forward	TAGTGGTCTGATTCGCTGCC
CYP86B1-Reverse	CTATCCCTCACCAGACCCGA
NCED1-Forward	CCAGCACTAATCGATTCC
NCED1-Reverse	GAGAGTGGTGATGAGTAA
NCED2-Forward	CATGGAAAGAGGAAGTTG
NCED2-Reverse	GAAGCAAGTGTGAGCTAAC
Ao5b-Forward	TTGGCGTTGTGATTGCTGAGAC
Ao5b-Reverse	AAAACGGGGGAGGATGGAAGTA
ABA8-OH1-Forward	AGCACGGACCGTCAAAGTC
ABA8-OH1-Reverse	TGAGAATGCCTACGTAGTG
ABA8-OH2-Forward	GAGATGCTGGTGCTCATC
ABA8-OH2-Reverse	ACGTCGTCGCTCGATCCAAC
BG8-Forward	CCCCGGCCAGGCGTATTCC
BG8-Reverse	TCCCAGGCTTATTCGTCATCCA
PYL4-Forward	CCCCCTCCGGTCAACTCTCG
PYL4-Reverse	CCACCACCACCACCACGGATTT
PP2C4-Forward	TGGCCTCTGGGATGTATTGTCG
PP2C4-Reverse	GAGCCGCTGGATCTGGGGAGTC
SnRK2-Forward	GCTGCGTCCCTGCTTCGTA
SnRK2-Reverse	CGCTTCGTGGCCTTATTGTTG

Table S2 The gene information of key DEGs in response to copper stress (P-value < 0.05)

Gene ID	Symbol	Description	Log_2FC	P-value
Cell wall modification				
HORVU.MOREX.r2.1HG0000810	WAK2	Wall-associated receptor kinase	-1.92	1.59E-05
HORVU.MOREX.r2.1HG0004550	WAK4	Wall-associated receptor kinase	1.55	2.16E-02
HORVU.MOREX.r2.3HG0186650	WAK1	Wall-associated receptor kinase	1.77	6.98E-03
HORVU.MOREX.r2.3HG0182520	WAK5	Wall-associated receptor kinase	2.01	1.73E-02
HORVU.MOREX.r2.5HG0420200	WAK3	Wall-associated receptor kinase	1.70	1.53E-03
HORVU.MOREX.r2.6HG0449500	WAK8	Wall-associated receptor kinase	1.95	2.33E-02
HORVU.MOREX.r2.3HG0274770	PAE6	Pectin acetylesterase 6	-2.25	3.22E-03
HORVU.MOREX.r2.3HG0274790	PAE5	Pectin acetylesterase 5	-2.09	8.34E-03
HORVU.MOREX.r2.5HG0438710	PAE3	Pectin acetylesterase 3	-4.94	9.07E-08
HORVU.MOREX.r2.1HG0048290	PME41	Pectin methylesterase 41	1.70	3.42E-03
HORVU.MOREX.r2.2HG0082500	PME4	Pectin methylesterase 4	2.17	3.33E-04
HORVU.MOREX.r2.5HG0356750	PME3	Pectin methylesterase 3	-1.94	4.29E-04
HORVU.MOREX.r2.7HG0601520	PME1	Pectin methylesterase 1	-1.65	2.41E-03
HORVU.MOREX.r2.1HG0002940	OMT1	O-methyltransferase family	-3.61	2.63E-04
HORVU.MOREX.r2.1HG0009370	OMT9	O-methyltransferase family	-5.51	3.37E-06
HORVU.MOREX.r2.1HG0009380	COMT	O-methyltransferase family	-5.48	3.90E-06
HORVU.MOREX.r2.4HG0276750	OMT2	O-methyltransferase family	4.38	3.92E-06
HORVU.MOREX.r2.6HG0449080	IGMT4	O-methyltransferase family	-4.94	4.47E-06
HORVU.MOREX.r2.7HG0547010	CCR2	Cinnamoyl-CoA reductase	1.51	1.71E-03
HORVU.MOREX.r2.7HG0621570	IGMT1	O-methyltransferase family	-5.22	5.56E-06
HORVU.MOREX.r2.2HG0092440	PRX1	Class III peroxidases	-2.34	3.40E-02
HORVU.MOREX.r2.2HG0092500	PRX2	Class III peroxidases	-1.50	4.80E-02
HORVU.MOREX.r2.3HG0211680	PRX72	Class III peroxidases	-2.93	4.05E-05
HORVU.MOREX.r2.3HG0211690	PRX2	Class III peroxidases	-5.08	1.81E-05
HORVU.MOREX.r2.3HG0211730	PRX36	Class III peroxidases	-3.46	7.14E-04
HORVU.MOREX.r2.3HG0211760	PRX9	Class III peroxidases	-4.80	4.41E-05
HORVU.MOREX.r2.5HG0404500	PRX17	Class III peroxidases	1.56	6.70E-05

HORVU.MOREX.r2.3HG0254020	LAC12	Laccase multi-copper oxidoreductase	-2.89	8.98E-04
HORVU.MOREX.r2.4HG0319180	LAC5	Laccase multi-copper oxidoreductase	-2.95	2.46E-04
HORVU.MOREX.r2.5HG0385060	LAC12	Laccase multi-copper oxidoreductase	-1.79	1.68E-03
HORVU.MOREX.r2.1HG0059450	LAC4	Laccase multi-copper oxidoreductase	-4.42	7.68E-07
HORVU.MOREX.r2.2HG0111770	LAC17	Laccase multi-copper oxidoreductase	-2.60	1.01E-07
HORVU.MOREX.r2.3HG0252380	LAC2	Laccase multi-copper oxidoreductase	-2.90	2.93E-04
HORVU.MOREX.r2.4HG0326360	KCS1	3-ketoacyl-CoA synthase	-2.47	4.71E-03
HORVU.MOREX.r2.4HG0329430	KCS6	3-ketoacyl-CoA synthase	-3.69	6.52E-04
HORVU.MOREX.r2.7HG0572230	FAR1	Fatty acyl CoA reductase	2.12	1.11E-06
HORVU.MOREX.r2.7HG0538720	FAR4	Fatty acyl CoA reductase	-5.12	1.98E-04
HORVU.MOREX.r2.4HG0276830	FAR5	Fatty acyl CoA reductase	-3.68	6.54E-04
HORVU.MOREX.r2.3HG0251350	CYP86A1	Fatty acyl omega-hydroxylase	-2.60	1.16E-03
HORVU.MOREX.r2.1HG0034810	CYP86B1	Fatty acyl omega-hydroxylase	-1.66	7.41E-03
HORVU.MOREX.r2.6HG0499350	CYP86A4	Fatty acyl omega-hydroxylase	-1.84	2.60E-03
HORVU.MOREX.r2.2HG0107490	HHT1	Hydroxycinnamoyl-CoA acyltransferase	-2.39	1.28E-03
HORVU.MOREX.r2.2HG0107530	HHT2	Hydroxycinnamoyl-CoA acyltransferase	-2.22	2.74E-03
HORVU.MOREX.r2.4HG0321420	ABCG2	ABC transporter G family member	-2.64	2.94E-04
HORVU.MOREX.r2.3HG0253120	ABCG20	ABC transporter G family member	-2.85	1.36E-03
Translocation				
HORVU.MOREX.r2.2HG0088520	YSL6	Yellow stripe-like protein	-3.23	1.42E-02
HORVU.MOREX.r2.2HG0165820	YSL4	Yellow stripe-like protein	-2.09	3.93E-02
HORVU.MOREX.r2.1HG0057890	ZIP5	Zrt-/Irt-like protein	1.70	2.57E-03
HORVU.MOREX.r2.2HG0158440	ZIP3	Zrt-/Irt-like protein	2.55	2.37E-04
HORVU.MOREX.r2.3HG0273580	ZIP2	Zrt-/Irt-like protein	-3.46	3.31E-04
HORVU.MOREX.r2.7HG0603650	HMA2	Heavy metal ATPase	-2.32	9.96E-04
HORVU.MOREX.r2.7HG0606170	ATX1	Antioxidant protein	-3.26	1.15E-03
Detoxification				
HORVU.MOREX.r2.1HG0004210	MT2	Type 2 metallothionein-like	3.67	1.58E-03
HORVU.MOREX.r2.4HG0348200	NAS2	Nicotianamine synthase	-3.45	3.30E-02
HORVU.MOREX.r2.6HG0523410	NAS3	Nicotianamine synthase	-3.28	1.03E-02

HORVU.MOREX.r2.4HG0345860	NAS1	Nicotianamine synthase	-1.85	3.72E-02
HORVU.MOREX.r2.2HG0175140	HSP20-1	Heat shock protein 20 family	-2.09	3.33E-05
HORVU.MOREX.r2.3HG0187690	HSP20-2	Heat shock protein 20 family	-4.25	2.49E-03
HORVU.MOREX.r2.3HG0197320	HSP20-3	Heat shock protein 20 family	2.68	9.80E-03
HORVU.MOREX.r2.3HG0197340	HSP20-4	Heat shock protein 20 family	2.99	3.82E-03
HORVU.MOREX.r2.3HG0197310	HSP20-5	Heat shock protein 20 family	2.43	3.29E-04
HORVU.MOREX.r2.3HG0197330	HSP20-6	Heat shock protein 20 family	3.04	1.14E-03
HORVU.MOREX.r2.3HG0197300	HSP20-7	Heat shock protein 20 family	1.80	1.40E-03
HORVU.MOREX.r2.4HG0277610	HSP20-8	Heat shock protein 20 family	-1.56	3.68E-02
HORVU.MOREX.r2.4HG0334030	HSP20-9	Heat shock protein 20 family	-1.61	4.91E-02
HORVU.MOREX.r2.4HG0334490	HSP20-10	Heat shock protein 20 family	2.43	1.64E-03
HORVU.MOREX.r2.5HG0397460	HSP20-11	Heat shock protein 20 family	-1.51	1.66E-04
HORVU.MOREX.r2.6HG0515330	HSP20-12	Heat shock protein 20 family	2.03	7.94E-03
HORVU.MOREX.r2.7HG0551540	HSP20-13	Heat shock protein 20 family	2.12	3.46E-02
HORVU.MOREX.r2.7HG0551550	HSP20-14	Heat shock protein 20 family	1.50	1.51E-02
HORVU.MOREX.r2.7HG0551580	HSP20-15	Heat shock protein 20 family	1.61	1.70E-02
HORVU.MOREX.r2.7HG0555460	HSP20-16	Heat shock protein 20 family	2.41	4.38E-02
HORVU.MOREX.r2.2HG0084300	HSP60-1	Heat shock protein 60 family	-1.69	3.19E-02
HORVU.MOREX.r2.6HG0451590	HSP60-2	Heat shock protein 60 family	3.21	7.47E-05
HORVU.MOREX.r2.3HG0252650	HSP70-1	Heat shock protein 70 family	1.84	3.85E-04
HORVU.MOREX.r2.4HG0329540	HSP70-2	Heat shock protein 70 family	1.65	1.43E-03
HORVU.MOREX.r2.2HG0101570	HIPP23	Heavy-metal-associated isoprenylated plant protein	3.18	2.70E-03
HORVU.MOREX.r2.2HG0134510	HIPP43	Heavy-metal-associated isoprenylated plant protein	-1.77	1.89E-03
HORVU.MOREX.r2.2HG0135330	HIPP39	Heavy-metal-associated isoprenylated plant protein	2.85	2.46E-02
HORVU.MOREX.r2.2HG0163600	HIPP4	Heavy-metal-associated isoprenylated plant protein	1.74	1.64E-03
HORVU.MOREX.r2.2HG0167790	HIPP2	Heavy-metal-associated isoprenylated plant protein	-2.57	6.60E-03
HORVU.MOREX.r2.2HG0173360	HIPP44	Heavy-metal-associated isoprenylated plant protein	2.89	2.09E-04
HORVU.MOREX.r2.2HG0173500	HIPP45	Heavy-metal-associated isoprenylated plant proteinn	-2.83	1.85E-03
HORVU.MOREX.r2.2HG0173510	HIPP46	Heavy-metal-associated isoprenylated plant protein	1.91	5.25E-04
HORVU.MOREX.r2.3HG0209410	HIPP47	Heavy-metal-associated isoprenylated plant protein	1.85	2.37E-05

HORVU.MOREX.r2.3HG0221330	HIPP20	Heavy-metal-associated isoprenylated plant protein	-1.94	2.43E-03
HORVU.MOREX.r2.4HG0338470	HIPP33	Heavy-metal-associated isoprenylated plant protein	-2.86	3.11E-04
HORVU.MOREX.r2.6HG0453610	HIPP27	Heavy-metal-associated isoprenylated plant protein	3.07	4.93E-03
HORVU.MOREX.r2.7HG0620520	HIPP35	Heavy-metal-associated isoprenylated plant protein	-3.26	8.36E-04
Copper protein				
HORVU.MOREX.r2.1HG0038390	SKS2	Multicopper oxidase	-2.57	5.04E-03
HORVU.MOREX.r2.7HG0594750	MCO2	Multicopper oxidase	-1.62	2.54E-04
HORVU.MOREX.r2.2HG0113990	UCC1-1	Uclacyanin-like protein	-6.24	7.71E-08
HORVU.MOREX.r2.2HG0129660	UCC2-1	Uclacyanin-like protein	-3.62	3.26E-04
HORVU.MOREX.r2.3HG0241980	ENODL19	Early nodulin-like protein	2.11	2.44E-04
HORVU.MOREX.r2.2HG0153720	UCC3-1	Uclacyanin-like protein	-2.65	5.76E-04
HORVU.MOREX.r2.5HG0404380	UCC2-2	Uclacyanin-like protein	1.58	2.39E-02
HORVU.MOREX.r2.6HG0469140	ENODL18	Early nodulin-like protein	-1.97	2.77E-04
HORVU.MOREX.r2.6HG0497420	UCC3-2	Uclacyanin-like protein	-3.26	1.95E-04
HORVU.MOREX.r2.5HG0444530	ARPN1	Plantacyanin-like protein	-2.65	1.08E-03
HORVU.MOREX.r2.6HG0507710	ARPN2	Plantacyanin-like protein	1.54	1.53E-03
HORVU.MOREX.r2.3HG0244850	UCC1-2	Uclacyanin-like protein	-3.98	1.13E-03
HORVU.MOREX.r2.4HG0280990	ARPN3	Plantacyanin-like protein	1.79	1.25E-03
HORVU.MOREX.r2.6HG0506410	ENODL1	Early nodulin-like protein	-1.75	2.47E-02
HORVU.MOREX.r2.4HG0347290	ENODL8	Early nodulin-like protein	-2.09	3.98E-04
HORVU.MOREX.r2.3HG0245030	ENODL9	Early nodulin-like protein	-1.67	3.54E-02
HORVU.MOREX.r2.5HG0425180	ENODL20	Early nodulin-like protein	-1.69	4.77E-03
HORVU.MOREX.r2.7HG0551420	UCC1-3	Uclacyanin-like protein	-1.91	5.24E-04
Antioxidant				
HORVU.MOREX.r2.2HG0094720	CSD1	Cu/Zn superoxide dismutase	0.56	3.59E-03
HORVU.MOREX.r2.4HG0329510	CSD2	Cu/Zn superoxide dismutase	0.98	1.39E-04
HORVU.MOREX.r2.1HG0054390	POD1	Peroxidase superfamily protein	-6.29	1.51E-07
HORVU.MOREX.r2.1HG0054400	POD2	Peroxidase superfamily protein	-5.73	3.71E-07
HORVU.MOREX.r2.1HG0054410	POD3	Peroxidase superfamily protein	-5.50	8.44E-07
HORVU.MOREX.r2.1HG0054420	POD4	Peroxidase superfamily protein	-5.71	5.07E-07

HORVU.MOREX.r2.1HG0054440	POD5	Peroxidase superfamily protein	-6.07	3.51E-08
HORVU.MOREX.r2.2HG0159520	POD6	Peroxidase superfamily protein	-3.32	6.70E-05
HORVU.MOREX.r2.5HG0425690	POD7	Peroxidase superfamily protein	-3.37	1.79E-05
HORVU.MOREX.r2.7HG0584900	POD8	Peroxidase superfamily protein	2.28	5.53E-04
HORVU.MOREX.r2.7HG0604280	POD9	Peroxidase superfamily protein	-2.92	2.96E-04
HORVU.MOREX.r2.6HG0453490	CAT2	Catalase2	3.13	1.69E-03
HORVU.MOREX.r2.2HG0085360	APX3	Ascorbate peroxidase 3	-1.53	1.70E-03
HORVU.MOREX.r2.6HG0525590	APX1	Ascorbate peroxidase 1	-1.64	4.93E-03
HORVU.MOREX.r2.1HG0040650	GSTU16	Glutathione S-transferase	-2.02	1.77E-03
HORVU.MOREX.r2.1HG0040550	GSTU18	Glutathione S-transferase	-2.05	3.18E-03
HORVU.MOREX.r2.3HG0183910	GSTU15	Glutathione S-transferase	1.67	3.39E-02
HORVU.MOREX.r2.2HG0178450	GSTU20	Glutathione S-transferase	3.46	1.21E-05
HORVU.MOREX.r2.2HG0155370	GSTF3	Glutathione S-transferase	4.40	3.20E-04
HORVU.MOREX.r2.2HG0178460	GSTU19	Glutathione S-transferase	3.28	7.05E-04
HORVU.MOREX.r2.3HG0233440	GSTU24	Glutathione S-transferase	1.85	2.43E-04
HORVU.MOREX.r2.2HG0178440	GSTU25	Glutathione S-transferase	3.47	5.24E-04
HORVU.MOREX.r2.7HG0529160	GSTU8	Glutathione S-transferase	2.85	3.23E-04
HORVU.MOREX.r2.3HG0266820	GSTU7	Glutathione S-transferase	1.77	1.86E-03
HORVU.MOREX.r2.7HG0529420	GSTU1	Glutathione S-transferase	1.83	1.98E-03
HORVU.MOREX.r2.4HG0321340	GSTL2	Glutathione S-transferase	2.14	8.02E-04
HORVU.MOREX.r2.5HG0411910	GSTZ1	Glutathione S-transferase	1.68	1.52E-03
HORVU.MOREX.r2.7HG0612050	GSTU11	Glutathione S-transferase	-2.59	3.54E-04
Plant hormone signal transduction				
HORVU.MOREX.r2.1HG0060180	AUX1	Auxin influx transporter	1.72	9.14E-03
HORVU.MOREX.r2.4HG0291400	LAX2	LAX family of auxin influx carriers	-2.09	5.89E-04
HORVU.MOREX.r2.5HG0360080	IAA3	Aux/IAA protein family	-1.51	6.61E-04
HORVU.MOREX.r2.5HG0422820	IAA16	Aux/IAA protein family	-1.90	8.04E-04
HORVU.MOREX.r2.5HG0423400	IAA14	Aux/IAA protein family	-2.29	1.50E-05
HORVU.MOREX.r2.1HG0072210	ARF4	ARF family of transcription factors	1.76	9.96E-04
HORVU.MOREX.r2.3HG0244730	GH3.1	IAA-amido synthases	-1.68	2.05E-03

HORVU.MOREX.r2.3HG0242100	GH3.2	IAA-amido synthases	1.52	2.05E-02
HORVU.MOREX.r2.1HG0054200	GH3.4	IAA-amido synthases	1.52	1.19E-04
HORVU.MOREX.r2.5HG0409880	SAUR6	Auxin-regulated protein	2.01	2.15E-02
HORVU.MOREX.r2.5HG0409900	SAUR9	Auxin-regulated protein	1.70	9.69E-03
HORVU.MOREX.r2.5HG0409910	SAUR12	Auxin-regulated protein	2.04	2.21E-02
HORVU.MOREX.r2.6HG0463870	SAUR19	Auxin-regulated protein	-2.02	3.06E-04
HORVU.MOREX.r2.6HG0463880	SAUR32	Auxin-regulated protein	-2.63	1.44E-03
HORVU.MOREX.r2.6HG0513430	SAUR50	Auxin-regulated protein	1.76	2.37E-04
HORVU.MOREX.r2.2HG0079860	YUCCA9	Flavin monooxygenase	-1.83	6.90E-03
HORVU.MOREX.r2.2HG0172680	YUCCA3	Flavin monooxygenase	-2.66	4.48E-03
HORVU.MOREX.r2.4HG0297660	PIN1	Auxin efflux carrier	1.69	1.27E-03
HORVU.MOREX.r2.7HG0613500	PIN2	Auxin efflux carrier	-2.35	2.77E-03
HORVU.MOREX.r2.7HG0605640	ILL6	IAA amino acid conjugate hydrolase	1.58	2.37E-03
HORVU.MOREX.r2.2HG0140600	ARR3	Arabidopsis response regulator	-2.36	4.27E-04
HORVU.MOREX.r2.2HG0175470	ARR6	Arabidopsis response regulator	-3.10	7.03E-05
HORVU.MOREX.r2.6HG0526160	ARR8	Arabidopsis response regulator	-1.98	8.24E-06
HORVU.MOREX.r2.3HG0268300	ARR4	Arabidopsis response regulator	-2.06	9.63E-04
HORVU.MOREX.r2.5HG0381410	ARR9	Arabidopsis response regulator	-1.50	1.01E-02
HORVU.MOREX.r2.5HG0397180	CYP735A1	Cytokinin hydroxylases	-2.53	7.86E-04
HORVU.MOREX.r2.7HG0604580	XET22	Xyloglucosyl transferase	-1.88	1.41E-04
HORVU.MOREX.r2.7HG0604570	XET6	Xyloglucosyl transferase	2.68	2.19E-04
HORVU.MOREX.r2.5HG0387330	CYCD3	Cyclin D-type protein	1.80	6.39E-04
HORVU.MOREX.r2.2HG0080130	BR6OX	Brassinosteroid-6-oxidase	1.56	7.14E-03
HORVU.MOREX.r2.1HG0055970	TGA2	TGACG binding proteins	1.56	7.04E-04
HORVU.MOREX.r2.5HG0406840	TGA10	TGACG binding proteins	-1.77	3.75E-04
HORVU.MOREX.r2.5HG0392230	PRB1-2	Pathogenesis-Related Protein	4.68	4.03E-04
HORVU.MOREX.r2.5HG0431600	PRB1-3	Pathogenesis-Related Protein	3.76	3.32E-03
HORVU.MOREX.r2.5HG0392250	PR1a	Pathogenesis-Related Protein	3.90	4.58E-04
HORVU.MOREX.r2.7HG0540560	PR1	Pathogenesis-Related Protein	-5.20	1.23E-05
HORVU.MOREX.r2.7HG0549070	PR1c	Pathogenesis-Related Protein	3.07	1.92E-03

HORVU.MOREX.r2.7HG0549080	PR1b	Pathogenesis-Related Protein	3.16	6.72E-04
HORVU.MOREX.r2.2HG0167340	SnRK2	SNF1-related protein kinases	1.99	2.49E-03
HORVU.MOREX.r2.2HG0079050	PP2C4	Phosphatase 2C family protein	1.86	1.85E-02
HORVU.MOREX.r2.3HG0255020	EIN3	Ethylene-insensitive3 protein	2.25	1.96E-04

8. Acknowledgements

The past four years would be the most unforgettable time in my life. I experienced too many things. Fortunately, I met a lot of kind and helpful people. Although there are too many words to express enough of my appreciation, I still want to thank everyone I met and who helped me. First, I would like to thank my supervisor, Prof. Dr. Lukas Schreiber, sincerely. Thank him for giving me a chance in his group and for providing patient and careful guidance in my research. I also appreciate him caring about my life and health just like my family.

I would like to thank the China Scholarship Council (CSC) for giving me an opportunity to complete my PhD study in Germany.

I would like to extend my gratitude to all members of our institute and lab for their suggestions and help. It's my pleasure to get along with them for a wonderful four years. Thanks to Dr. Viktoria V. Zeisler-Diehl for patient and careful guidance in GC analysis and patient assistance in every reagent order. Thanks to Dr. Rochus B. Franke, Dr. Paul Grünhofer, Dr. Juila Holbein, Kiran Suresh, Lena Herzig, Jorge Carvajal and other colleagues for their suggestions and help with my experiment.

I would like to thank my friends and colleagues Hongjun Meng, Li Guo and Junwen Zhao for their support and companionship in my life and work. I would also like to express my sincere gratitude to my best friends Caiqiong Yang, Zhuo Xu, Baoyu Hu and Congwei Xie, who studied with me in Europe. I will always remember the wonderful and fun times we had traveling, enjoying delicious food and discussing life together. Of course, I would also like to thank my best friends Xinli Xiao, Xiyang Long and Xiaowen Zhang in far away China for your companionship, support and encouragement, which made my four-year study trip less boring and lonely.

I would also like to express my sincere gratitude to my parents and family for their unselfish love, support and encouragement. Last but not least, I would like to thank a lovely and elegant lady, my wife, Zhenzhen Shen, for her constant waiting, support, encouragement and companionship. Her presence in my life makes me feel that I am the luckiest and happiest man in the world.

Per aspera ad astra.